

21539791



This is to certify that the

thesis entitled

INVESTIGATIONS OF ENERGY TRANSPORT PROPERTIES IN HIGH PRESSURE MICROWAVE PLASMAS

presented by

Craig F. Hoekstra

has been accepted towards fulfillment of the requirements for

M.S. degree in _____CHE

Major professor

Date 8/24/88.

MSU is an Affirmative Action/Equal Opportunity Institution

O-7639





RETURNING MATERIALS:
Place in book drop to remove this checkout from your record. FINES will be charged if book is returned after the date stamped below.

INVESTIGATIONS OF ENERGY TRANSPORT PROPERTIES IN HIGH PRESSURE MICROWAVE PLASMAS

Ву

Craig Frederick Hoekstra

A THESIS

Submitted to
Michigan State University
in partial fulfillment of the requirements
for the degree of

MASTER OF SCIENCE

Department of Chemical Engineering

1988

ABSTRACT

INVESTIGATIONS OF ENERGY TRANSPORT PROPERTIES IN HIGH PRESSURE MICROWAVE PLASMAS

BY

Craig Frederick Hoekstra

Mechanisms of energy transfer to and within high pressure (200 - 1000 torr) helium and nitrogen microwave plasmas were studied. Emission spectroscopy was used to estimate electron temperatures within helium plasmas. Plasma diameter and volume measurements were taken on nitrogen and helium discharges. In a calorimetry experiment, the distribution of power to the cavity walls, cooling air and plasma gas was measured. A heat transfer model was used to calculate radial temperature profiles and mixing cup temperatures of the gas exiting the plasma region. Yttria has potential as a sheath material for a high temperature microwave resistant probe. Future research should focus on 400 to 1500 W plasmas which should be more stable and have higher electron densities.

Dedicated to Edward Waltz.

ACKNOWLEDGMENTS

I am thankful to Dr. Martin Hawley for his encouragement and interest throughout this investigation. I would like to thank Dr. Jes Asmussen and his graduate students, Jeff Hopwood and Leonard Mahoney, for their suggestions and guidance. I am especially grateful to Dr. Stanley Whitehair for helping me design my experiment and learn about microwave plasmas. Thanks should also be given to John Filpus and Nancy Gronlund for their patience and help in this endeavor.

Most of all, I would like to give thanks to my wife Karyn for enduring my late hours and lost weekends so that I might finish this project and my parents for making all this possible.

This research was supported in part by fellowships from Michigan

State University and by grants from the National Aeronautics and Space

Administration Lewis Research Center.

TABLE OF CONTENTS

| LIST OF FIGURESvi |
|---|
| LIST OF TABLESi |
| NOMENCLATURE |
| CHAPTER I INTRODUCTION |
| 1.1 History of Microwave Plasma Research |
| 1.2 Research Objectives |
| CHAPTER II MICROWAVE PLASMA SYSTEM |
| 2.1 Introduction |
| 2.2 Microwave Cavity and Plasma Containment Assembly |
| 2.3 Flow System |
| 2.4 Microwave System |
| CHAPTER III EMISSION SPECTROSCOPY MEASUREMENTS |
| 3.1 <u>Introduction</u> |
| 3.2 Equipment for Atomic-Electronic Temperature Measurements. 1 |
| 3.3 Experimental Procedures and Operating Conditions2 |
| 3.4 Discussion of Experimental Results |
| 3.5 <u>Summary</u> 3 |
| CHAPTER IV PLASMA VOLUME AND DIAMETER MEASUREMENTS |
| 4.1 <u>Introduction</u> |
| 4.2 Experimental Design |
| 4.3 Results for High Pressure Plasmas3 |
| 4.4 <u>Summary</u> 4 |
| CHAPTER V ENERGY BALANCE MEASUREMENTS |
| 5.1 <u>Introduction</u> |
| 5.2 Experimental System and Procedure |
| 5.3 Results of Calorimetry Experiment |
| 5.4 <u>Summary</u> 6 |
| CHAPTER VI COMPUTER MODELING OF PLASMA SHEATH |
| 6.1 <u>Introduction</u> |
| 6.2 Development of Computer Program |
| 6.3 Results from Simulation Runs70 |
| 6.4 <u>Summary</u> 8 |
| CHAPTER VII MICROWAVE PROBE DEVELOPMENT |
| 7.1 <u>Introduction</u> 8 |
| 7.2 Testing Materials for Probe8 |
| 7.3 Discussion of Results8 |
| 7.4 Summary8 |

| CHAPTER VIII CONCLUSIONS | |
|---|-------|
| 8.1 <u>Introduction</u> | 91 |
| 8.2 Spectroscopy Measurements | 91 |
| 8.3 Plasma Volume and Diameter Results | 92 |
| 8.4 Energy Balance Measurements | |
| 8.5 Heat Conduction Model Results | |
| 8.6 Probe Development | |
| 8.7 <u>Summary</u> | 94 |
| CHAPTER IX RECOMMENDATIONS | |
| 9.1 Introduction | 97 |
| 9.2 Spectroscopy | |
| 9.3 Plasma Volume and Diameter Measurements | |
| 9.4 Energy Balance | |
| 9.5 Computer Modeling | |
| 9.6 Probe Development | .101 |
| REFERENCES | . 102 |
| APPENDIX | |
| Computer Program for Sheath Modeling | . 104 |
| Experimental Procedures for Starting a Plasma | |
| Safety Considerations | |

LIST OF FIGURES

| Figure Figure | | Microwave Electrothermal Thruster Concept |
|------------------|--------------|---|
| Figure | 2 1 | Quartz Tube Assembly10 |
| Figure | | Cross Section of Microwave Cavity Applicator11 |
| Figure | | Picture of Assembled Microwave Cavity Applicator13 |
| Figure | | Gas Flow System |
| | | |
| Figure | 2.5 | Microwave System |
| Figure | 3.1 | Emission Spectroscopy System |
| Figure | 3.2 | Spectral Response Configuration23 |
| Figure | 3.3 | Electronic Temperatures versus Pressure27 |
| Figure | | Helium Energy Level Diagram30 |
| Figure | | Electronic Temperatures versus Flow Rate |
| Figure | | Electronic Temperatures versus Coolant Flow Rate34 |
| 6 | | |
| Figure | 4.1 | Discharge Volume Measurement Setup38 |
| Figure | 4.2 | Helium Plasma Diameters versus Pressure40 |
| Figure | 4.3 | Nitrogen Plasma Diameters versus Pressure41 |
| Figure | 4.4 | Plasma Diameters versus Pressure42 |
| Figure | | Plasma Optical Measuring Device |
| | | • |
| Figure | 5.1 | Electromagnetic Field Pattern for the |
| | | Microwave Cavity Applicator50 |
| Figure | 5.2 | Calorimetry System54 |
| Figure | | Microwave Power Absorbed by Cooling Water56 |
| Figure | | Percent Power Absorbed by Gas58 |
| Figure | | Percent Power Absorbed by Cooling Air60 |
| Figure | | Gas Flow Rate Dependent Data (He) |
| 116410 | 3.0 | tab 120% hate bependent bata (he) |
| Figure | 6.1 | Computer Modeling of Plasma Energy Transfer to |
| | | the Air Cooled Wall by Non-Reacting Gases64 |
| Figure | 6.2 | Illustration of Different Types of |
| | | Boundary Conditions67 |
| Figure | 6.3 | Non-Plasma Gas Axial Temp. Profiles (Base Case)72 |
| Figure | 6.4 | N ₂ Non-Plasma Gas Axial Temp. Profiles |
| | | (Expanding Gas Boundary Conditions)74 |
| Figure | 6.5 | Non-Plasma Gas Exit Temp. Radial Distributions |
| | | (Base Case) |
| Figure | 6.6 | Non-Plasma Gas Exit Temp. Radial Distributions |
| - 5 | - | (Expanding Gas Boundary Condition) |
| Figure | 6.7 | Non-Plasma Gas Exit Temp. (200 Torr) |
| Figure | | N ² Non-Plasma Cas Frit Temp (600 Torr) 78 |
| Figure | | N2 Non-Plasma Gas Exit Temp. (1000 Torr) |
| Figure | | N Cas Frit Tamparatures (Missing Cum Asserses) |
| TRULE | 0.10 | no cas pure remberacares (mixing cab userages) |

| Figure 7.1 | High Temperature, Microwave-Tolerant Probe | |
|------------|--|----|
| | Development | 85 |
| Figure 7.2 | Microwave Heating of Yttria Probe | 89 |

LIST OF TABLES

| Table 3.1 | Transition Probabilities, Wavelength of Transition, Energies and Degeneracies of the Atomic Electronic Levels for Helium and Nitrogen Gases | | |
|-----------|---|--|--|
| Table 4.1 | Helium and Nitrogen Plasma Volumes in Pressures from 200 - 1000 Torr48 | | |
| Table 5.1 | Calorimetry Experimental Conditions53 | | |
| Table 6.1 | Experimental Conditions for Computer Simulation71 | | |
| Table 8.1 | Summary of Experimental Parameters96 | | |

NOMENCLATURE

```
- transition probability
Anm
        - the electron ionization energy (eV)
Ср
        - constant pressure heat capacity
        - energy of the initial electronic state
        - thrust force
        - gravitational acceleration.
g
        - degeneracy of the initial state of transition
H
        - enthalpy per gram
hc
        - heat transfer coefficient (Bennett and Myers [1974])
        - measured emission line intensity
,
k
        - thermal conductivity of nitrogen (Cal/s cm K) (Chpt 6)
        - Boltzman Constant (Chapter 3)
^{\lambda}nm
        - wavelength of the transition
ṁ
        - mass flow rate of propellant
        - the electron level
        - the number of moles of gas entering in the initial
           plasma volume
        - the electron density (cm^{-3})
Ne
Νi
        - molar flux of gas (gmoles/s)
        - the number of moles of gas in the plasma volume
np
           after being heated to 1500 K
        - microwave power input to the cavity system
pabs
        - microwave power absorbed by the quartz tube cooling air
pair
        - microwave power absorbed and kept in the plasma gas
pgas
        - microwave power absorbed by the cavity cooling water
        - percent of total input power absorbed by the cooling air
*Pair
        - percent of total input power absorbed by the plasma gas
*Pgas
        - percent of total input power absorbed by the cooling water
        - heat flux in the r direction (E/L_2^2t)
\mathbf{q}_{\mathbf{z}}
        = heat flux in the z direction (E/L't)
        - density (M/L)
R
        - the gas law constant
Re
        - Reynolds Number
        = spectral response function
RΪ
        - plasma non-plasma interface (cm)
R2
        - interface between the quartz tube and non-reacting gas (cm)
T
        - temperature of gas
T<sub>b</sub>
        - the plasma boundary temperature
        - the electronic temperature (eV)
Te
Telec
Ti
Ti
        - atomic electronic temperature (K)
        - the initial gas temperature (298 K)
        - the plasma gas temperature (1500 K)
        = velocity in the z direction (L/t)
        - the ionic charge
```

Chapter I

Introduction

1.1 History of Microwave Plasma Research

"All rocket motors are based on the same principle, mass is accelerated and expelled" (Cornelisse [1979]).

It seems appropriate that this investigation begin with a statement of the fundamental idea behind the development of rocket propulsion systems. Before discussing the current research and development of the microwave electrothermal rocket engine, it is important to understand the chemical rocket motor. Although the chemical rocket engine is not used to propel all types of spacecraft, the underlying principles are very basic and provide the necessary background for discussion of more modern propulsion systems.

Chemical rocket engines need oxygen to combust the propellant fuel. The main products are gases which are heated by the chemical energy released during combustion. Typical gas temperatures for a chemical rocket engine vary between 2000 and 3500 K (Cornelisse [1979]). Since the hot gases are contained in a relatively small volume, the thermal expansion of these gases causes a high pressure flow. The high pressure flow is expanded and accelerated by a nozzle, resulting in a force on the rocket motor.

Along with chemical combustion, nuclear reaction and electrical power are possible energy sources for rocket propulsion (Sutton [1976]). The nuclear rocket engine heats the propellant by nuclear

reaction instead of by a combustion process. This type of engine is still in the experimental stage. The electrical rocket motor uses many different coupling mechanisms to change electrical energy into heat energy in providing thrust for the spacecraft.

Although the chemical rocket motor is well suited for many different propulsion situations, the electrical rocket motor has created its own niche by satisfying the long term propulsion needs of deep space exploration. Long periods of flight in deep space require two propulsion design criteria, long engine life and low propellant consumption rates or high specific impulse. Specific impulse is defined as "the ratio of thrust to propellant mass flow expressed in units of seconds" (Sutton [1976). The formula for calculating the specific impulse of a rocket engine is as follows:

$$I_{sp} = \frac{F g_{c}}{m g}$$

where F = thrust force

m = mass flow rate of propellant

g = gravitational acceleration.

g - gravitational constant

The three fundamental types of electrical propulsion are electrothermal, electrostatic, and electromagnetic. The electrothermal propulsion system electrically heats the propellant and expands the gas at supersonic speeds through a nozzle similar to the chemical rocket motor. Acceleration of the propellant particles in the electrostatic system is achieved by the interaction of electrostatic fields on charged propellant particles. The electromagnetic propulsion system uses the interaction of electric and magnetic fields to create a plasma used to accelerate the propellant gas. The electrothermal propulsion systems are expected to achieve a higher specific impulse than the chemical rocket motor and a higher thrust to weight ratio than the electrostatic thruster.

One type of electrothermal propulsion system is the microwave thruster. Figure 1.1 illustrates how beamed or on-board microwave power can be used by a microwave thruster to sustain a plasma. Although the microwave thruster creates a plasma during operation, it is not classified as an electromagnetic thruster because it uses a nozzle to accelerate the propellant gases. The electromagnetic thruster does not require a nozzle because it uses electromagnetic fields to establish high particle velocities.

Because the microwave electrothermal thruster does not require contact with the working fluid, it has advantages over other electrothermal thrusters such as the DC arcjet and resistojet. Propulsion systems that require thermal mechanisms of energy transfer to the propellant eliminate the use of chemically active gases such as 0_2 (Whitehair [1986]). The DC arcjet uses electrodes, which can erode during operation, to heat the propellant. The resistojet suffers from a similar drawback in that the propellant picks up energy from contact with heating coils.

Microwave electrothermal thrusters use a microwave generated plasma to heat the propellant. Although the use of a plasma as a source of heating of rocket propellant was first suggested by Stewart

Microwave Electrothermal Thruster Concept

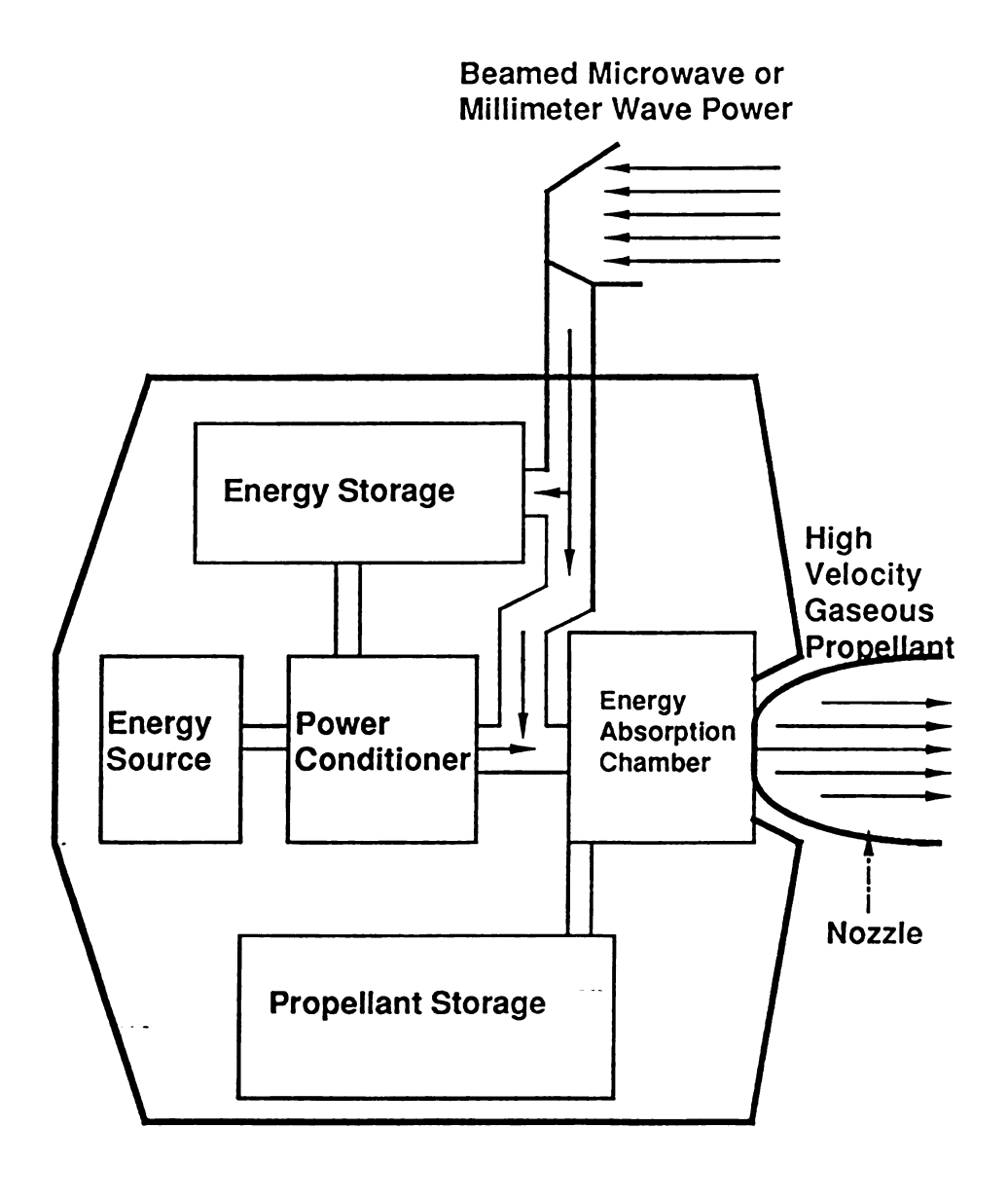


Figure 1.1 Microwave Electrothermal Thruster Concept

[1966] in his paper on "New Possibilities for Solar-System

Exploration," a full scale microwave electrothermal thruster is yet to be constructed.

The term "plasma" is a relatively new one. Back in the 17th century, the first observation of a gas discharge was made during electrostatic investigations (Howatson [1965]). In 1939, however, Langmuir [1939] named this same phenomena "plasma oscillations". In time, the expression of plasma oscillations has been shortened to plasma. Now, the terms gas discharge and plasma have come to mean the same thing; a gas with positive and negative particles which has no net charge. It is believed that 99% of the matter in the universe exists in the plasma state (Mark [1968] and Krall [1973]).

Microwave plasmas are created by electromagnetic fields (Figure 1.2) which accelerate free electrons in the working gas. The accelerated electrons collide with atoms and molecules of the gas, and causes the gas to ionize and previously bound electrons to be stripped off. This method differs from other methods which use high temperatures to create the necessary thermal agitation to create a plasma (Thompson [1962]). The distinction between a plasma and a normal gas is that a plasma can sustain an electrical current while a normal gas is an insulator. In this case, a normal gas is defined as a gas composed of neutral species.

The search for a greater understanding of the plasma heat and mass transfer mechanisms has motivated research at Michigan State University for more than twenty years. To bring the development of the microwave electrothermal thruster closer to realistic operating

Microwave Discharge Properties

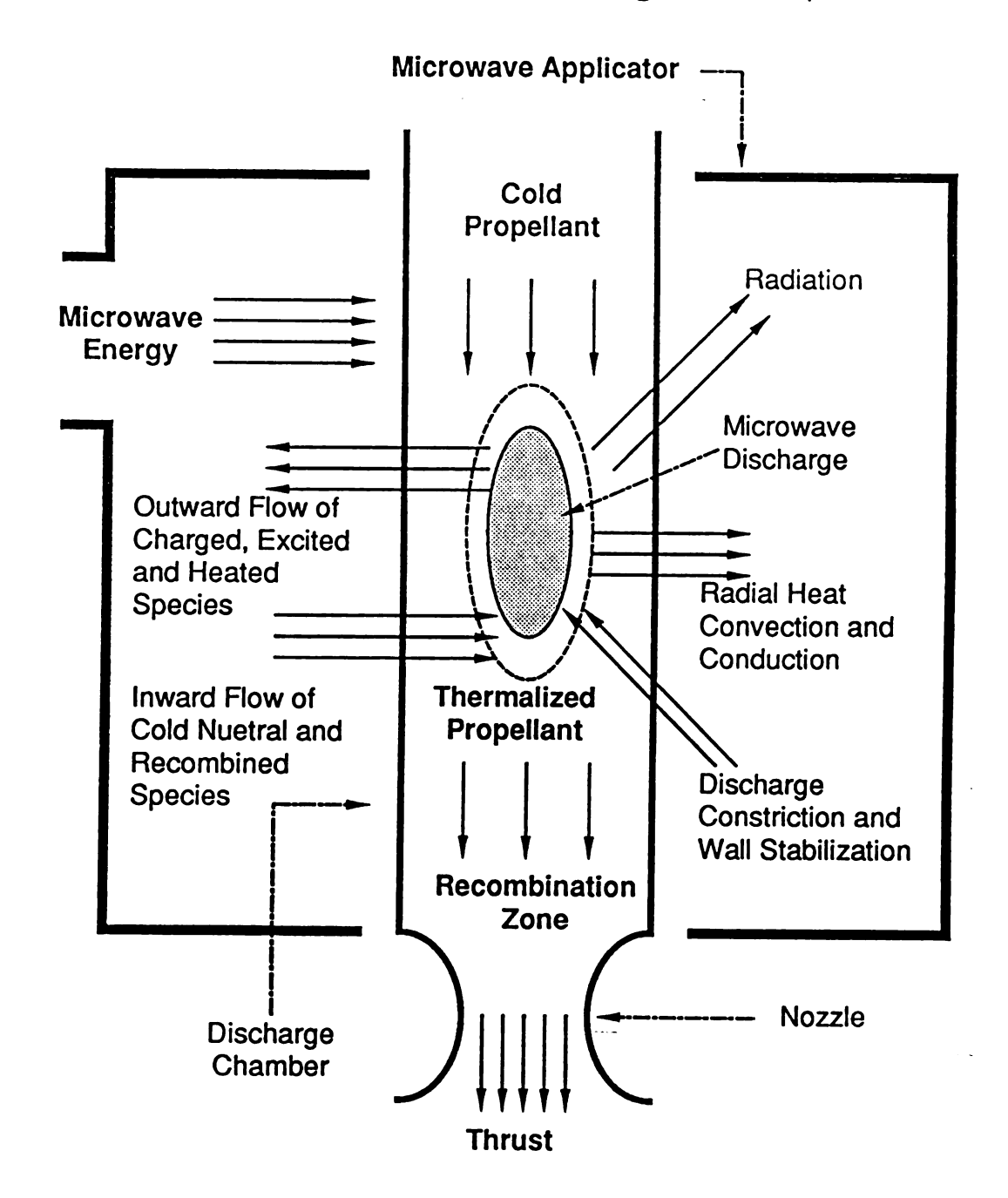


Figure 1.2 Microwave Discharge Properties

conditions, current research focuses on high pressure (200 - 1000 torr) plasmas.

1.2 Research Objectives

The research objectives are to study and develop diagnostic techniques for high pressure (200 - 1000 torr) and high power (100 - 250 W) microwave plasmas. Experiments include electron temperature and cavity efficiency measurements, plasma volume and diameter measurements, and the initial development of a microwave resistant temperature probe. Also, a computer program is used to model the conductive heat transfer from the plasma to the wall of the plasma chamber and calculate radial temperature distributions downstream from the plasma. The information gathered during this investigation should help build the knowledge base necessary to eventually construct a full scale microwave electrothermal thruster.

Emission spectroscopy, photographic methods and an energy balance of the microwave discharge system are techniques used in this study to observe the mechanisms of energy transfer within high pressure microwave discharges. Emission spectroscopy measurements are used to calculate the atomic-electronic (bound electron) temperatures of plasma gases and to get an idea of the relative population of electron states whose transitions are in the visible region of the spectrum. Plasma volume and diameter measurements are made for use in a heat transfer model and also to help further the understanding of the chemical processes inside high pressure plasmas. The energy balance experiment is used to measure the percentage of input power absorbed

by the microwave cavity, input gas, and cooling air flow during different operating conditions.

Another objective of this investigation is to model the heat transfer in nitrogen gas from the microwave plasma to the quartz tube wall by conduction. From this model, radial temperature distributions of the gas exiting the plasma region can be calculated and then used in other calculations which include mixing cup temperatures and plasma recombination models.

A ceramic probe sheath for a 400 °C maximum temperature fluoroptic probe is being designed in an attempt to calculate the temperature of the plasma gas inside the microwave field. Currently there is no method of calculating this temperature with a high degree of accuracy. This method will utilize the measuring of the unsteady state temperature rise of the ceramic probe sheath to calculate the exact temperature of the system from standard curves.

Chapter II

Microwave Plasma System

2.1 Introduction

Chapter II contains a description of the equipment necessary to generate a high pressure microwave plasma. The total microwave plasma system is broken down into three major sections; the cavity and plasma containment assembly, the gas flow systems, and the microwave system. In the first section (Section 2.2), the materials and construction necessary to make the microwave resonant cavity and the plasma containment assembly are specified. In Section 2.3, the equipment used in the working gas and cooling flow systems is discussed, while the Section 2.4 deals with the equipment necessary to construct a 500 W (maximum) microwave power system.

2.2 Microwave Cavity and Plasma Containment Assembly

The plasma is generated in a quartz tube which is placed inside a cylindrical microwave cavity. The quartz tube containing the plasma is 33 cm O.D. and is surrounded by a 50 cm O.D. air cooling tube. Both tubes are 2 1/2 feet long and are epoxied to aluminum collars which feed the necessary gases (See Figure 2.1). The cavity, which is machined in brass, consists of three major parts: a cylindrical body, a sliding short, and a tuning probe.

The microwave cavity is used to produce the necessary electromagnetic fields to maintain a plasma. The cavity body (Figures 2.2

Quartz Tube Assembly

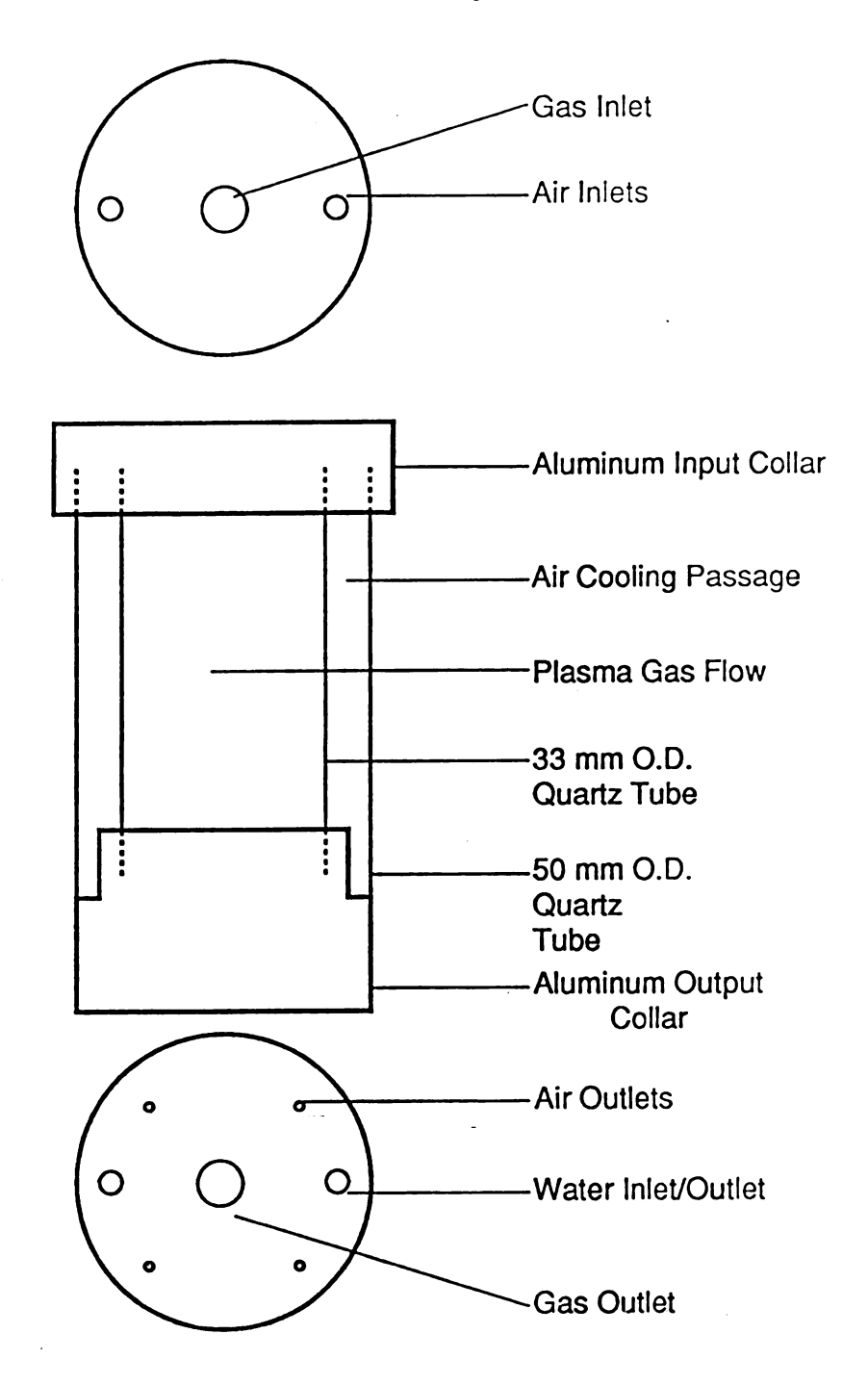


Figure 2.1 Quartz Tube Assembly

Cross Section of Microwave Cavity Applicator

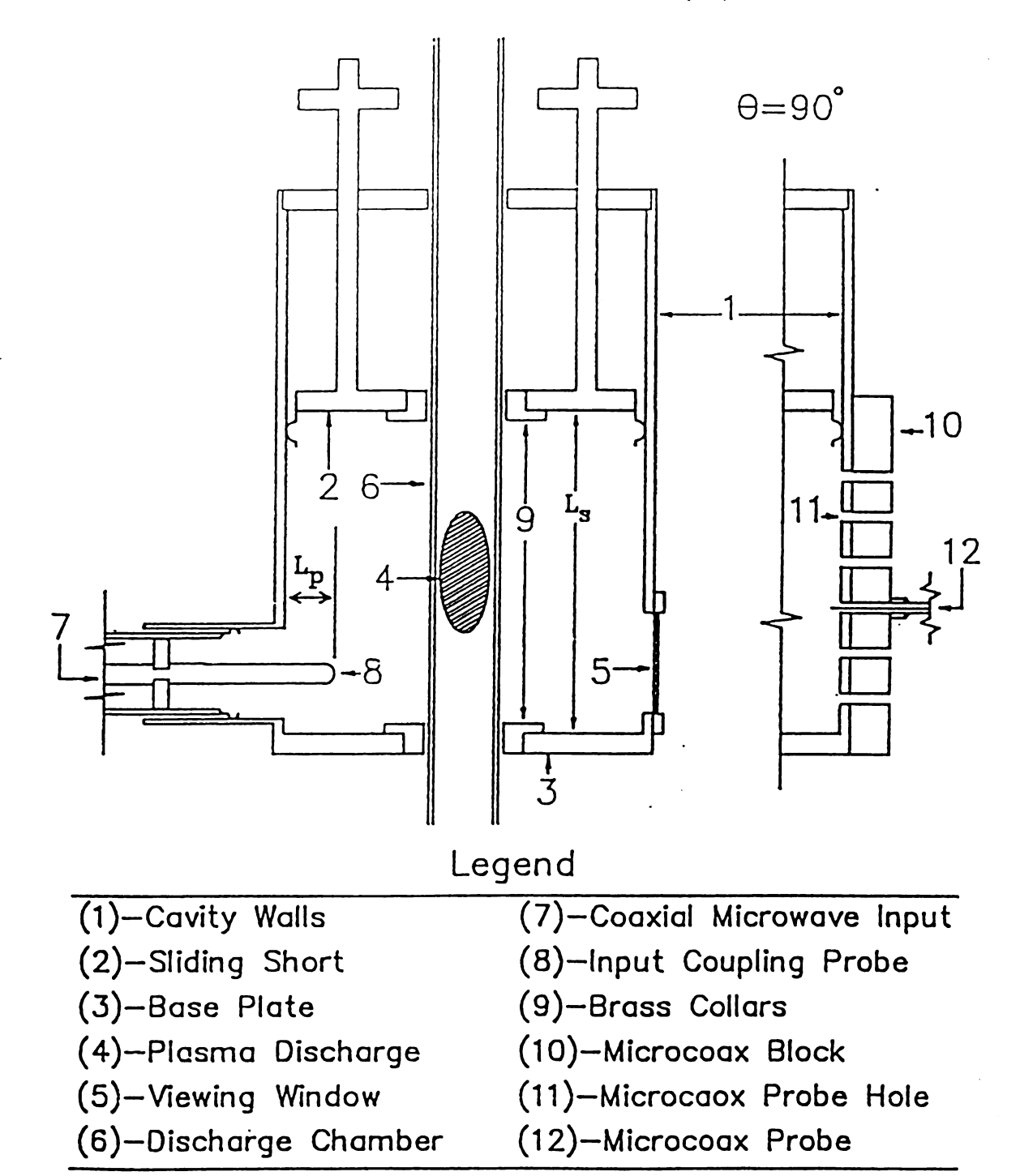


Figure 2.2 Cross Section of Cavity Applicator
Reproduced with permission from S. Whitehair

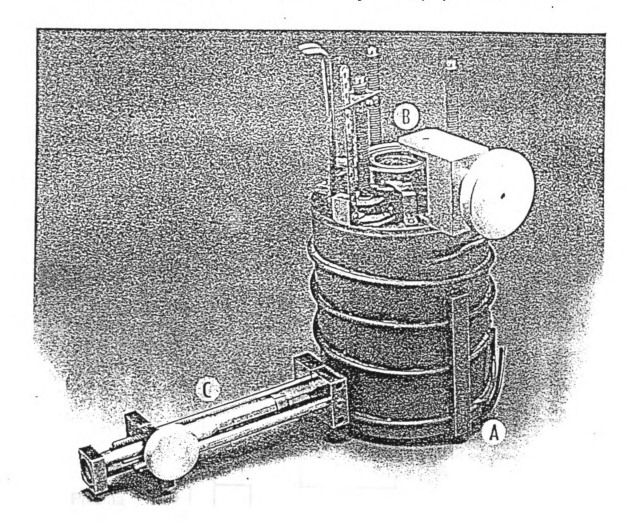
and 2.3) is made from a 17.8 cm I.D. brass pipe. Attached to the cavity is a tuning probe and a sliding short which can be adjusted so that the reflected power from the cavity is at a minimum and a resonant mode is attained. A resonant mode represents an eigenvalue of the solution to Maxwell's equations. For these experiments the TM_{012} and TM_{011} resonant modes are used.

The sliding short is a brass disk with finger stock on the outside edges so that electrical contact is made with the cavity body. To change the resonance length, the short is pushed or pulled inside the cavity body. The movement of the short allows the cavity length to vary from 6 to 16 cm (Whitehair [1986]). Attached near the bottom of the cavity body is the tuning probe. The tuning probe is an antenna which is pushed into the cavity to input microwave power. Movement of the tuning probe and the short is necessary during the tuning of the cavity to produce a plasma by allowing maximum transfer of power to the discharge. The plasma discharge can be seen through two copper screen windows located at 90° angles from the tuning probe.

2.3 Flow Systems

A schematic diagram of the flow system is contained in Figure 2.4. Flows of 99.99% pure helium and nitrogen are regulated using a back pressure regulator and a 3/4 in. valve in front of the vacuum pump. For no-flow experiments, the valve is opened just enough to fill the quartz tube with gas at the needed pressure and then closed off during the experiment. The pressure of the plasma chamber is measured using a Heise gauge with a range from 1-1600 torr. Although

Picture of Assembled Microwave Cavity Applicator



Legend

- (A) Brass Microwave Cavity Body
 (note microcoax block in lower corner)
- (B) Sliding Short Actuator
- (C) Tuning Probe Actuator

Figure 2.3 Picture of Assembled Microwave Cavity Applicator Reproduced with permission from S. Whitehair

Gas Flow System

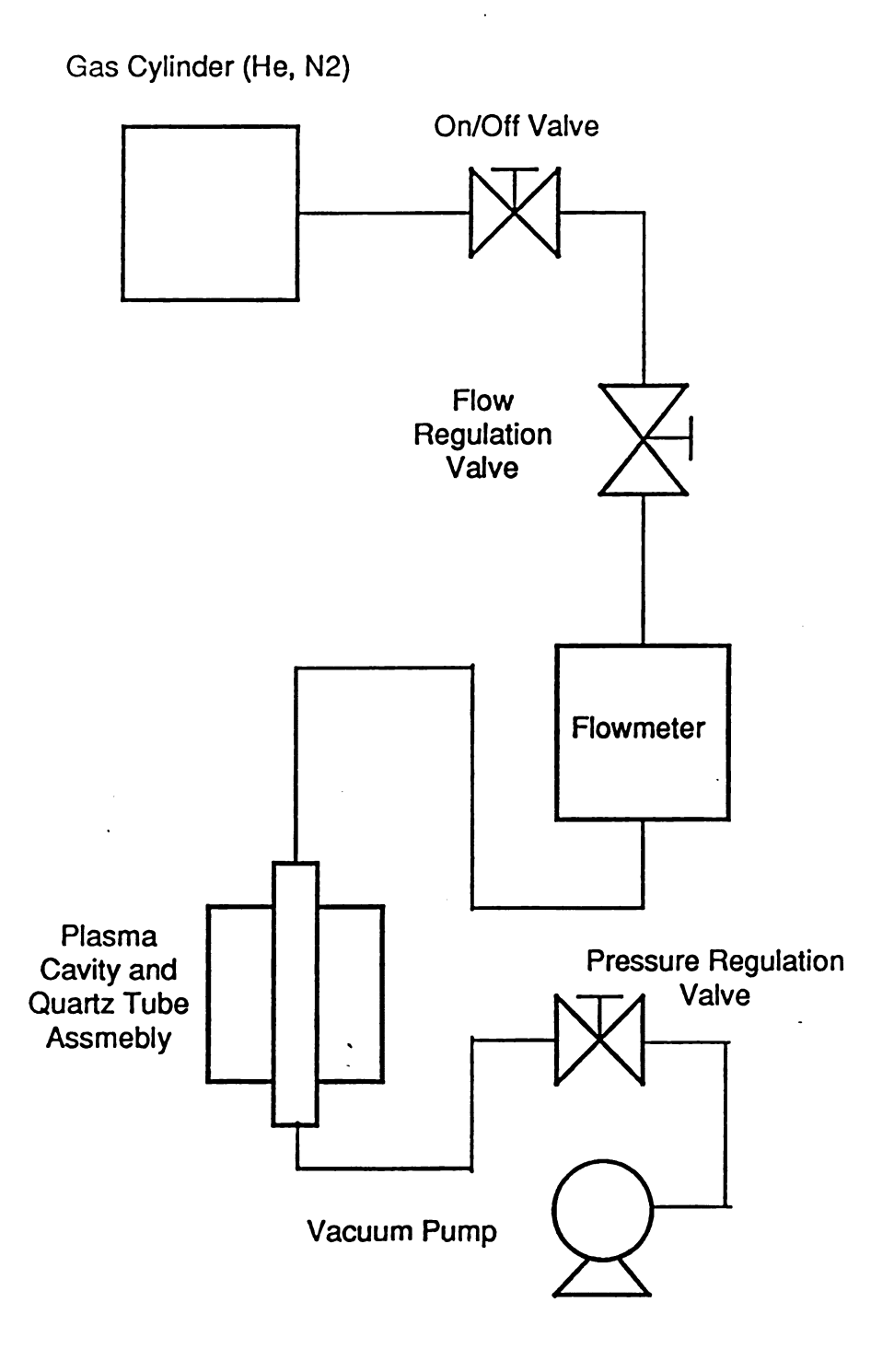


Figure 2.4 Gas Flow System

this flow system has a maximum flow rate of 7000 sccm due to the metering system, most experiments are run at lower flow rates because of plasma instabilities caused by high flow rates at 250 W microwave input power levels.

The plasma chamber is cooled by air flowing through a second quartz tube with an outer diameter of 50 mm. The air flow rate needed to sufficiently cool the plasma chamber in this experiment is 2.0 scfm. Further cooling of the exhaust gas is accomplished by a water cooled collar which seals the ends of the plasma chamber and the air cooling tube. Water cooling of the exhaust collar is done so that the hot exhaust gases will not destroy any seals inside the vacuum pump or decompose the epoxy bond between the collar and the quartz flow tubes.

The resonance cavity and the sliding short have copper tubing soldered onto them for water cooling. This water cooling is regulated separately from the water cooling of the aluminum collars so that water will not condense inside the cavity and change its electromagnetic field characteristics.

2.4 Microwave System

A schematic diagram of the microwave system is contained in Figure 2.5. A Micro-Now Model 420B1 Microwave Power Oscillator is used to send 0 - 400 W of power at a fixed frequency of 2.45 GHz to the cavity input probe. Although the oscillator has a maximum power rating of 500 W, losses from the microwave cable, circulator, and bidirectional coupler cause the power to drop to 400 W maximum power by the time it reaches the cavity. Once the power reaches the input

Microwave System

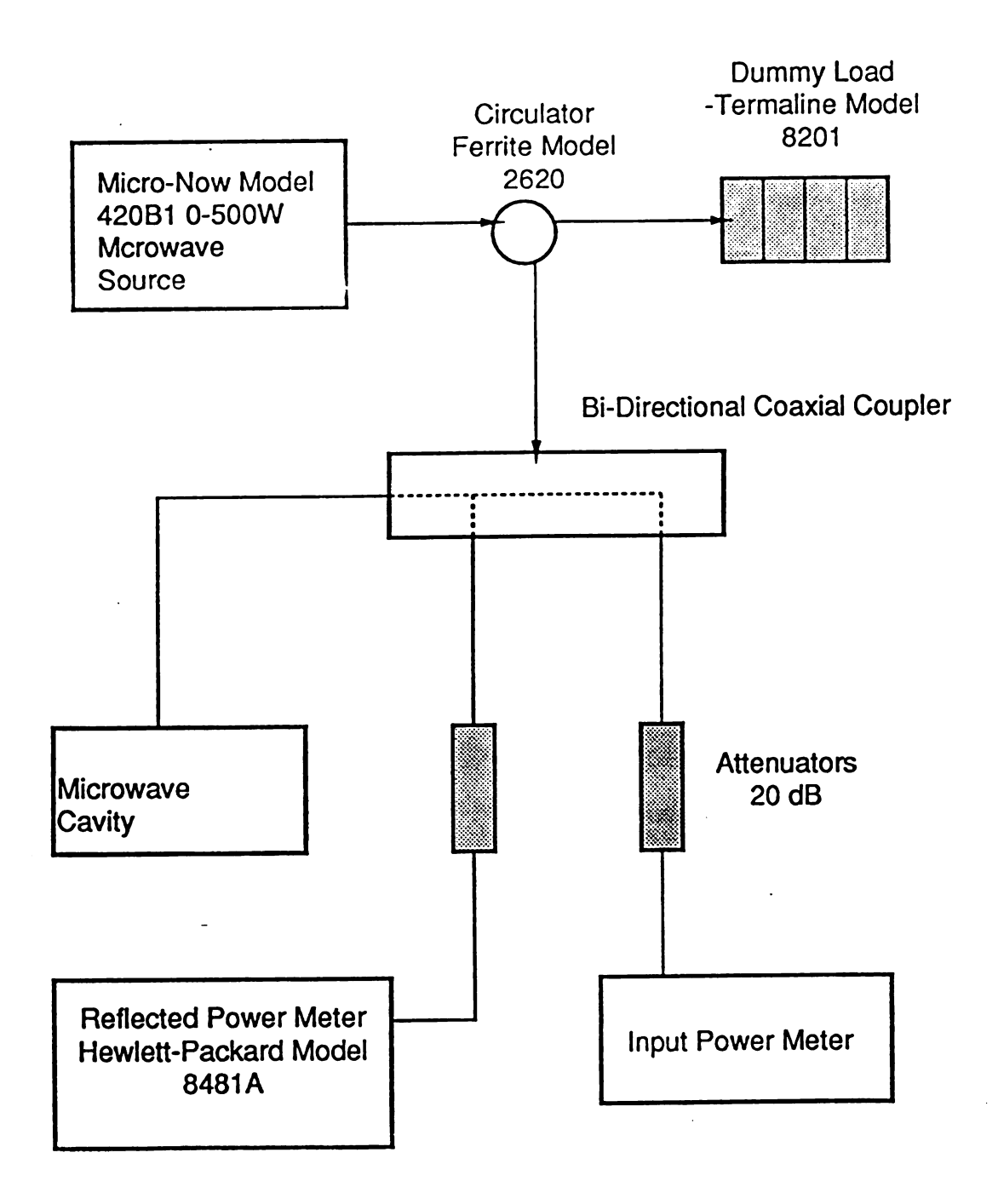


Figure 2.5 Microwave System

probe, it is electromagnetically coupled into the cavity.

The microwave oscillator is connected to a Ferrite Model 2620 500 W circulator. The circulator provides at least 40 dB of isolation between the incident and reflected power (Whitehair [1986]). The circulator serves two purposes; to protect the magnetron in the oscillator from reflected signals, and to increase the accuracy of the power measurements. The circulator is connected to a 500 W Termaline Model 8201 dummy load, which absorbs the reflected power, and a bidirectional coaxial coupler. The coupler allows the input and reflected power levels to be monitored through 20 dB attenuators attached to Hewlett Packard 8431A Power Meters. After the coaxial coupler, the microwave radiation is sent to the cavity.

Chapter III

Emission Spectroscopy Measurements

3.1 Introduction

The goals of emission spectroscopy measurements are to a) gather atomic-electronic temperatures in helium and nitrogen high pressure (200 to 1000 torr) plasmas and b) study the effect of pressure on the atomic-electronic states within these plasmas. In a previous investigation (Chapman [1986]), atomic-electronic temperatures in a low pressure (0.7-10 torr) hydrogen plasma were determined from measurements of the Balmer line series, and a strong dependence of the calculated temperature on the selection of lines was noted. This dependence was attributed to a non-equilibrium distribution of the electronic states and appeared to decrease as the plasma pressure increased.

For an atomic electronic transition the equation for the measured line intensity can be written as

$$\ln \frac{I_{\text{meas }nm}}{R_{\lambda} g_{\text{n}} A_{\text{nm}}} = \text{Const.} - \frac{E_{\text{n}}}{k T_{\text{elec}}}$$

where

 I_{meas} - measured emission line intensity

 λ_{nm} - wavelength of the transition

E - energy of the initial electronic state

T elec - atomic electronic temperature

 $\mathbf{g}_{\mathbf{n}}$ - degeneracy of the initial state of transition

 A_{nm} - transition probability

R_{λ} - spectral response function

Table 3.1 summarizes the necessary data needed to calculate the atomicelectronic temperatures for the four emission lines chosen for nitrogen and helium (Tourin [1966]). These lines were chosen because of their relatively high intensities as listed in the CRC Handbook of Chemistry and Physics [1984].

3.2 Spectroscopy System

A diagram of the spectroscopy system is given in Figure 3.1. The emission of helium and nitrogen plasmas is measured by a 0.5 m McPherson Model 216.5 Monochromator with a Harrison Model 6110A DC Power Supply. For the atomic transitions, a diffraction grating blazed at 3000 Å with 1200 grooves/mm is used. The output from the monochromator is processed using a Keithley Model 616 PMT attached to a Honeywell Model 196 Dual Pen Chart Recorder. The monochromator is positioned approximately 60 cm from the plasma with the use of an optical lens system. A low pass filter made with a 2000 μ F 10 V capacitor and a 1 K Ω 1/2 W resistor is used between the electrometer and the chart recorder to get minimize any high frequency noise.

The lens system consists of two 25 cm focal length glass lenses which concentrate the light into the monochromator. The decision to use the lens system is based on research conducted by Brake [1983] and Hopwood [1986] in which it was concluded that better resolution of atomic lines was achieved with this system. In this investigation, the monochromator is placed to measure the most intense emission.

Table 3.1. Transition Probabilities, Wavelength of Transition, Energies and Degeneracies of the Atomic Electronic Levels for Helium and Nitrogen Gases.

| Level | A _{nm} (sec ⁻¹) | λ _{nm} (Å) | E _n (J) | g _n | | |
|----------|--------------------------------------|---------------------|----------------------------|----------------|--|--|
| Nitrogen | | | | | | |
| n | 4.000 x 10 ⁶ | 4109.95 | 2.1959×10^{-18} | 6 | | |
| n | 1.580 x 10 ⁶ | 4935.12 | 2.1152 x 10 ⁻¹⁸ | 2 | | |
| n+1 | 2.820 x 10 ⁵ | 5281.20 | 2.1263 x 10 ⁻¹⁸ | 6 | | |
| n+2 | 6.400 x 10 ⁵ | 5829.54 | 2.2384 x 10 ⁻¹⁸ | 6 | | |
| Helium | | | | | | |
| n | 9.478 x 10 ⁶ | 3888.65 | 3.6862 x 10 ⁻¹⁸ | 9 | | |
| n+1 | 1.338 x 10 ⁷ | 5015.68 | 3.6690×10^{-18} | 3 | | |
| n+2 | 1.980 x 10 ⁷ | 4921.9 | 3.8030 x 10 ⁻¹⁸ | 5 | | |
| n+2 | 2.460 x 10 ⁷ | 4471.48 | 3.8030×10^{-18} | 15 | | |
| | | | | | | |

Emission Spectroscopy System

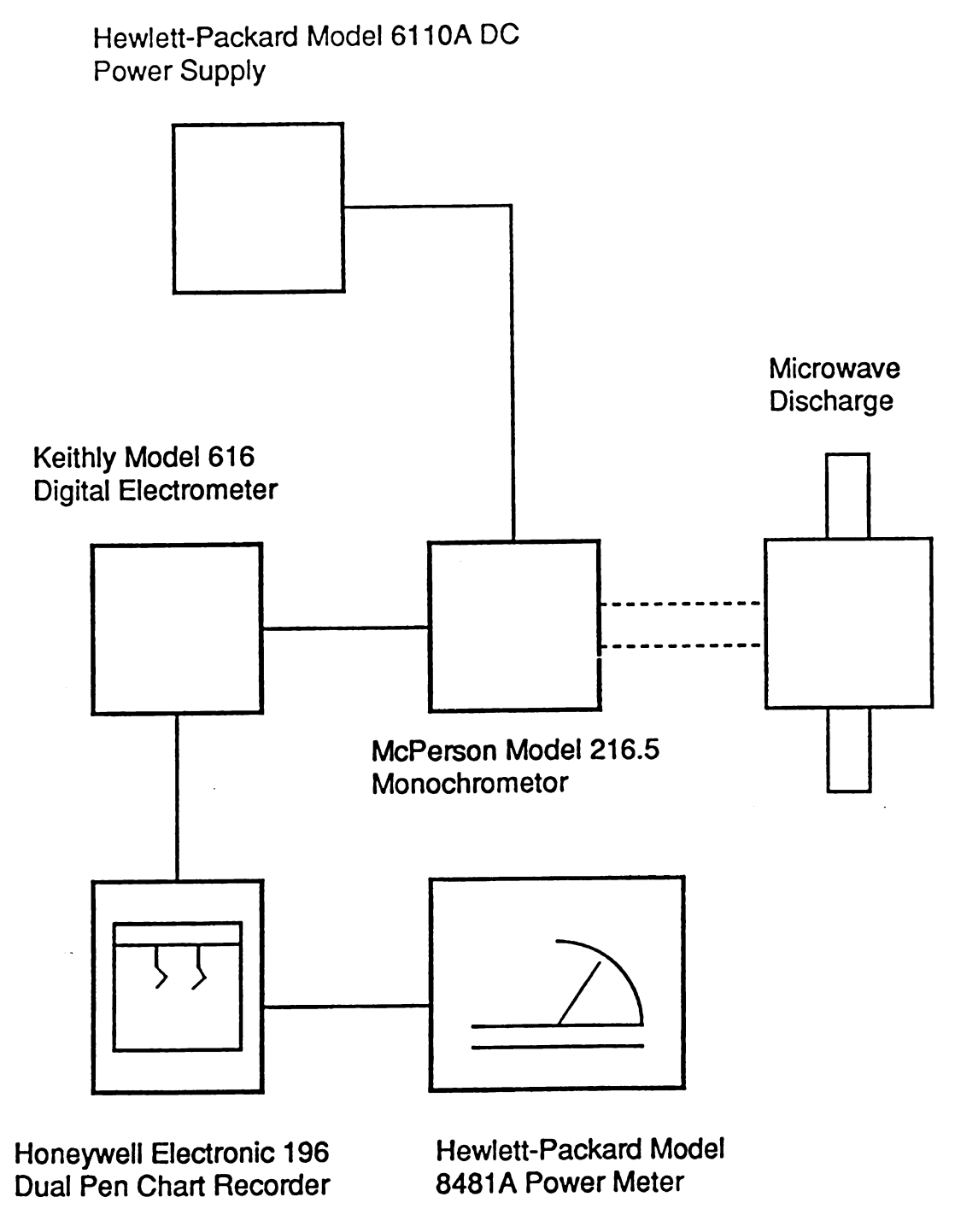


Figure 3.1 Emission Spectroscopy System

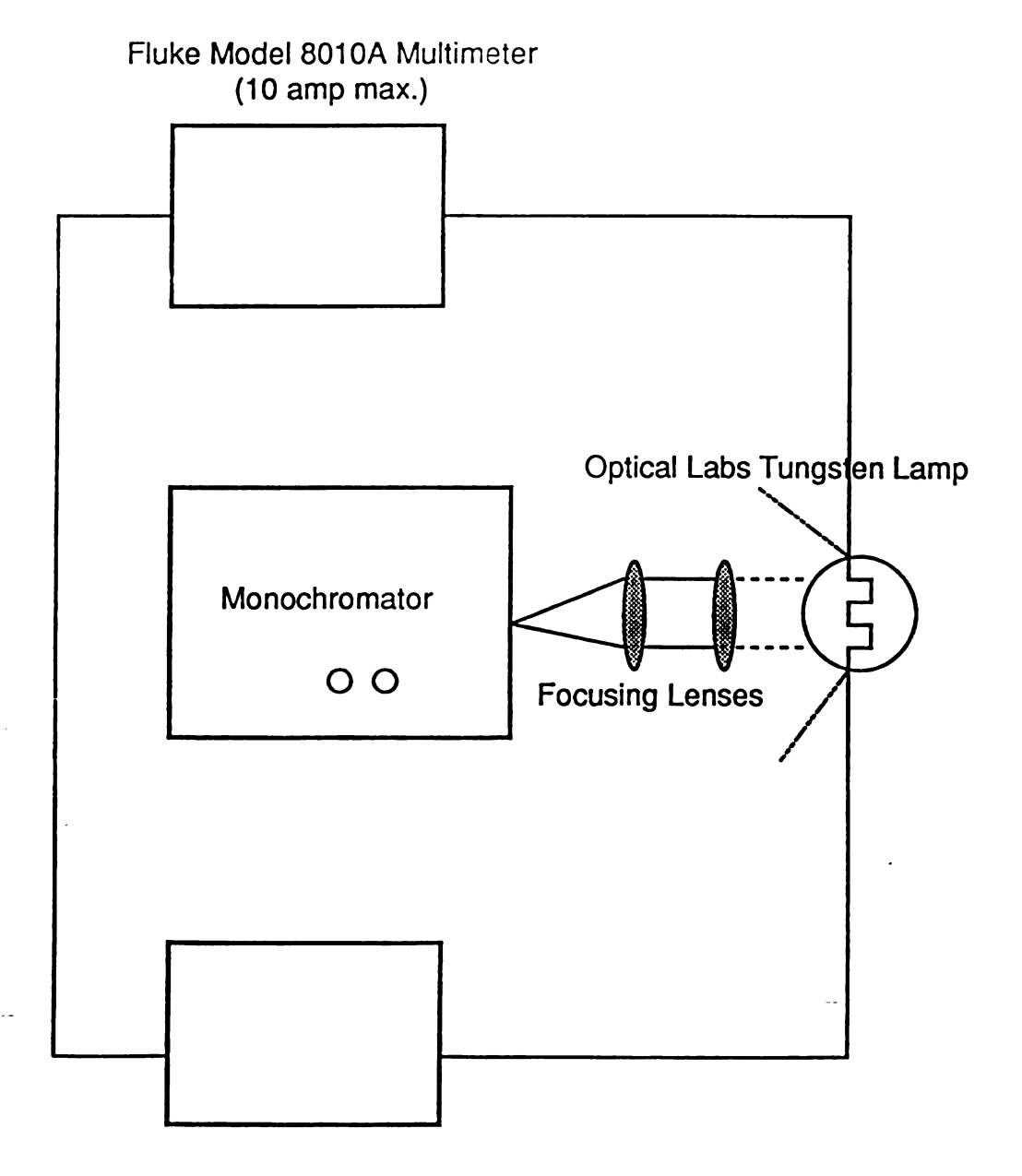
The spectral response function for this experimental configuration is calibrated using a 45 watt quartz-halogen tungsten coiled-coil filament lamp. The lamp is operated at 6.5 amperes DC delivered by a Hewlett-Packard Model 6282A DC Power Supply through a Fluke Model 8010A Digital Multimeter (Figure 3.2). The spectrum obtained from the lamp measurements is checked against the calibration standard from the lamp to get the response function at the desired wavelengths.

3.3 Experimental Procedures and Operating Conditions

The experimental procedure for calculating electronic temperatures involves four basic steps, starting a plasma, finding transition lines of measurable intensity, finding the intensity of those lines, and calculating the electronic temperature from those intensity measurements. Of these steps, the second one is most difficult. Finding lines of measurable intensity is difficult because the spectrometer must be set up with the proper parameters (slit width, scan speed, etc.) so that the readings give the best representation of the actual spectra. Although steps three and four seem simple in comparison to step two, other problems can still cause large error in the electronic temperature calculation.

The first step is to create a plasma. The experimental set-up for creating a plasma is discussed in Chapter 2 and a complete listing of the steps necessary for creating a plasma can be found in the Appendix. To start a plasma, the plasma containment chamber should be air cooled and evacuated below 10 torr with the working gas flow being

Spectral Response Configuration



Hewlett-Packard Model 6282A DC Power Supply

Figure 3.2 Spectral Response Configuration

no greater than 60 sccm. Once the water cooling of the cavity is begun, the microwave power can be coupled into the cavity. Strong resonant fields within the cavity break down the gas and form the plasma.

Before attempting a scan of the plasma spectra (Step 2), it is important to know the transitions possible in the working gas. The CRC Handbook of Chemistry and Physics [1984] has tables of possible tansitions and their relative intensities for many different gases. This table is also useful for obtaining the degeneracies of the initial states and transition probabilities needed in the electronic temperature equation. Even though the relative intensities given in the CRC Handbook do not represent the actual intensities present in a microwave plasma, they provide a starting point for finding the desired transitions. The last phase of this step includes both finding the best slit width and scan speeds and taking preliminary scans of the total wavelength region to be studied. The optimum slit width and scanning speed are found by finding an intense peak and using successive iterations of these parameters until a Maxwellian distribution type peak is attained. Once the slit width and scan speed are known, a scan of the desired wavelength region is taken so that observable transitions can be identified. These scans should be done at both maximum and minimum operating pressures because the relative intensities of the peaks vary with pressure.

During the measurement of peak intensities (Step 3), two experimental techniques facilitate the taking of accurate and reproducible data. The first experimental technique involves scanning

from 5 Å above to 5 Å below the desired transition. Using this technique allows more measurements to be taken under consistent plasma conditions. The second experimental technique involves monitoring the input power level to the plasma to ensure that the transition intensities remain constant. If the power level changes during a peak measurement by even a slight amount, the peak height can be drastically affected. Power level effects can cause up to a 20% change in the intensity of a peak.

Once the transition intensities are known, they can be easily inserted into the electronic temperature equation previously discussed in Section 3.1 (Step 4). To reduce the amount of error in calculating the electronic temperatures, the use of as many intensity measurements as possible is necessary. Although these steps do not cover all the aspects and possible problems that can occur during an experiment, they provide guidelines for taking electronic temperature measurements.

3.4 Discussion of Experimental Results

Unfortunately, the electronic temperatures for nitrogen could not be calculated because the vibrational transition lines are so large that they hide any electronic transitions that might be visible.

Brake and Hopwood also noted this difficulty in their study (Hopwood et al. [1986]). At first, it was thought that a good estimate could be made on the height of the transitions, but this was soon abandoned because of the uncertainty as to which lines were being studied.

Helium is a monatomic gas which has no vibrational lines to hinder

experimental measurements.

In general, the electronic temperatures for a helium gas plasma increase with an increase of pressure (Figure 3.3). It can be noted, however, that the increase of electronic temperature with increasing pressure tends to level off between 600 and 800 torr. These results are consistent with those measured by Hopwood and Brake. At an input power of 246 W, the electronic temperatures increased from 4347 K at 200 torr to 5344 K at 800 torr with a He flow rate of 60 sccm.

Initially, the electronic temperature versus pressure measurements were to be taken in no flow conditions (steady state discharge), but the hydrogen and nitrogen impurities in the gas made the spectroscopic measurements difficult to interpret. At an input power of 172 W, the electronic temperatures increased from 3600 K at 200 torr to 4950 K at 700 torr. It was impossible to sustain a helium plasma above 700 torr with an input power of 172 W. The maximum pressure for a 246 W helium plasma was found to be 1040 torr.

It is important to note the difference between electronic temperature and <u>electron</u> temperature. The atomic-electronic temperature (electronic temperature) is the temperature of the "bound" electrons and is often referred to as the excitation temperature. If the electronic states are in equilibrium with the free electron gas, the electronic temperature is the same as the electron temperature (Brake [1983]). The equilibrium of the electronic states depends on the collision frequency and electron density. At low pressures (0-600 torr) the electronic temperature is not the same as the electron temperature because there are not enough collisions between the free

Electronic Temperatures vs. Pressure Helium Plasmas

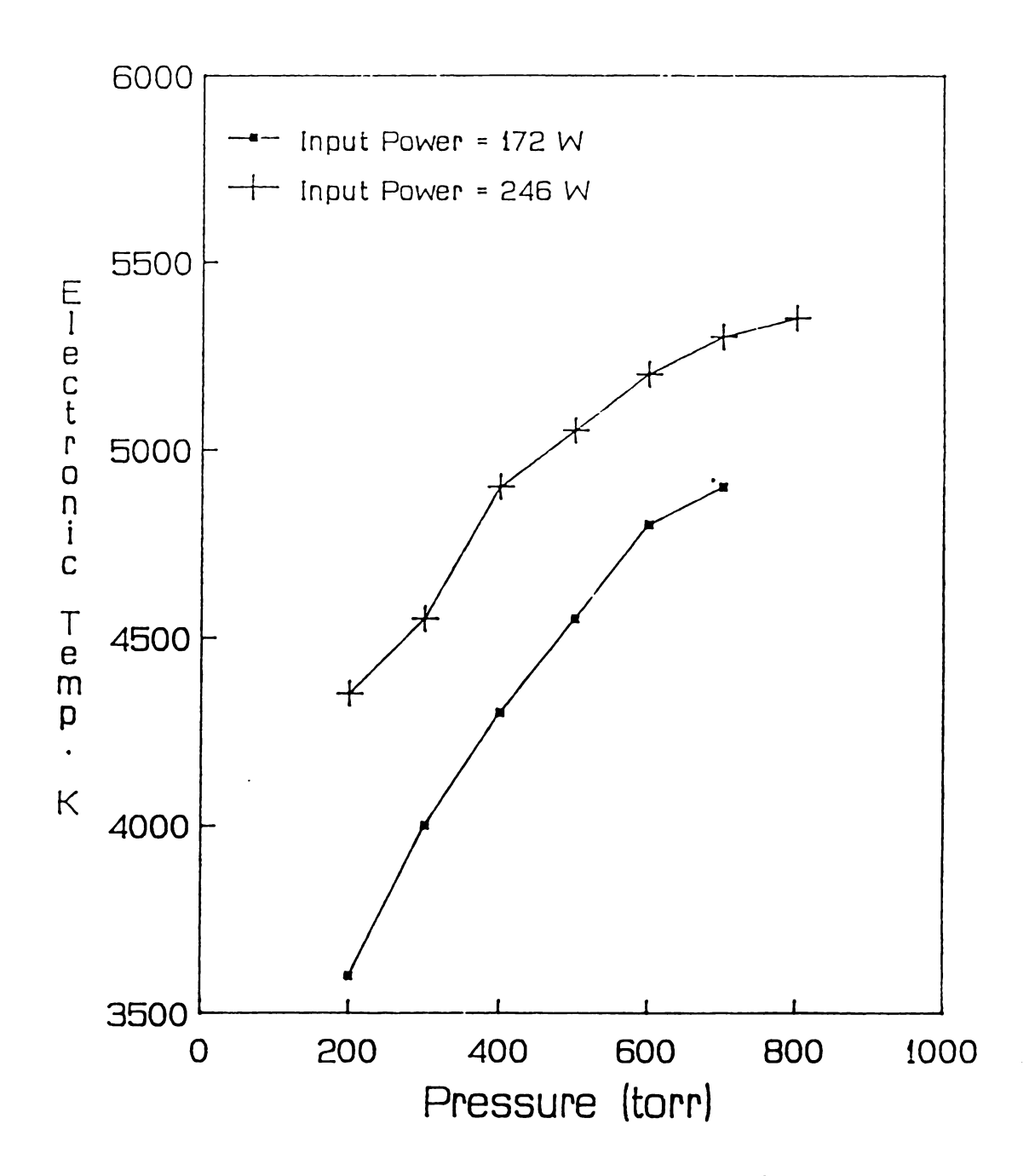


Figure 3.3 Electronic Temperatures versus Pressure

electron gas and the electronic states. If one were to plot the electron temperature versus pressure, the electron temperature would "decrease" with an increase of pressure until it reached equilibrium with the atomic electronic states.

From the plot of electronic temperature versus pressure and power (Figure 3.3), the electronic temperatures are shown to increase with pressure and microwave input power. Although electronic temperature is a good estimate of free "electron" temperature, the electronic temperature does not vary with pressure in the same manner as the electron temperature. An increase in pressure causes a decrease in the electron temperature due to a greater frequency of energy exchange between the electrons, ions, and neutrals (Hellund [1961]). However, in this investigation, the electronic temperature is observed to increase with an increase in plasma pressure. An explanation for the discrepancy between electron and electronic temperature behavior, is that the plasma does not satisfy the local thermodynamic equilibrium (LTE) condition. According to Bekefi [1976], in his book "Principles of Laser Plasmas," LTE occurs if the electron density satisfies the following equations:

Ne
$$\geq 1.4 \times 10^{14} T_e^{0.5} \chi(m,n) cm^{-3}$$

or

Ne
$$\geq$$
 (2 x 10¹⁸ Z⁶ T_e^{0.5}) / (n^{8.5}) cm⁻³

where n =the electron level (n=3)

Ne = the electron density (cm^{-3})

 T_{e} - the electron temperature (eV)

 χ - the electron ionization energy (eV)

Z = the ionic charge

Using information for helium n=3 level electrons, the electron density must be greater than or equal to $7 \times 10^{13} \, \mathrm{cm}^{-3}$ for the system to be in LTE. Helium plasmas in the 200 - 1000 torr pressure range, with microwave input powers up to 400 W, do not satisfy this condition. Hopwood and Brake [1986] reported electron densities on the order of $10^{12} \, \mathrm{cm}^{-3}$ for helium plasmas produced under these conditions. Therefore, one must be careful when assuming that the electronic temperature is equal to the electron temperature in a high pressure plasma (>300 torr). Even though the microwave plasmas produced in this study have a low electron density and the electronic temperature does not equal the electron temperature, the electronic temperature measurement is important because it gives an idea of the approximate electron temperature.

During the investigation of electronic temperatures, it was noted that as the pressure was increased, the relative population of some excited states changed. The diffraction grating available for the monochromator limited this study of line intensities in the 3000 to 5500 Å range. Figure 3.4 shows the energy level diagram for helium. The most intense atomic electronic line at all pressures (200-800 torr) was the 5016 Å line which signifies the helium electron transition from the 3¹P to the 2¹S level. The intensity of the second most populated state of helium electron transitions changes with pressure. At 200 torr, the 3889 Å line is more intense than the 4471 Å line, and from 500-600 torr, the lines were of the same intensity.

Helium Energy Level Diagram

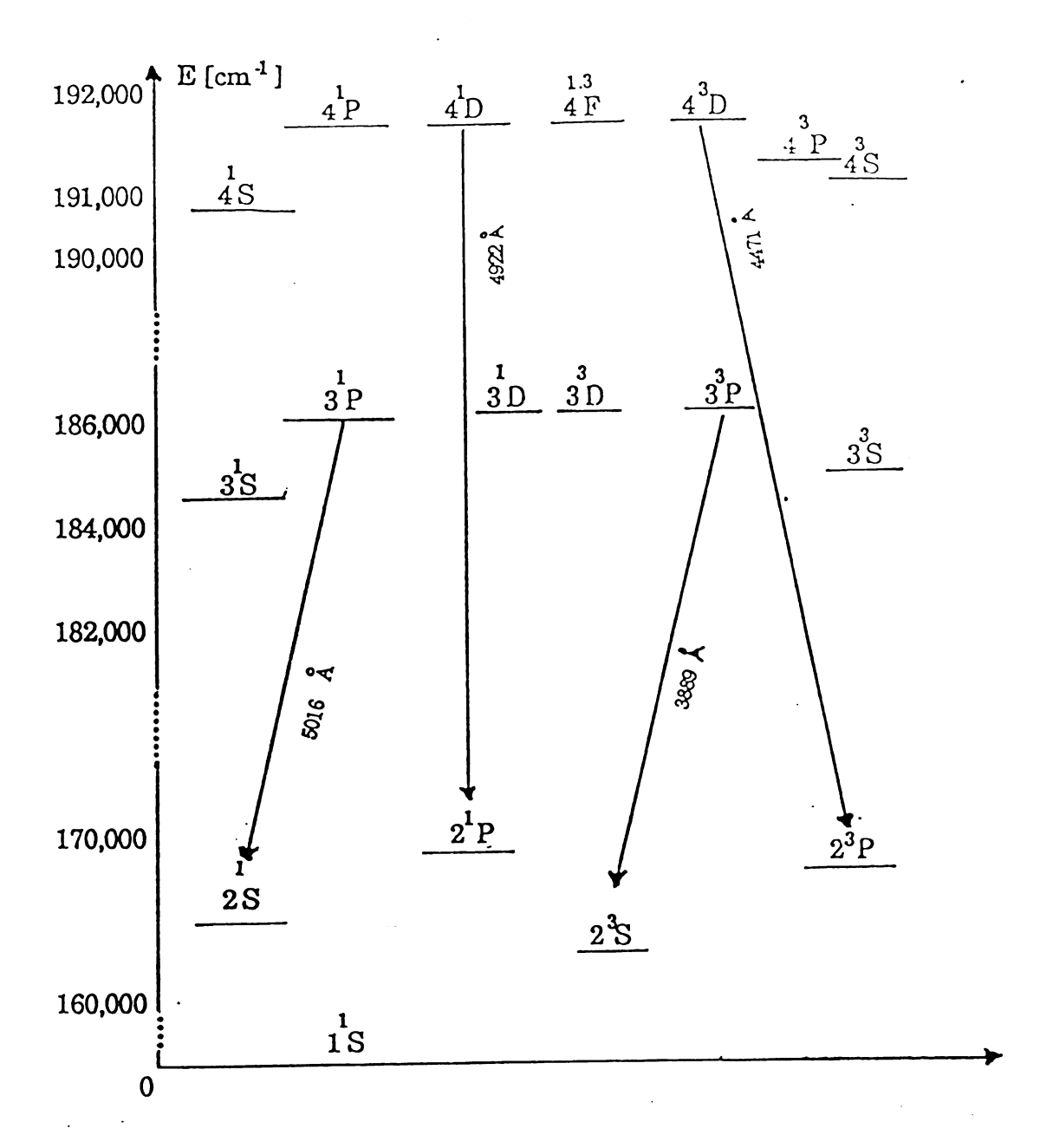


Figure 3.4 Energy-Level Diagram of Helium

As the pressure was increased further, the 4471 Å line became stronger than the 3889 Å line by a factor of 1.4. The 4471 Å line signifies the electron transition from the 4^3D level to the 2^3P level, and the 3889 Å line signifies the electron transition from the 3^3P level to the 2^3S level. The lowest intensity line that could measured with sufficient accuracy was the 4922 Å line which signifies the electron transition from the 4^3D level to the 2^3P level. The 4922 Å line is 5 times smaller than the 5016 Å line for all pressures. The only other helium electron transition that was observed was the 5047 Å line which was detected at pressures above 600 torr.

Impurities in the helium gas and leakage of the flow system caused other lines to be observed in this study. At 3063 Å, the OH impurity was discovered, and at 3360 Å \Rightarrow the NH spectra was evident. The most intense impurity lines were the hydrogen lines. The H $_{\beta}$ line could always be counted on to peg the chart recorder needle when searching for helium lines, and the H $_{\gamma}$ line was another common nonhelium line. The impurity of the plasma can be noted visually at low pressures by the pinkish color of the discharge instead of the yellow discharge color which was reported in French studies. The pinkish color may be attributed to air leakage into the system because the plasma became clear at high pressures (above 1 atm).

The objective of the next experiment was to measure electronic temperatures as a function of helium flow rate (Figure 3.5). At 600 torr and above, the electronic temperature should be close to the electron temperature. Results for the 600 torr experiment are inconclusive in the 280-840 sccm flow rate range because the

Electronic Temperatures vs. Flow Rate Helium Plasmas

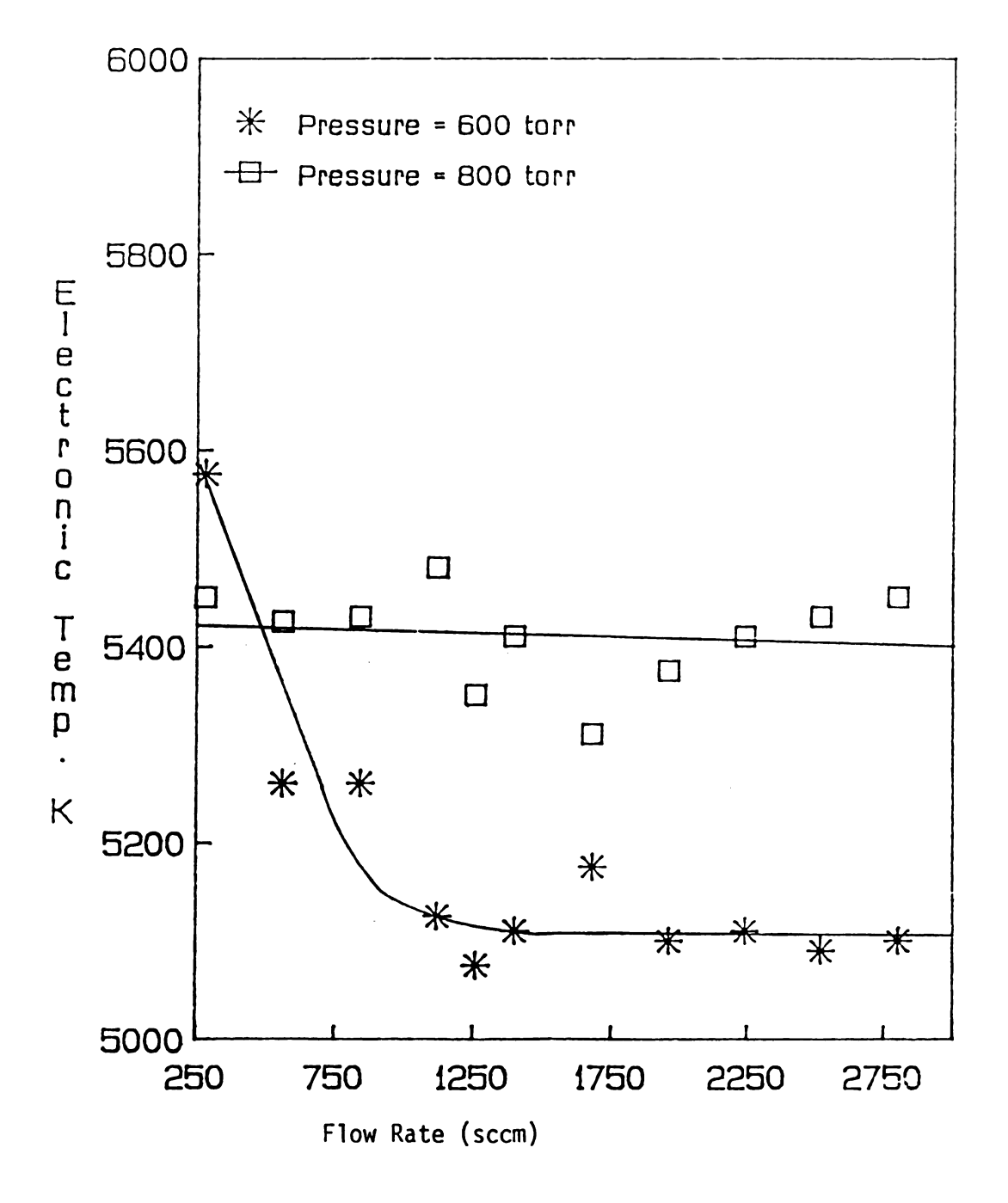


Figure 3.5 Electronic Temperatures versus Flow Rate

characteristics of this curve could not be duplicated at the higher pressure. It can, however, be concluded that the electron temperature is not affected to a high degree by the plasma gas flow rate. Although the 800 torr graph tends to have a negative slope with increasing flow rate, the data is not precise enough to make a definite statement. In summary, changing the helium flow rate from 840 to 2500 sccm has little or no effect on the electron temperatures of plasmas in the pressure range of 600-800 torr.

Since it is believed that the wall recombinations in the plasma region are affected by the boundary condition at the quartz tube wall, a third experiment was undertaken to determine the electron temperatures as a function of the cooling air flow rate (Figure 3.6).

Because the error in calculating electron temperatures (Brake [1983]) was greater than the negative slope of the line of best fit through the data, it must be concluded that the cooling air flow rate has no effect on the electron temperature.

3.5 Summary

It is commonly assumed that free and bound electrons are in local thermodynamic equilibrium in a plasma environment. Classical theory [Hellund, 1961] predicts that as pressure increases, free electron temperature decreases. However, measurements in this study show that the bound electron temperature increases with an increase in pressure. This apparent discrepancy is due to local thermodynamic equilibrium not being attained between the free and bound electrons in the operating conditions of this study.

Electronic Temp. vs. Coolant Flow Rate Helium Plasmas

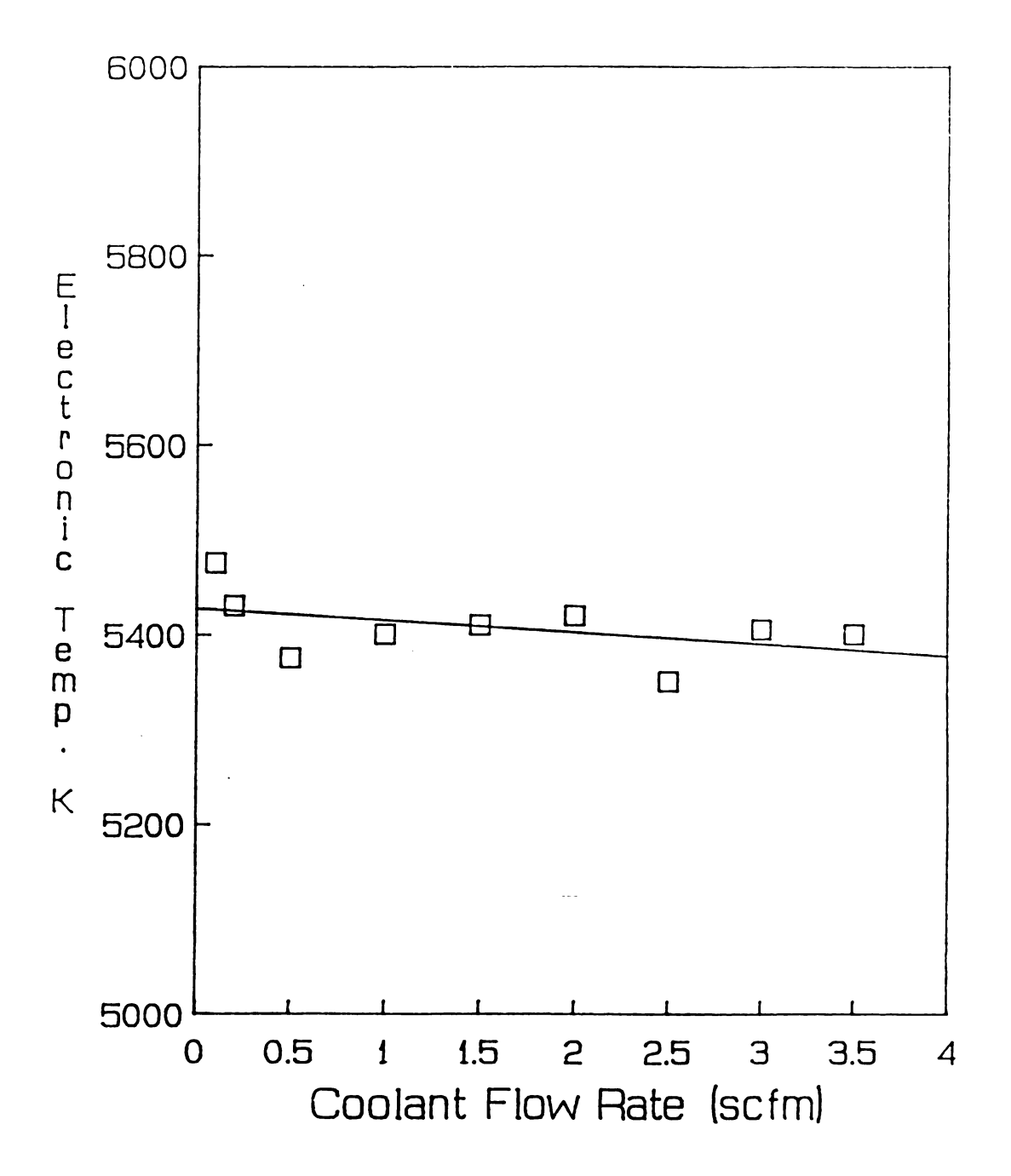


Figure 3.6 Electronic Temperatures versus Coolant Flow

Free electron temperatures for helium plasmas are found to be affected by pressure and microwave power input. At 200 torr, these temperatures are 3600 K for a 172 W input and 4400 K for a 246 W input. As the pressure is raised from 200 to 800 torr, these temperatures increase by 1000 K. At these input power levels and pressures, the electronic temperature does not equal the electron temperature due to local thermodynamic equilibrium constraints. The electronic temperatures are not affected by cooling air and helium flow rates in the ranges of 0 to 4 scfm and 280 to 2520 sccm, respectively. The only case where helium flow rate has an affect on the electronic temperatures is at 600 torr. With a flow rate change of 280 to 1000 sccm, the electronic temperature changes from 5500 K to 5100 K.

Chapter IV

Plasma Diameter and Volume Measurements

4.1 Introduction

One aspect of a microwave induced plasma is its change in size and shape with pressure. The purpose of this study is to measure the plasma diameter and volume of 200 - 1000 torr helium and nitrogen discharges as a function of pressure. These measurements can be used in a heat transfer model of the plasma and also to help further the understanding of the chemical processes inside the plasma (Rogers [1982]). The plasma measurements are taken at pressures of 200-1000 torr and a microwave input power of 246 W under no flow conditions. No flow conditions are used so that maximum stability of the plasma is achieved. Air cooling (3.5 scfm) is used to protect the quartz tube walls from the heat generated by the plasma.

4.2 Experimental Design

Plasma dimensions are calculated from 35 mm slide pictures. The images are measured and compared with a standard grid pattern which is photographed and projected at the same distance. Although this procedure seems uncomplicated, the unsteady nature of high pressure plasmas causes many problems to arise. An example of one of the problems encountered is the migration of high pressure nitrogen plasmas from one side of the quartz tube to the other without establishing any kind of pattern.

Using a tripod, a 35 mm camera is positioned approximately one half inch from the microwave cavity window (see Figure 4.1). The pictures are taken using a 58 mm lens with a 10 mm extension.

Ektachrome 200 ISO color slide film is preferred over 400 ISO black and white print film because it provides better resolution. Each plasma is photographed using three different aperture and shutter speed settings: f4 at 1/250 s, f2.8 at 1/250 s and f2.8 at 1/500 s.

This range of settings was chosen based on Whitehair's work [1987].

4.3 Results for High Pressure Plasmas

For this experiment the best aperture and shutter speed settings are f2.8 and 1/250 s, respectively. High pressure plasmas are observed to have two distinct regions, a more intense white inner region surrounded by a diffuse colored outer region. The outer region is orange in nitrogen and a cross between maroon and purple in helium. To characterize the microwave discharges, two diameters are measured. For the purposes of this study, the two regions are considered as areas of strong and weak electromagnetic coupling, respectively. A high pressure helium plasma (400-1000 torr) has a cylindrical inner region and a diffuse dumbbell-shaped outer region. The inner region nearly fills the "waist" region of the dumbbell, and therefore the diameter of the "waist" region is taken to be the diameter of the strong coupling region. The largest diameter of the plasma is taken to be the weak coupling diameter. A high pressure nitrogen plasma (400-1000 torr) has two cylindrical regions with rounded ends. The inner and outer regions of a nitrogen plasma are separated by a color

Discharge Volume Measurement Setup

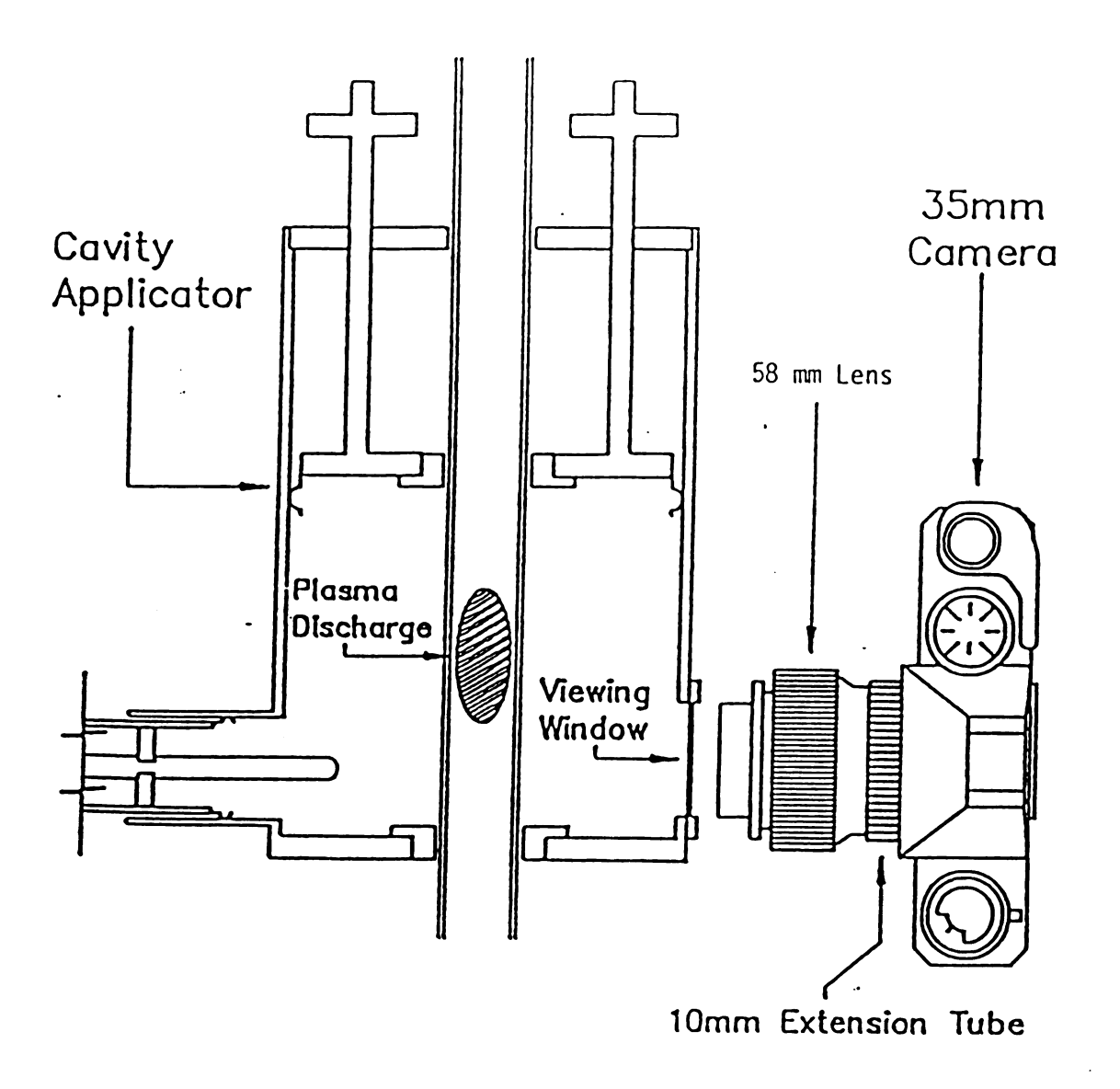


Figure 4.1 Experimental Setup for Plasma Discharge Volume and Radius Measurements

Reproduced with permission from S. Whitehair

change from white to orange.

Figures 4.2 and 4.3 show the diameters of the coupling regions as a function of pressure in helium and nitrogen, respectively. At 200 torr, the helium plasma fills the whole quartz tube and the two regions are indistinguishable. From 400-1000 torr, the difference between the diameters of the weak and strong coupling regions remains constant for helium, and decreases with increasing pressure for nitrogen. Figure 4.4 illustrates that helium plasmas change more in diameter with pressure than nitrogen plasmas.

There is a distinct change of behavior in helium plasmas as the pressure is changed from 200-300 torr. In this pressure regime, the plasma diameter decreases from the entire quartz tube diameter to about half the tube diameter. Nitrogen discharges exhibit this behavior around 100-200 torr. An explanation for the difference in pressure where this phenomenon is observed, is that nitrogen has a larger collision cross-section than helium. Thus, the probability of an ion diffusing to the wall is lower at a given pressure for nitrogen than for helium. To further support this argument, Hellund ("The Plasma State" [1961]) states that nitrogen molecules do not have a high degree of dissociation in the plasma. Therefore, not only one, but two molecules create the large collision cross section in nitrogen.

Another explanation for the difference between the pressure ranges in which this behavior is observed in helium and nitrogen discharges is due to the fact that nitrogen is a diatomic gas.

Because nitrogen is diatomic and has vibrational modes which absorb

He Plasma Diameters vs Pressure Strong and Weak Coupling Regions

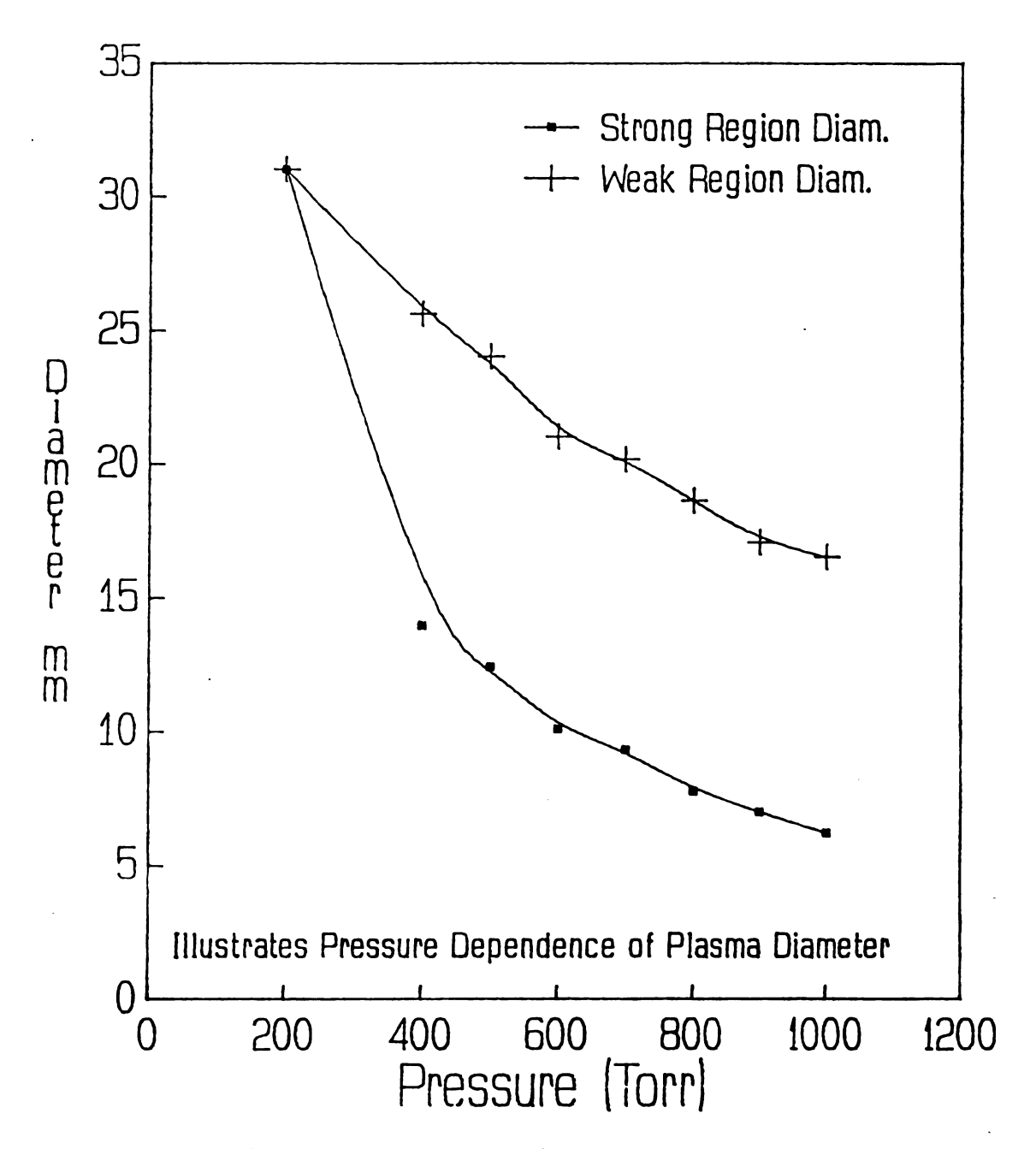


Figure 4.2 Plasma Diameters (He) versus Pressure

N2 Plasma Diameters vs Pressure Strong and Weak Coupling Regions

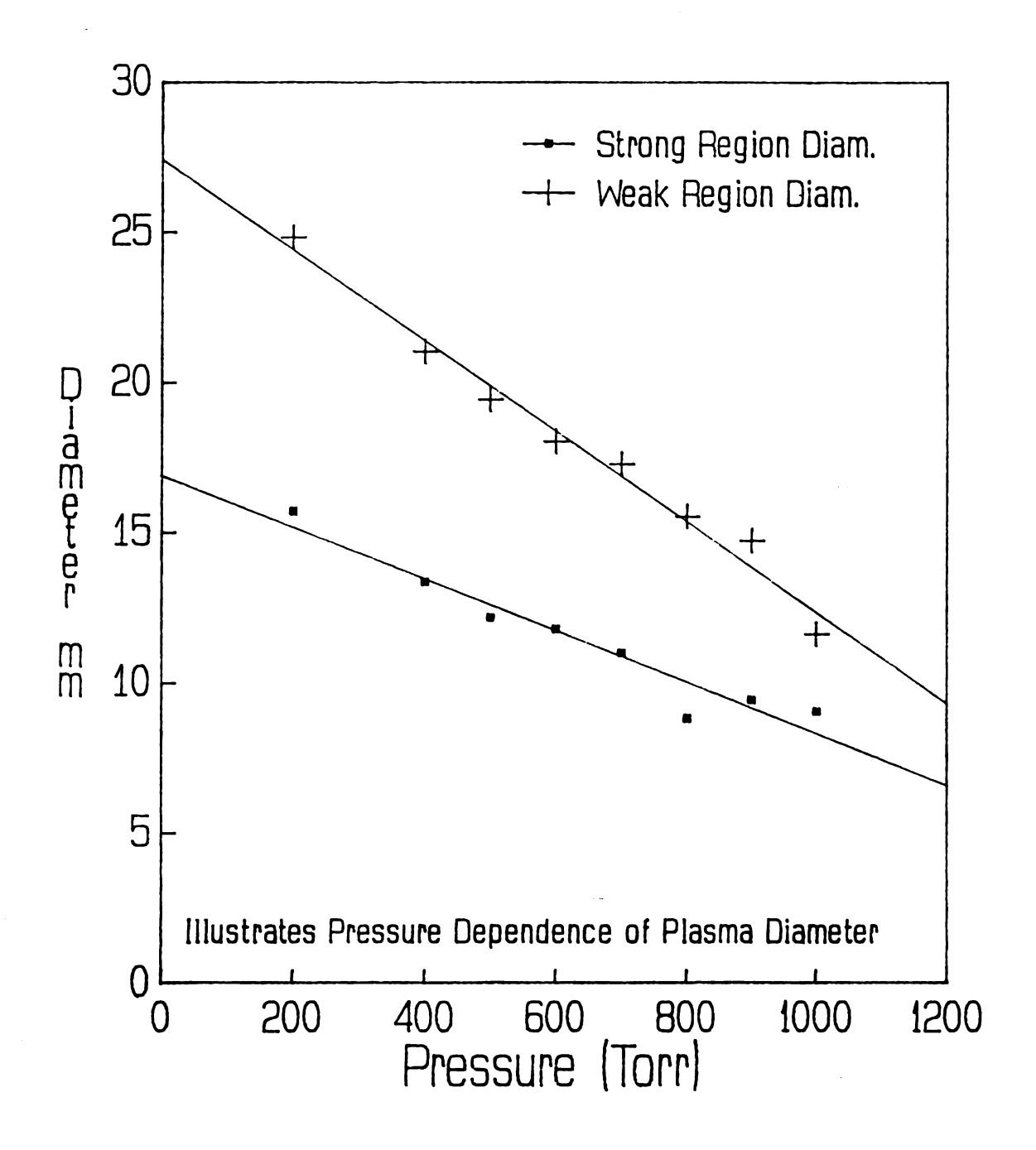


Figure 4.3 Nitrogen Plasma Diameters versus Pressure

He & N2 Plasma Diam. vs. Pressure Strong Coupling Region

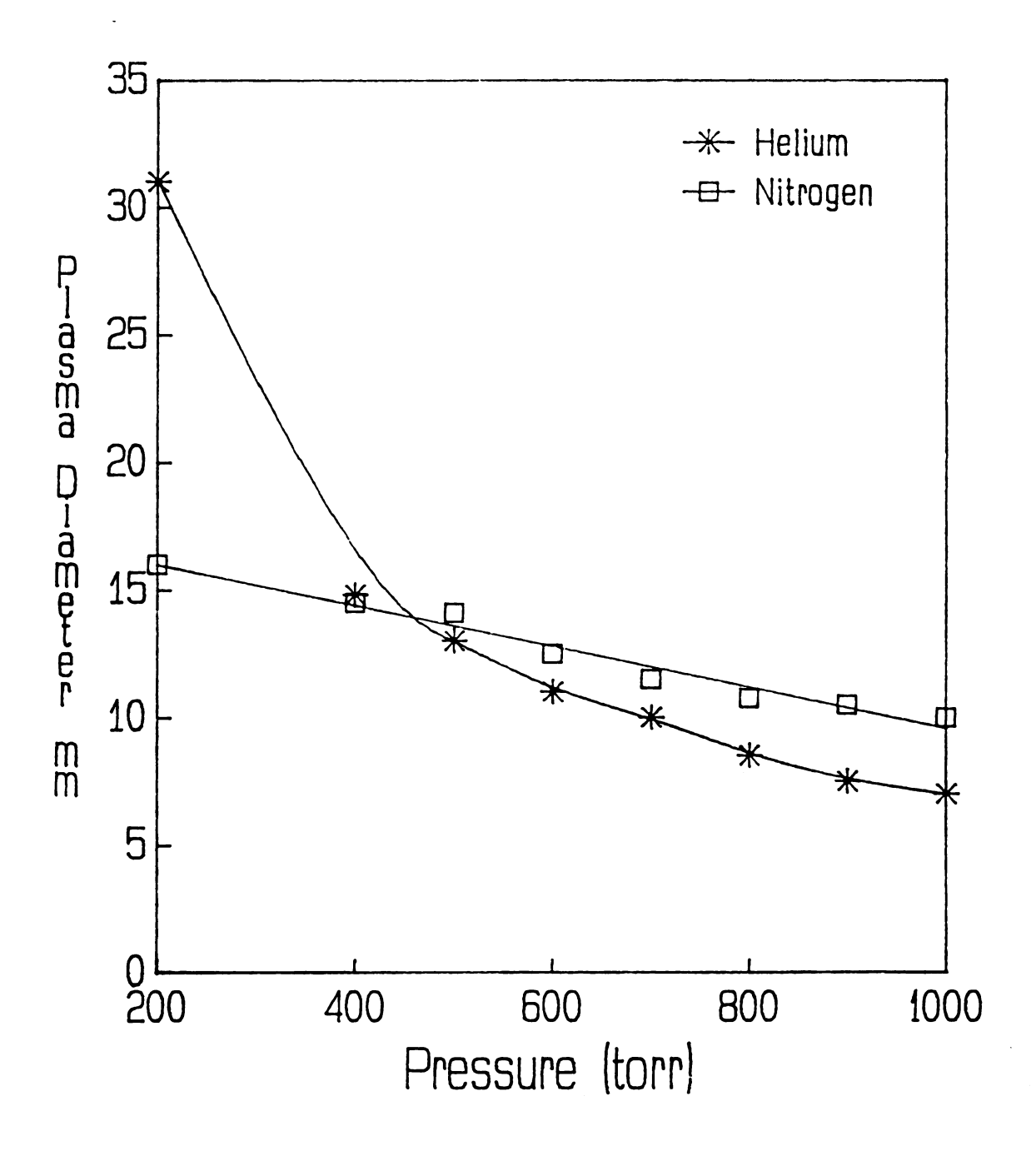


Figure 4.4 He and N2 Strong Coupling Diameters versus Pressure

energy, it takes more energy to keep it fully ionized (i.e. to fill the whole tube) than helium requires at a given pressure. It is believed that the vibrational excitations of nitrogen influence the plasma diameter through ionization rates, and as the pressure is increased above 100 torr, these excitations are more readily damped than the electronic excitations of helium. The electronic excitations of helium are damped in the 200-400 torr pressure region. Above 400 torr, helium and nitrogen plasmas display similar behavior.

A possible explanation for this phenomenon involves the concept of three-body collisions. The recombination processes within a plasma require a three-body collision to reduce excess energy from the binding electron before electron capture can occur. The third body, which does not recombine, receives the excess kinetic energy of the binding electron. The third body can be the containment wall, as in low pressure plasmas, or another particle, as in high pressure plasmas. During low pressure operations, low particle densities cause the formation of a plasma on the containment wall because the wall is needed as the third body in the recombination process. At high pressures, the corresponding high particle density results in a shortened mean free path. This, in turn, renders the containment wall unnecessary as the third body in the recombination process.

An optical measuring device was designed and built to compare plasma diameters resolved with the photographic method and plasma diameters measured by the human eye. A beneficial consequence of this invention is that it provides a back-up method of measuring plasma diameters if the photographic method should fail.

Figure 4.5 illustrates the optical measuring device. To use this device, the iris is placed at the cavity window and the operator looks through the small hole at the other end. To take a measurement, the operator closes the iris until the outer edges of the plasma are encircled within the iris. The iris diameter is then measured with calipers. This measurement is then multiplied by a calibration factor. The easiest method for obtaining the calibration factor is to focus the iris on the plasma containment tube which is of known diameter, and then calculate the multiplier necessary to convert the iris measurement to the tube diameter.

Measurements taken using this technique were found to agree within 5% of the measurements taken with the photographic technique. The optical measuring device's measurements were usually smaller than the photographic measurements. This can be explained as a problem with either containment tube glare causing problems with the photographic technique or a problem caused by squeezing the plasma (with the iris) in the optical measuring technique. Not only does this method help validate the diameter measurements taken by the photographic method, but also it provides another means for quickly obtaining data during other experiments.

The plasma volume measurements for helium are made by cutting the dumbbell-shaped 2-dimensional areas into rectangular and semi-circular sections. Assuming that the plasma is cylindrically symmetric, the rectangular sections can be calculated as cylindrical volumes and the semi-circular sections can be calculated as hemi-spherical volumes. Then, all the individual volumes are added up to represent the total

OPTICAL MEASURING DEVICE (OMD)

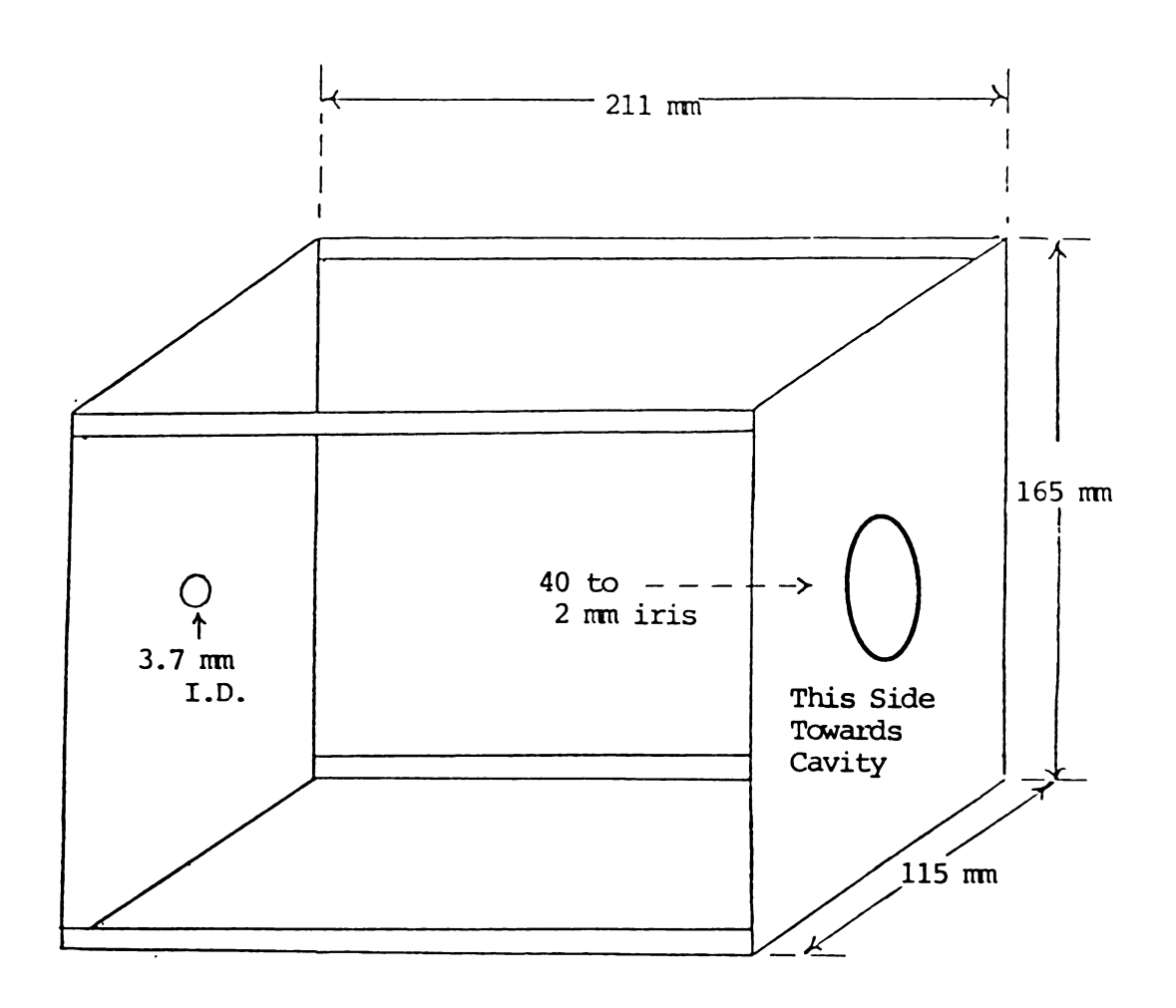


Figure 4.5 Optical Measuring Device used to calculate plasma diameters.

plasma volume. For nitrogen, the dumbbell shape is not present, and the plasma volumes are best approximated as cylinders. In Table 4.1, the volumes of strong and weak coupling regions are listed for helium and nitrogen for pressures from 200-1000 torr. It can be seen that the plasma volumes follow the same trend as the plasma diameters; plasma volumes in helium change more with pressure than those in nitrogen. Volumes of strong coupling regions in helium vary from 46.7 cm³ at 200 torr to 4.59 cm³ at 1000 torr. The volumes of similar regions in nitrogen change from 14.5 cm³ at 200 torr to 2.8 cm³ at 1000 torr.

4.4 Summary

Plasma diameter and volume measurements in the 200 to 1000 torr pressure range for helium and nitrogen discharges are taken in a 31 mm I.D. quartz containment tube for a microwave input power of 246 W.

Both helium and nitrogen discharges are found to have a "threshold" pressure where the plasma volume and diameter change dramatically.

Above this "threshold" pressure the plasma diameter and volume become linearly dependent upon pressure. The diameter of the strong electromagnetic coupling region in this pressure range for helium and nitrogen discharges varies from 31 to 7 mm and from 17 to 13 mm respectively. The plasma volumes vary from 46.71 to 4.59 cm³ for helium discharges and from 14.5 to 2.83 cm³ for nitrogen discharges. Since the scope of this experiment is in the pressure range of 200 torr and above, the "threshold" pressure for nitrogen plasmas is not observed. Nitrogen, since it is a diatomic, has a lower "threshold"

pressure, around 100 torr for 246 W input power.

This study builds upon the work of Whitehair [1986]. Whitehair calculated plasma volumes in helium, nitrogen and oxygen discharges for pressures in the range of 40-760 torr in quartz tubes of 12, 25, and 37 mm inner diameter (See Table 4.1). Although his work was similar to this experiment, he worked at higher microwave powers (over 400 W compared to 246 W), and at a lower maximum pressure (760 torr compared to 1000 torr). Whitehair's results showed similar trends to those observed in this study, since helium plasma volumes changed more than nitrogen plasma volumes for the 200-760 torr range (9.3 cm³ and 1.3 cm³, respectively). It is interesting to note that the plasma volumes calculated by Whitehair correspond with the strong coupling volumes calculated in this study. Whitehair's measurements are based on the assumption that the strong coupling region marked the entire plasma. Since the position of the plasma boundary is still being debated by researchers in this field, the strong and weak coupling region measurements are reported in this (Hoekstra) study.

Table 4.1. Helium and Nitrogen Plasma Volumes in Pressures from 200 - 1000 Torr. Experimental parameters are: power = 246 W, no flow conditions, 31 mm I.D. quartz containment tube, and 3.5 scfm air cooling.

| Press. | | -31 m | m 245 | W | Whitehair's 25 He | mm | 37 | mm |
|--------|------|-------|-------|-----|----------------------|-----|------|-----|
| | | | | | | | | |
| 200 | 46.7 | 14.5 | 30.4 | 2.4 | 10.9 | 2.0 | 13.0 | 5.9 |
| 400 | 18.3 | 12.5 | 3.4 | 1.4 | - | - | - | - |
| 500 | 15.0 | 10.4 | 1.9 | 1.3 | 3.8 | 2.0 | 5.6 | 3.4 |
| 600 | 11.7 | 10.0 | 1.2 | 1.2 | 3.3 | 2.4 | 4.7 | 4.6 |
| 700 | 10.5 | 7.8 | 1.0 | 1.0 | - | - | - | - |
| 800 | 8.1 | 6.2 | 0.6 | 0.8 | 2.5 | 2.0 | 3.7 | 4.5 |
| 900 | 5.8 | 5.4 | 0.5 | 0.7 | • | - | - | - |
| 1000 | 4.6 | 2.8 | 0.4 | 0.6 | 2.1 | - | - | - |
| | | 2.3 | · · · | 0.3 | | | | |

Chapter V

Energy Balance Measurements

5.1 Introduction

The purpose of this experiment is to measure the energy distribution between the cavity walls, cooling air and plasma gas for high pressure nitrogen and helium microwave plasmas in the ${\rm TM}_{012}$ and ${\rm TM}_{011}$ electromagnetic resonant modes. The ${\rm TM}_{011}$ mode is chosen so that this work can be contrasted with Chapman's study [1986], and the ${\rm TM}_{012}$ mode is chosen to be consistent with the atomic-electronic temperature experiment.

The electromagnetic field patterns of the TM_{012} mode are double those of the TM_{011} mode (see Figure 5.1). Since the short length of the TM_{012} mode is double that of the TM_{011} mode, the TM_{012} mode has 1.6 times more surface area than the TM_{011} mode.

An energy balance around the microwave system can be written as

 P_{abs} is the microwave power absorbed by the plasma system. It is calculated by measuring the amount of power put into the system by the microwave source and subtracting the amount of energy reflected out of the system. P_{water} is the amount of power absorbed by the microwave cavity and is calculated by measuring the flow rate and temperature change of the cooling water. P_{air} is the amount of power absorbed by the air cooling of the quartz plasma containment tube and is calcu-

Electromagnetic Field Pattern for the Microwave Cavity Applicator

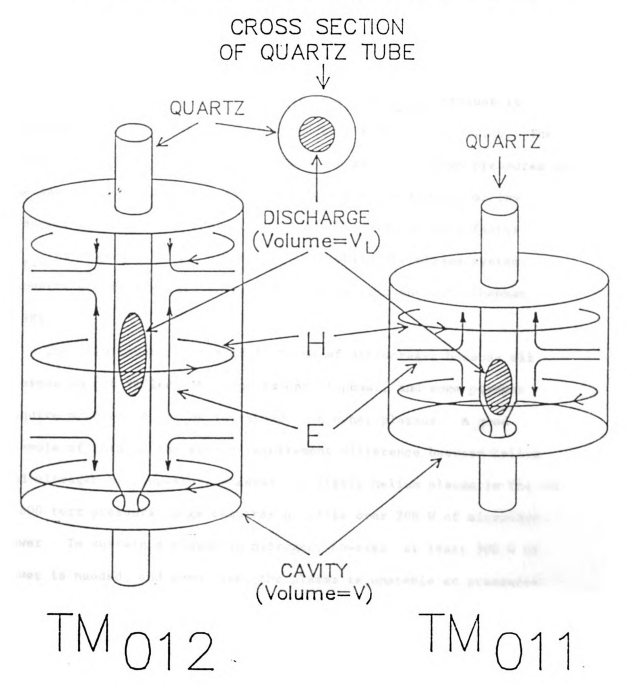


Figure 5.1 Electric and Magnetic Field Patterns for the Cavity Applicator Reproduced with permission from S. Whitehair

lated by measuring the flow rate and temperature change of the cooling air. The air cooling is necessary to keep the quartz containment tube from melting due to the extreme temperature of the plasma. An emission radiation term has been neglected since the system is almost entirely enclosed (Chapman [1986]). P_{gas} is the amount of energy in the plasma gas (He or N_2) that exits the system and is calculated by subtracting P_{air} and P_{water} from P_{abs} .

In this study, the important parameter is $P_{\rm water}$ because it indicates the amount of power absorbed by the microwave cavity. The calculation of $P_{\rm gas}$ is made to measure the effect of high pressures on the amount of power in the exit gas since earlier studies on low pressure plasmas (less than 10 torr) concentrated on this factor. " $P_{\rm gas}$ is regarded as the efficiency with which the plasma system converts electromagnetic energy into gas kinetic energy" (Chapman [1986]).

The results are presented in terms of percentages because all plasmas do not reflect the same amount of power, and some plasmas require more energy to be sustained than other plasmas. A good example of this is the energy requirement difference between helium and nitrogen high pressure plasmas. A stable helium plasma in the 200 - 800 torr pressure range requires a little over 200 W of microwave power. To sustain a plasma in nitrogen, however, at least 300 W of power is needed, and even then, the plasma is unstable at pressures over 400 torr. In this study, the power level was limited to a maximum of 300 W due to limitations of the microwave source and power cables.

The calculations for percent of power absorbed by the gas, air, and water and the error estimates for them are as follows:

$$P_{gas} = 100 \times P_{gas}/P_{abs}$$
 $\Delta P_{gas} = 3 - 4$

From these calculations, the data for helium and nitrogen can be compared directly without further manipulations.

Previous work by Chapman [1986] concluded that the amount of energy absorbed by the microwave cavity walls was independent of the resonant mode (See Table 5.1 for Chapman's operating conditions). Chapman's basis for this conclusion was that he found no difference in the amount of energy absorbed by the microwave cavity in the $\rm TE_{111}$ and $\rm TM_{011}$ resonant modes. Although the $\rm TM_{011}$ and $\rm TE_{111}$ resonant modes used in Chapman's experiment have different electromagnetic field distributions, they have similar short lengths. For an empty cavity, the $\rm TE_{111}$ mode has a short length of 6.45 cm, while the $\rm TM_{011}$ mode has a short length of 7.2 cm. The short length determines both the surface area exposed to heat and microwave radiation and the electromagnetic mode. Since Chapman chose resonant modes with similar cavity surface areas, it is not surprising that he found little or no difference in the amount of energy absorbed by the microwave cavity.

5.2 Experimental System and Procedure

Experimental measurements are taken with a setup as shown in

Table 5.1. Calorimetry Experimental Conditions

| Parameters | This Investigation | Chapman [1984] |
|-------------------------|---------------------------------------|---------------------------------------|
| | | |
| Gas | He, N ₂ | Н ₂ , N ₂ , Не |
| Flow Rate | 0 - 2000 sccm | 0 - 100 sccm |
| Pressure | 200 - 800 torr | 0 - 10 torr |
| Cooling Flow Rate | 0.5 scfm | 7.0 scfm |
| Quartz Tube Diameter | 31 mm I.D. | 22 mm I.D. |
| Electromagnetic Modes | TM ₀₁₁ , TM ₀₁₂ | TM ₀₁₁ , TE ₁₁₁ |
| Microwave Input Power | 230 W, 300 W | 100 W (max) |
| Driving Frequency | 2.45 GHz | 2.45 GHz |
| Electronic Temperatures | $3.5 - 5.4 \times 10^3 \text{ K}$ | $3.0 - 5.5 \times 10^3 \text{ K}$ |
| Reynolds Number (Re) | < 200 | < 10 |
| Short Length | 7.2 - 14.4 cm | 6.45 - 7.2 cm Probe |
| Depth | 0.1 - 3.0 cm | Unknown |

Calorimetry System

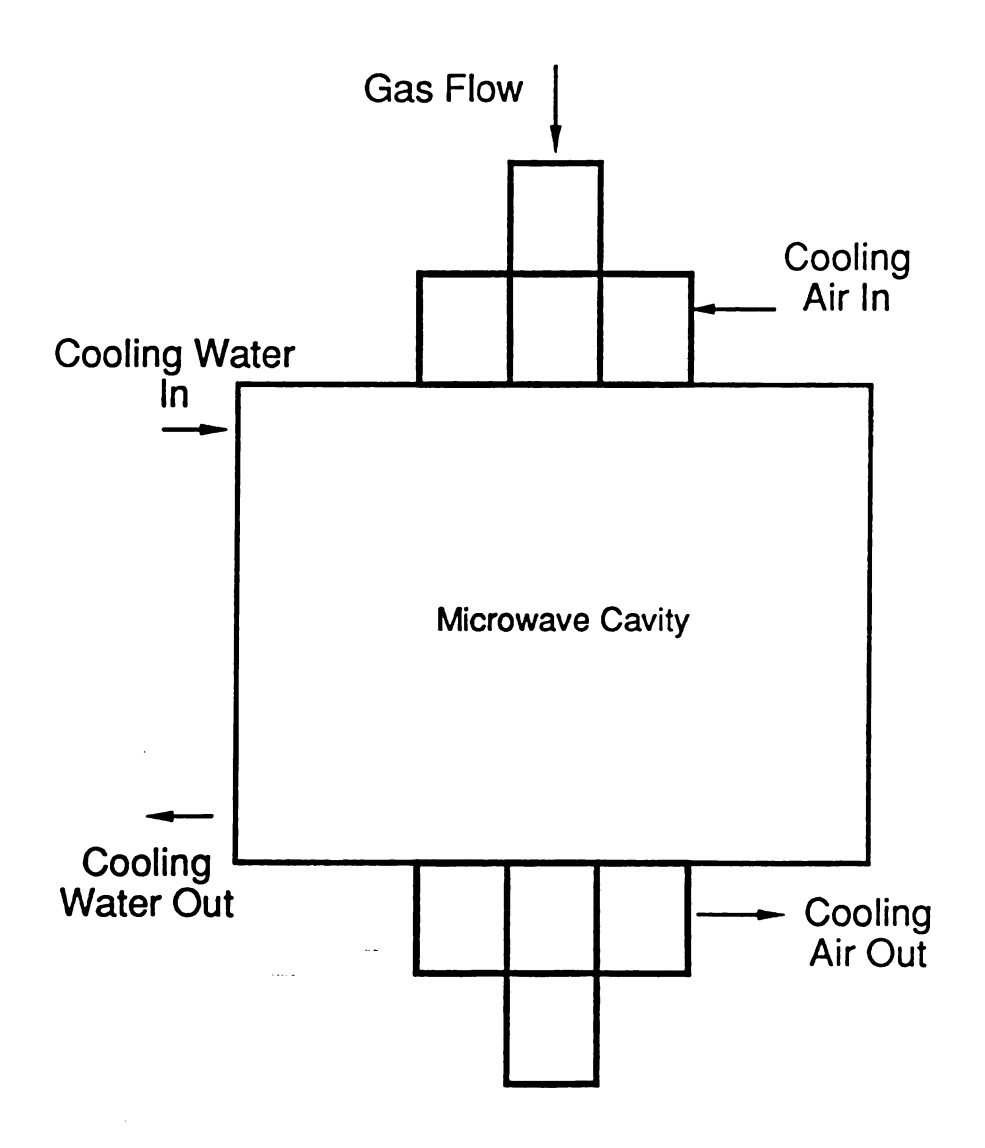


Figure 5.2 Calorimetry System

Figure 5.2. The inputs and outputs of the water and air cooling streams are monitored using type T thermocouples connected to Omega Model TAC80 thermocouple to millivolt converters. The thermocouple to millivolt converters are connected to digital voltmeters so that the temperature can be read directly. The flow rates of these coolant streams are kept constant and measured using calibrated flow meters. Typically, for experiments using the TM₀₁₂ mode, the water temperature rises 23 °C, while in the TM₀₁₁ mode, the water temperature rises about 11 °C. The air flow rate is kept high enough so that heat transfer by convection from the quartz containment tube to the cavity wall is negligible. Typical air flow rates and temperature rises are 0.35 1/s and 240 °C, respectively.

The microwave plasma generator and its supporting equipment are discussed in Chapter II. The experimental conditions are shown on Table 5.1. To make sure the energy balance is closed, no-flow experiments are done in both electromagnetic modes (TM_{012} and TM_{011}). The energy balance for this experimental setup is within 3 % of closure, which is considered accurate enough for this study.

Nitrogen plasmas with 300 W input power are too unsteady above 400 torr for energy balance work. A nitrogen plasma can be formed above 400 torr, but it cannot be sustained for the 1-2 hours necessary for a data point to be calculated. Generally, a data point is taken when the air and water temperatures have been stabilized for more than 30 minutes.

Power Absorbed By Water He and N2 Data

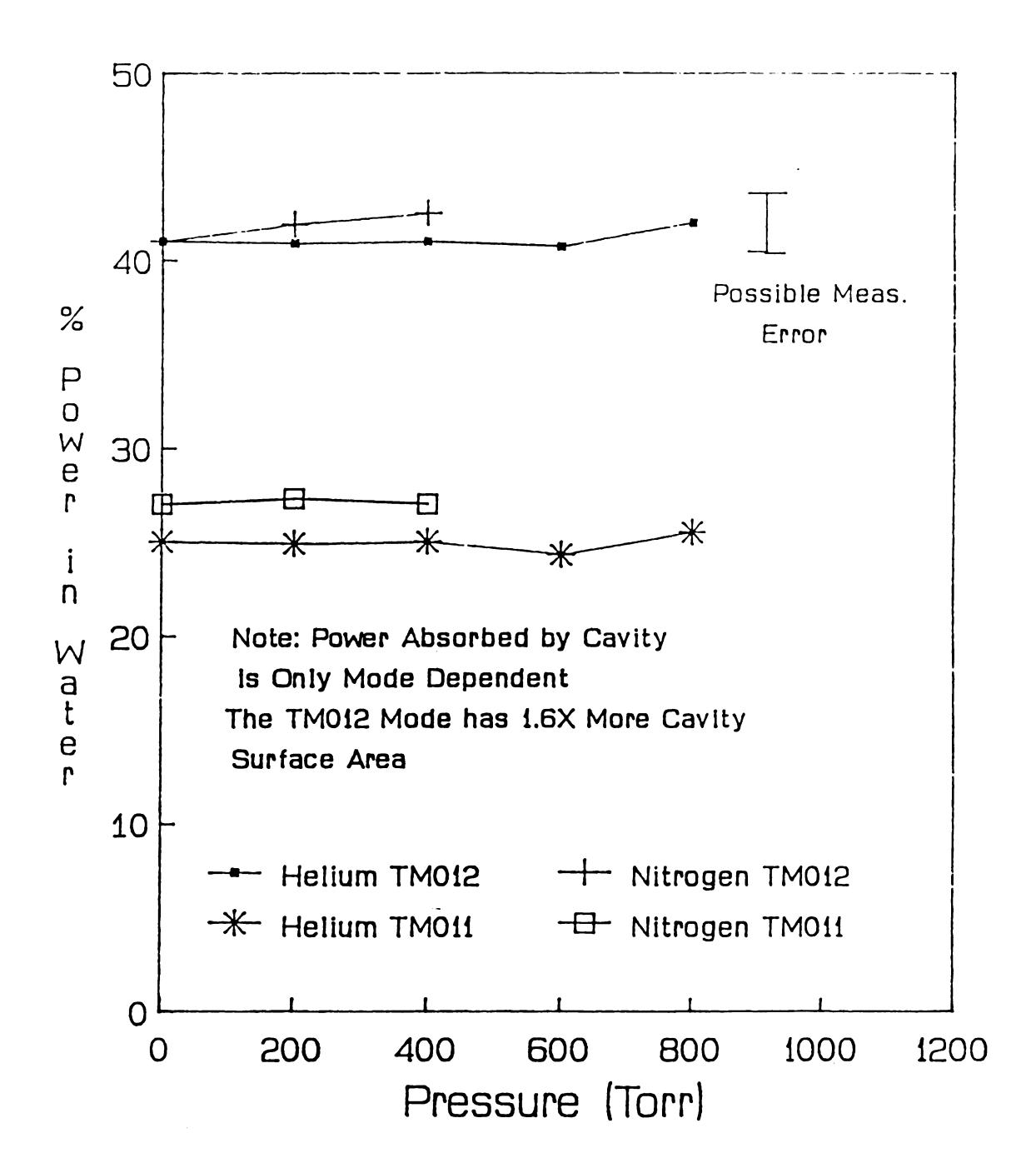


Figure 5.3 Power Absorbed by Water

5.3 Results from Calorimetry Experiments

Figure 5.3 illustrates the percent power absorbed by the microwave cavity for nitrogen and helium plasmas using the TM_{011} and TM_{012} modes. The power absorbed by the cavity is dependent on the cavity surface area and independent of gas and coolant flow rates. The TM_{012} mode absorbs 41% of the input power, while the TM_{011} mode absorbs approximately 25%. Within experimental error, these numbers are the same for both helium and nitrogen plasmas.

It is interesting to note that if the amount of power absorbed by the TM_{011} mode is multiplied by the difference in surface area (1.6X) the result is close to the amount of power absorbed by the TM_{012} mode. Therefore, it can be concluded that the surface area of cavity exposed to the microwave plasma environment is proportional to the losses incurred by the system to the cooling water. In other words, the more surface area exposed to the microwave environment, the more losses incurred by that system.

Previous studies by Chapman [1986] reported energy losses for a cavity in the TM₀₁₁ mode of 15 - 23%. The differences between his results, and the results of this study are caused by the use of different operating conditions. One of the differences in these studies is the air cooling rate. In Chapman's study, the air cooling rate was 7.0 scfm. Since his cooling rate was much higher than the cooling rate of this study (0.5scfm), the amount of I.R. losses to the cavity would be less in his experiments. Considering the differences in operating conditions, Chapman's measurements substantiate the results presented in this study.

% Power Absorbed By Gas Versus Pressure

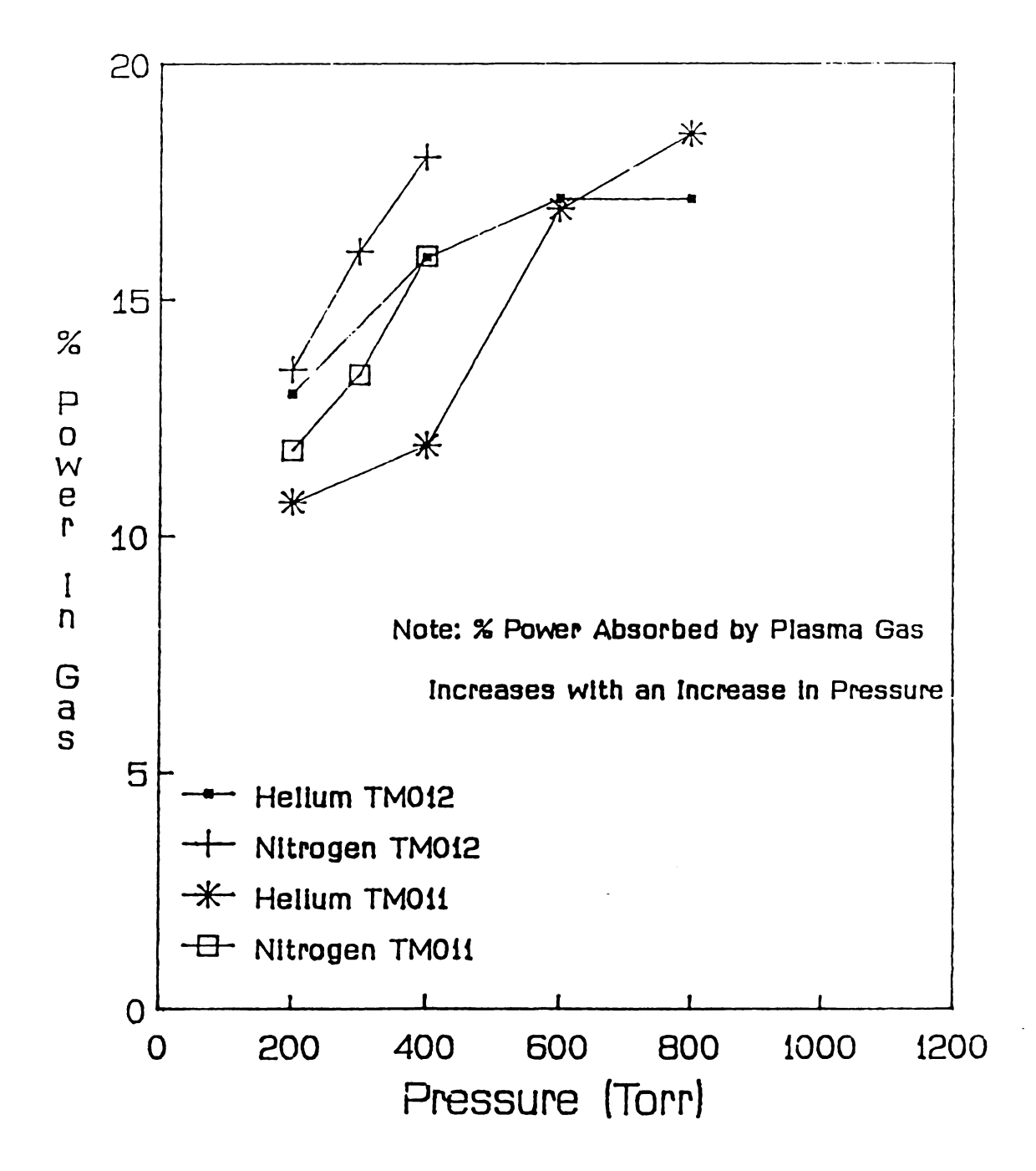


Figure 5.4 Percent Power Absorbed by Plasma Gas

Figure 5.4 illustrates the percent power absorbed by the working gas versus pressure. From this plot, it can be concluded that the plasma gas absorbs between 10 and 18 % of the total input power.

Another interesting fact is that as the pressure increases, the energy absorbed by the plasma gas increases. Although it is difficult to establish any mode dependence because of the error in the energy balance measurements, it can be noted that nitrogen tends to retain more power than helium.

The plot of percent power absorbed by cooling air versus pressure (Figure 5.5) illustrates the mode dependence of the partition of energy between the three sources of heat loss. The energy loss difference between the TM₀₁₂ mode and the TM₀₁₁ mode due to water cooling of the microwave cavity is made up in the difference in the amount of energy lost to the air cooling of the quartz tube. The TM₀₁₂ mode has a % P_{air} of 44% while the TM₀₁₁ mode has a % P_{air} of about 60%. The loss of energy due to the cooling air increases by almost 8% with an increase in pressure from 200 - 800 torr. As the pressure increases, the energy lost by the cooling air is gained by the plasma gas. A possible explanation is that when a plasma shrinks from high pressure, conduction is less effective because energy must be transferred over a longer distance.

In only one case is the plasma gas flow rate a factor in the percent of energy absorbed by cooling air and plasma gas (See Figure 5.6). The percent of energy absorbed by the gas is flow rate dependent in the 200 torr experiment with helium gas. The percent power absorbed by the gas increases from 0 - 16% as the flow rate

% Power Absorbed By Cooling Air Versus Pressure

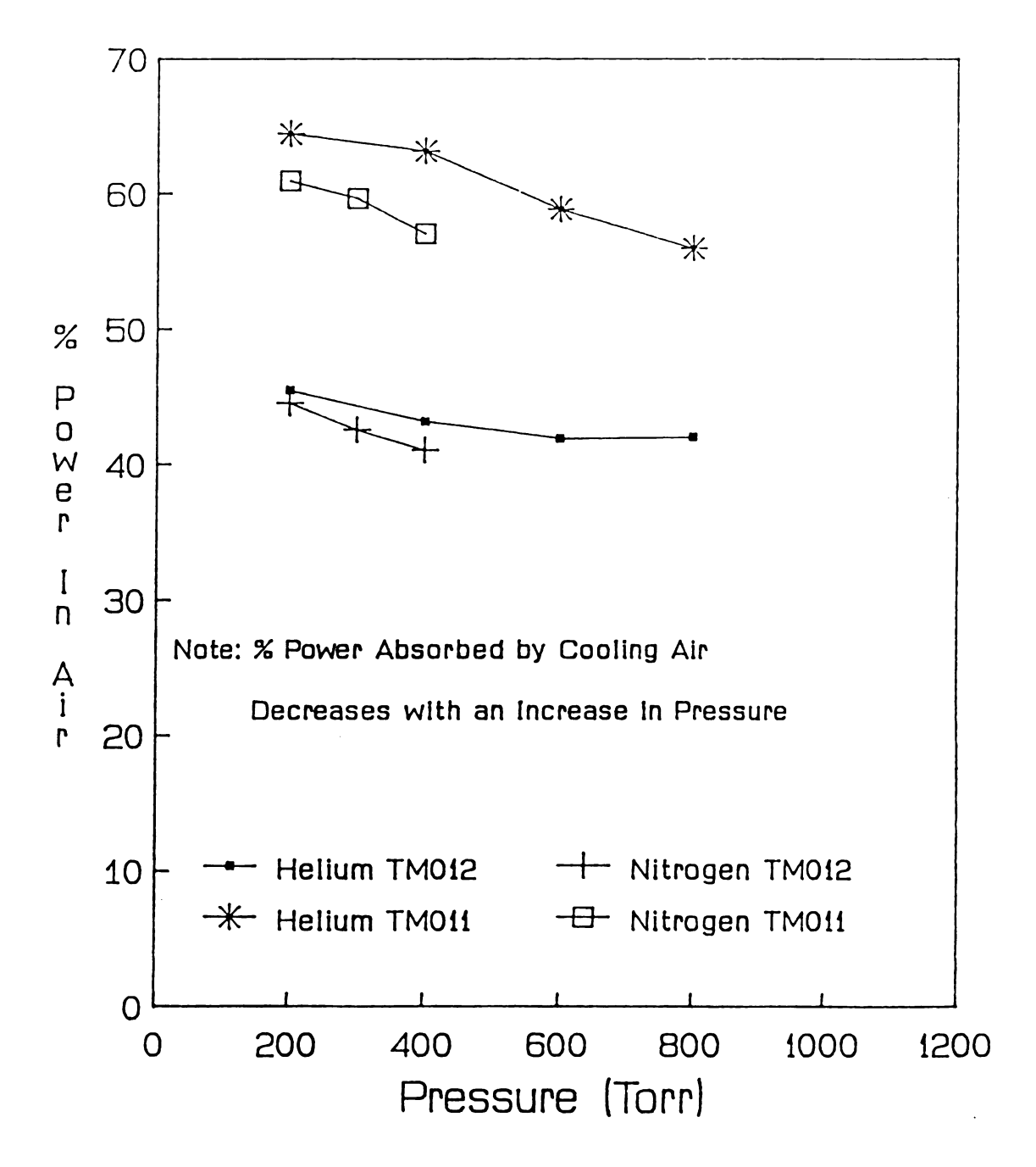


Figure 5.5 Percent Power Absorbed by Cooling Air

Gas Flow Rate Dependent Data Helium, 200 Torr

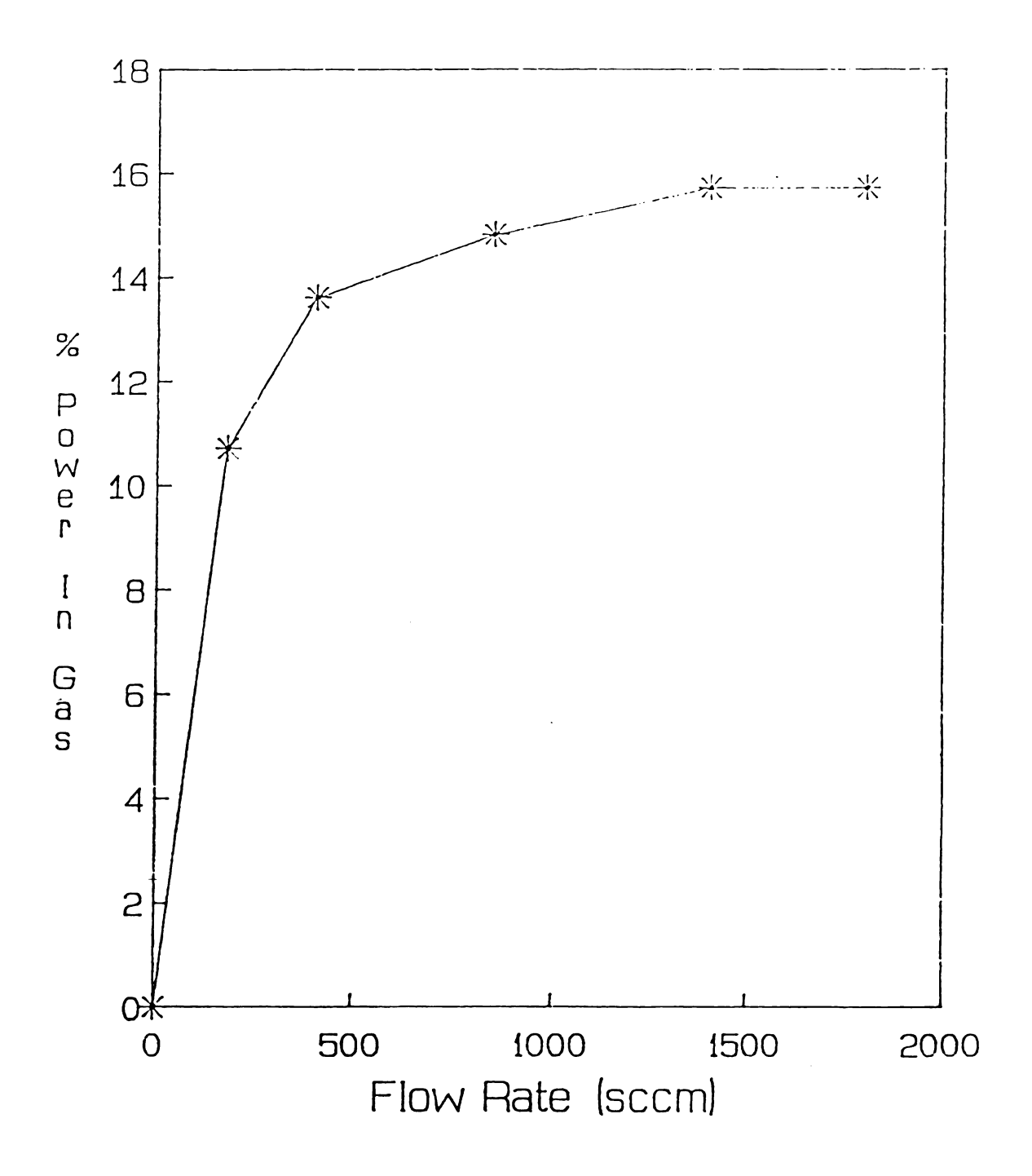


Figure 5.6 Gas Flow Dependent Data for Helium at 200 Torr.

changes from 0 - 2000 sccm. These results concur with those of Chapman for low pressure hydrogen plasmas, but differ from all other data gathered during this research. A plausible explanation for this behavior is that the %P becomes saturated with regard to ionization at high pressures and becomes no longer dependent on flow rate.

5.4 Summary

The results of the calorimetry experiment indicate that the amount of energy absorbed by the microwave cavity is dependent on the surface area of cavity exposed to the microwave environment. In other words, the amount of energy absorbed by the cavity is dependent on the short length of the cavity. The energy balance measurements indicate a 25% energy loss to the cooling water in the TM_{011} mode and a 41% loss in the TM_{012} mode. For high pressure (200-1000 torr) plasmas, the energy absorbed by the cavity is independent of both plasma pressure and working gas flow rate.

The amount of energy absorbed by the cooling air and plasma gas is pressure dependent but only flow rate dependent in one experiment. For most cases, the % P_{gas} varies from 10 - 16% as the pressure is increased from 200 - 800 torr. The % P_{air} is mode dependent and varies in this pressure range from 74 - 68 % in the TM_{011} mode and from 46 - 40% in the TM_{012} mode. The difference in the amount of energy absorbed by the cooling air in the two electromagnetic modes is equal to the difference in the amount of energy absorbed by the microwave cavity in the two modes.

Chapter VI

Computer Modeling of Plasma Sheath

6.1 Introduction

The purpose of this investigation is to model the heat transfer in nitrogen gas from the microwave plasma to the quartz containment tube wall due to conduction (See Figure 6.1). The reason for this is twofold: to revise existing plasma models, and to get an estimate of the heat loss due to conduction. Filpus (1986) developed a recombination model which calculated the axial and radial temperature distributions due to recombination processes downstream of the plasma. It is important to note, however, that his model started from the downstream end of the plasma. To begin his calculations, he had to guess the radial temperature distribution of the gas at this point. It is hoped that this conduction model, which calculates the radial temperature gradients formed at the end of the plasma region, will enable further use of the Filpus program to generate more accurate results. Another future application for this program is to complement Morin's (1985) plasma model by taking into consideration the entire discharge region. Morin modeled the collision induced heating of a weakly ionized dilute gas in steady flow, low pressure hydrogen plasmas. Modifying the plasma collision model to account for high pressures and adding a conduction model would lead to a much improved model of the whole discharge region.

The second reason for computing the radial temperature gradients

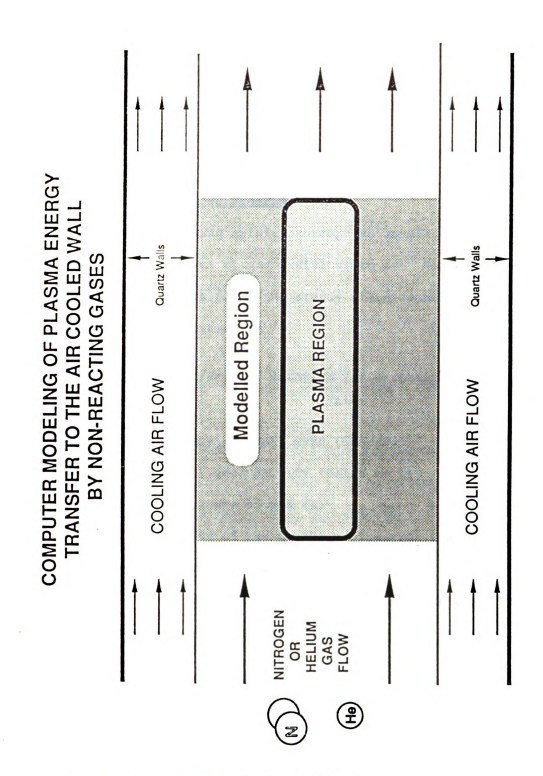


Figure 6.1 Computer Simulation Diagram

at the end of the plasma region is to get a feel for the amount of heat lost to the air cooled wall due to conduction. In both this investigation and an earlier investigation (Chapman [1986]), energy balance measurements were taken on microwave plasma discharge experiments. Results from this computer model should help in the analysis of future energy balance measurements.

6.2 <u>Development of Computer Program</u>

Consider a gas flowing axially through an annular element of length Δz , internal radius r, and radial width Δr . Neglecting axial diffusion and radial mass flux, the steady state enthalpy balance yields the following equation.

$$2\pi r \Delta r \rho u \overline{H} \mid -2\pi r \Delta z k (\partial T/\partial r) \mid -2\pi r \Delta r \rho u \overline{H} \mid +2\pi r \Delta z k (\partial T/\partial r) \mid = 0$$

$$z \qquad r \qquad z + \Delta z \qquad r + \Delta r$$

where \overline{H} - enthalpy per unit mass (Cal/gram)

k = thermal conductivity (Cal/s cm K)

T - temperature of gas (K)

u = velocity of gas in the z direction (cm/s)

 ρ - density of working gas (g/cm³)

Dividing through by $2\pi\Delta r\Delta z$, and taking the limits as Δr and Δz go to zero, the following equation is derived.

$$\rho ur(\partial \overline{H}/\partial z) - [\partial/\partial r(kr\partial T/\partial r)] = 0$$

For an ideal gas, a substitution can be made for $dH = \overline{C}pdT$.

$$\rho ur \overline{C} p(\partial T/\partial z) - [\partial/\partial r(kr\partial T/\partial r)] = 0$$
 where $\overline{C}p$ = constant pressure heat capacity (Cal/g K)

A substitution of $G = \rho u$ (the mass flux) is made and the equation is rearranged to obtain the working equation. Assuming the mass flux (G) remains constant, the following equation is valid.

$$\partial T/\partial z = 1/(G\overline{C}pr)\partial/\partial r[rk(\partial T/\partial r)]$$

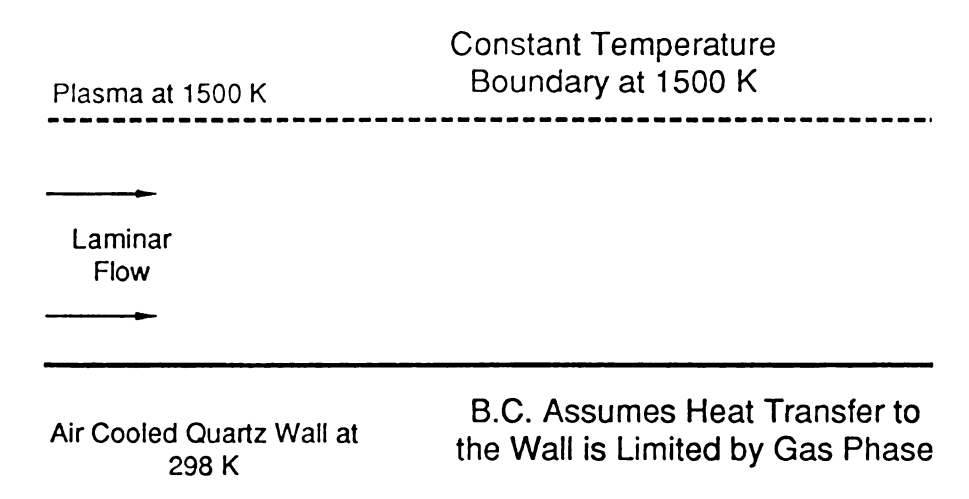
where $G = \text{mass flux } (g/\text{cm}^2 \text{ s})$

In solving this differential equation, many assumptions and substitutions are made. The assumptions are a) laminar flow. conditions, b) ideal gas conditions, c) modeling the plasma as a cylinder whose diameter is equal to its length, and d) neglecting any temperature change of the gas exiting downstream of the plasma. A parabolic velocity profile is used to calculate the initial mass flux. Also, an nth order fit of the thermal conductivity data for nitrogen found in the CRC Handbook of Chemistry and Physics (1986) is substituted for k (- aT n). The nth order fit of the thermal conductivity data yielded values of 0.825 and 5.26 x 10 $^{-7}$ for n and a, respectively (for k in units of Cal/(cm s K) and T in units of C).

Figure 6.2 illustrates the two sets of boundary conditions that are used to solve the differential equation. The difference between the two sets of boundary conditions is in the treatment of the interface between the plasma and non-plasma gases. The first set, which from now on will be referred to as the "base case", assumes that the plasma, non-plasma boundary region is at a constant temperature which is equal to that of the plasma. The second set, which will be referred to as the "expanding gas" boundary condition, allows energy transfer across the plasma, non-plasma interface due to expansion of

Illustration of Different Types of Boundary Conditions

Base Case Boundary Conditions



Expanding Gas Boundary Conditions

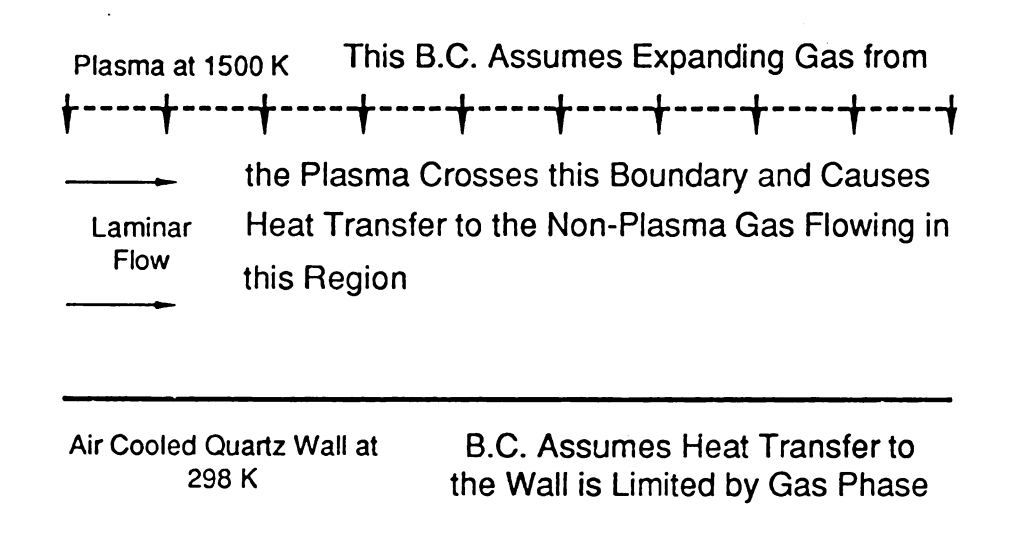


Figure 6.2 Illustration of Different Types of Boundary Conditions

gases from the plasma region. The two sets of boundary conditions are:

Boundary Base Case Expanding Gas B.C.

r = Rl Tp = 1500 K $-(3\pi r lk) \partial T/\partial r = [NiCp(1-Ti/Tp)(Tp-Tb)]$

r = R2 $\partial T/\partial r = (hc/k)(Tc-Tw)$ $\partial T/\partial r = (hc/k)(Tc-Tw)$

where Rl = radial position of the plasma non-plasma interface (cm)

R2 - radial position of the interface between the quartz tube and non-reacting gas (cm)

Ti = input temperature of gas (298 K)

Tp = gas temperature of the plasma (K)

Tb - temperature of the 1st element of non-plasma gas (temperature of non-plasma gas at R1 (K))

k - thermal conductivity of nitrogen (Cal/s cm K)

Ni - molar flux of gas (gmoles/s)

Cp = heat capacity of nitrogen (Cal/gmole K)

hc = heat transfer coefficient (Bennett and Myers [1974])

The expanding gas boundary condition is used to account for energy that passes through the plasma, non-plasma boundary due to the temperature induced expansion of the plasma gas. The derivation of the expanding gas boundary condition starts with the assumption of an ideal plasma gas volume. Assuming equimolar counter diffusion, the total mass of the plasma region does not change due to expansion of the plasma gas.

The derivation starts off simply from the following relation;

$$n_i R T_i - n_p R T_p$$

where n - the number of moles of gas entering in the initial plasma volume

 $n = the \ number \ of \ moles \ of \ gas \ in \ the \ plasma \ volume \ after \ being \ heated \ to \ 1500 \ K$

 $T_{.}$ - the initial gas temperature (298 K)

 T_{p} = the plasma gas temperature (1500 K)

R - the gas law constant

Rearranging the above equation and dividing by the ideal gas constant R, yields $n_{_{\mbox{\scriptsize D}}}$ as a function of temperatures and $n_{_{\mbox{\scriptsize I}}}$.

$$n_p - n_i(T_i/T_p)$$

Subtracting $n_{\mathbf{i}}$ from $n_{\mathbf{i}}$ represents the number of moles crossing the plasma, non-plasma boundary from the interior of the plasma. With this information, the energy losses from the plasma volume due to temperature induced expansion can be expressed as follows;

molar flow across boundary = $(n_i - n_p) - n_i(1 - T_i/T_p)$

(Note: moles are replaced by equimolar counter diffusion)

total energy loss = $n_i Cp(1 - T_i/T_p)(T_p - T_b)$.

where T_b - the plasma boundary temperature

Cp - constant pressure heat capacity

To account for axial energy losses, the energy loss equation is multiplied by a factor of two thirds. This quantity is derived by taking the radial surface area of the plasma (assuming a cylindrical plasma with the plasma diameter equal to the height of the cylinder) and dividing it by the total surface area of the plasma. From these calculations, the expanding gas boundary condition is derived for the inner boundary of the computer simulation.

$$-(3\pi r l k) \partial T/\partial r = [NiCp(1-Ti/Tp)(Tp-Tb)]$$

The first integration method used for solving this equation was a modified Bulirsch-Stoer algorithm (1966) used in the DREBS routine from the IMSL computer library. The Bulirsch-Stoer algorithm uses a rational function for extrapolation and is based on the midpoint rule in a slightly modified form due to Gragg (1965). Comparison of the Bulirsch-Stoer algorithm with the Runge-Kutta method shows clearly that rational extrapolation yields more accurate results and needs fewer operations in order to obtain these results. After many attempts were made at integrating the differential equation using this routine, it was decided that the system was too stiff for this algorithm.

A computer program was then written which incorporated the DIVPAG (IMSL) subroutine which is a linear multi-step method of Adams-Moulton (Hindmarsh [1974]). Utilizing this subroutine on the Vax microcomputers, satisfactory results were obtained at the cost of 8 days computation time. The program was then transferred to an IBM model 3090 mainframe computer, and the computation time was decreased to less than 12 hours depending on the tolerance limits.

6.3 Results of Simulation Runs

Figure 6.3 shows the axial temperature profiles for nitrogen gas flowing past a 1500 K plasma assuming base case boundary conditions at 200 torr. Even though the base case boundary conditions neglect important energy and mass transfer phenomena, a 300 °C temperature difference at the air-cooled boundary is obtained. From this data calculated with simple boundary conditions, it is evident that

Table 6.1. Experimental Conditions for Computer Simulation

| Gas | Nitrogen |
|---------------------------|-----------------|
| Plasma Temperature | 1500 K |
| Gas Inlet Temperature | 298 K |
| Pressure | 200 - 1000 Torr |
| Plasma Diameter | 2.9 - 1.7 cm |
| Plasma Tube Diameter | 3.1 cm I.D. |
| Air Cooling Tube Diameter | 4.8 cm I.D. |
| Bulk Air Flow | 50 cm/s |
| Gas Flow | 5,000 cm3/min |
| Radial Calc. Points | 8 |
| Computer Tolerance | 0.001 |
| Simulation Stepsize | 0.01 cm |

N2 Non-Plasma Gas Axial Temp. Profiles Base Case, 200 Torr

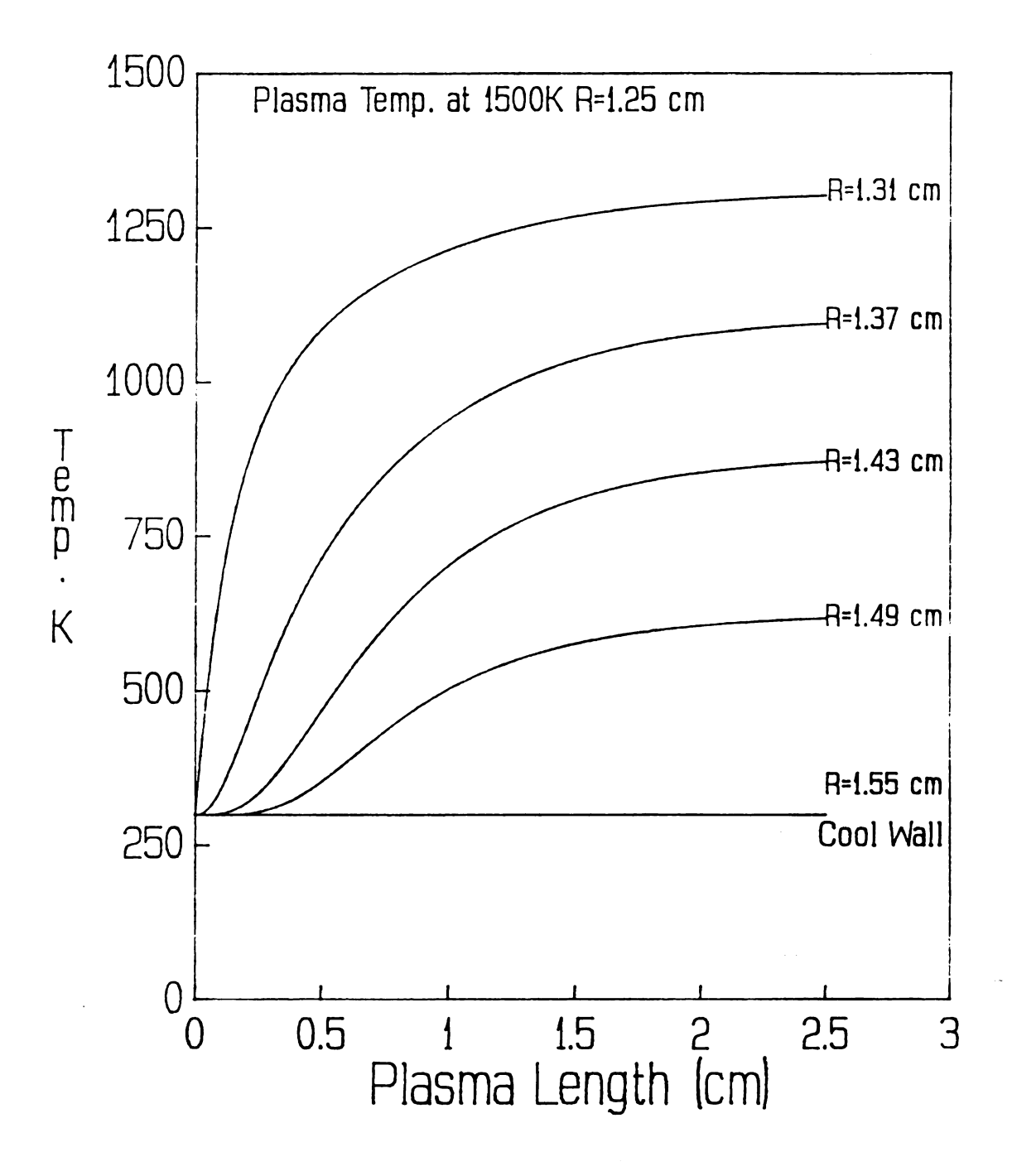


Figure 6.3 Nitrogen Gas Axial Temperature Profiles with Base Case Boundary Conditions

conduction may play an important role in energy losses to the air cooled plasma containment wall.

Figure 6.4 shows the effect of the expanding gas boundary condition. It is interesting to note the sharp temperature gradient of the 1.29 cm radial profile caused by the interfacial mass transfer. The temperature difference at the nitrogen gas wall interface for the expanding gas boundary condition is 370 °C. Therefore, the interfacial temperature increases by about 100 °C due to the expanding gas boundary condition.

The effect of pressure on the nitrogen gas exit temperature radial profiles is illustrated in Figures 6.5 and 6.6. From these figures, it can be concluded that the radial exit temperature profiles change from linear to hyperbolic with an increase in pressure. It is interesting to note the inflection of the first radial element for the expanding gas boundary condition case. Once again, this phenomena can be attributed to energy transfer due to mass transfer across the plasma boundary.

The next three figures in this section (Figures 6.7, 6.8, and 6.9) contain results obtained by changing the input parameters of the base case heat conduction model for three different pressures. From these graphs the inflection of the temperature profiles caused by the expanding gas boundary condition is easily observed. Changing the plasma gas temperature to 2500 K causes the nitrogen gas-wall interface to have a 500 °C temperature difference in the 200 Torr simulation, but it does not have a noticeable effect on the interfacial temperatures for the 600 and 1000 torr cases.

N2 Non-Plasma Gas Axial Temp. Profiles Expanding Gas B.C., 200 Torr

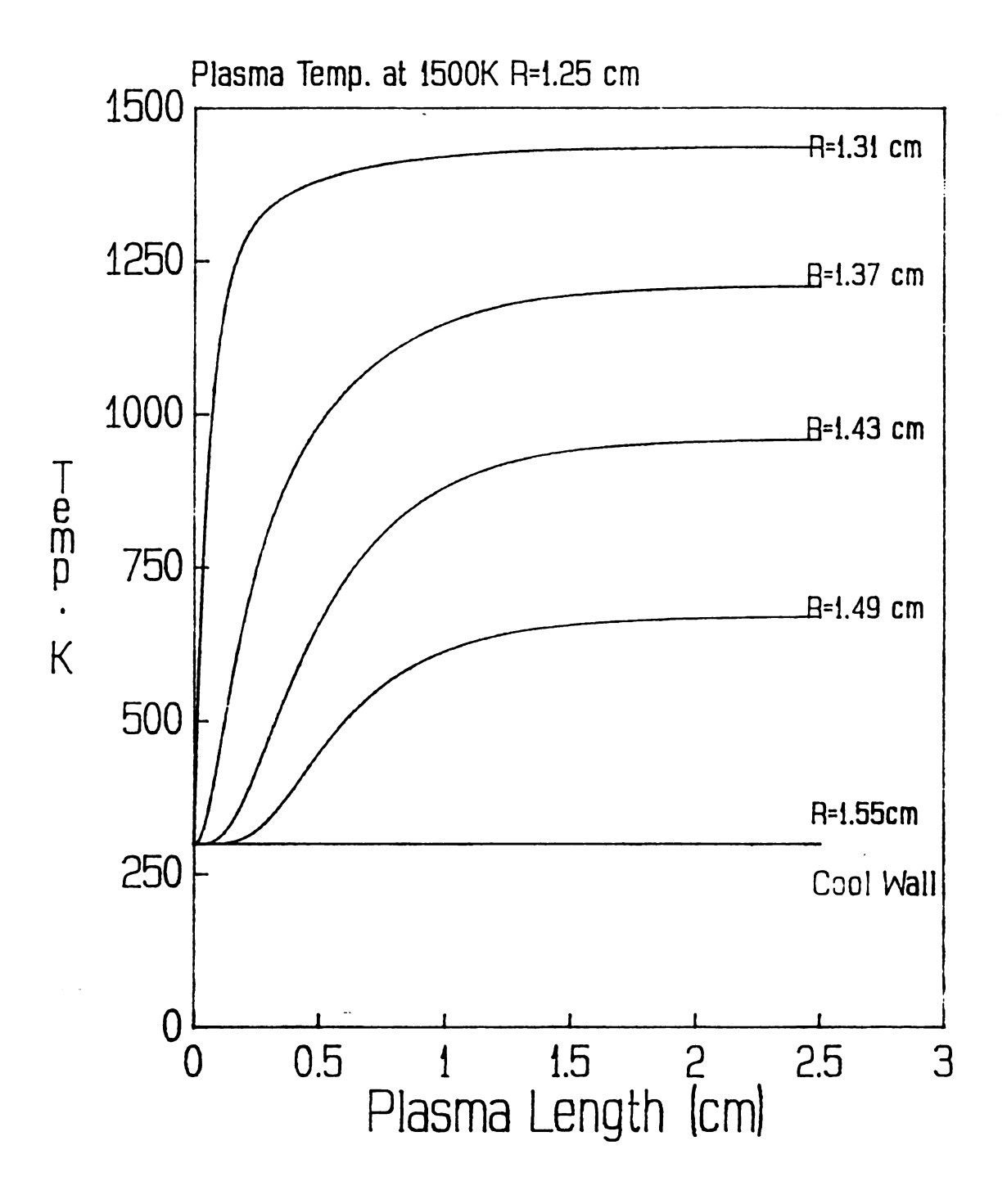


Figure 6.4 Nitrogen Gas Axial Temperature Profiles with Expanding Gas Boundary Condition

N2 Non-Plasma Gas Exit Temp. Radial Distributions

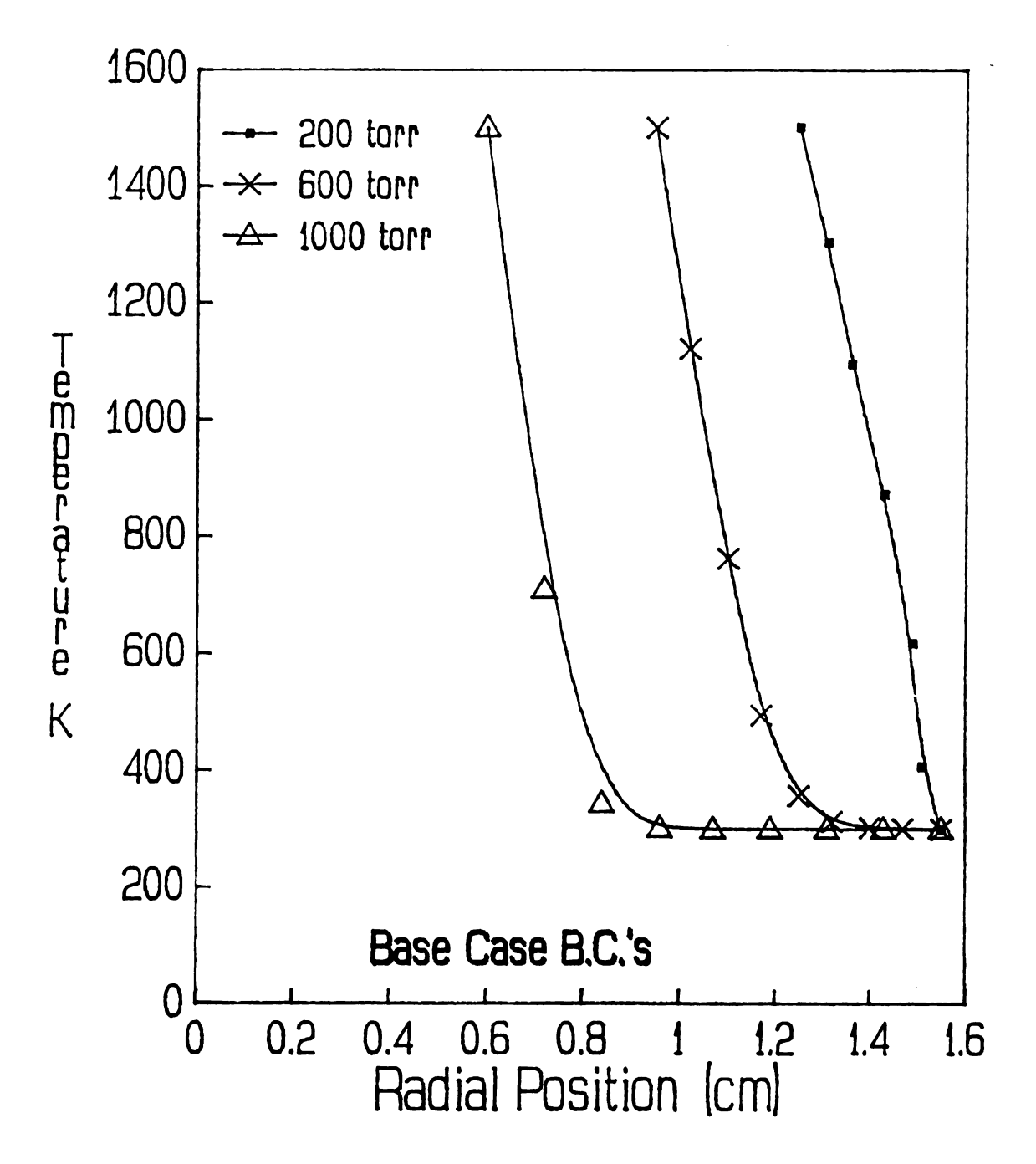


Figure 6.5 Radial Temperature Distributions of Exit Gas Calculated with Base Case Boundary Conditions

N2 Non-Plasma Gas Exit Temp. Radial Distributions

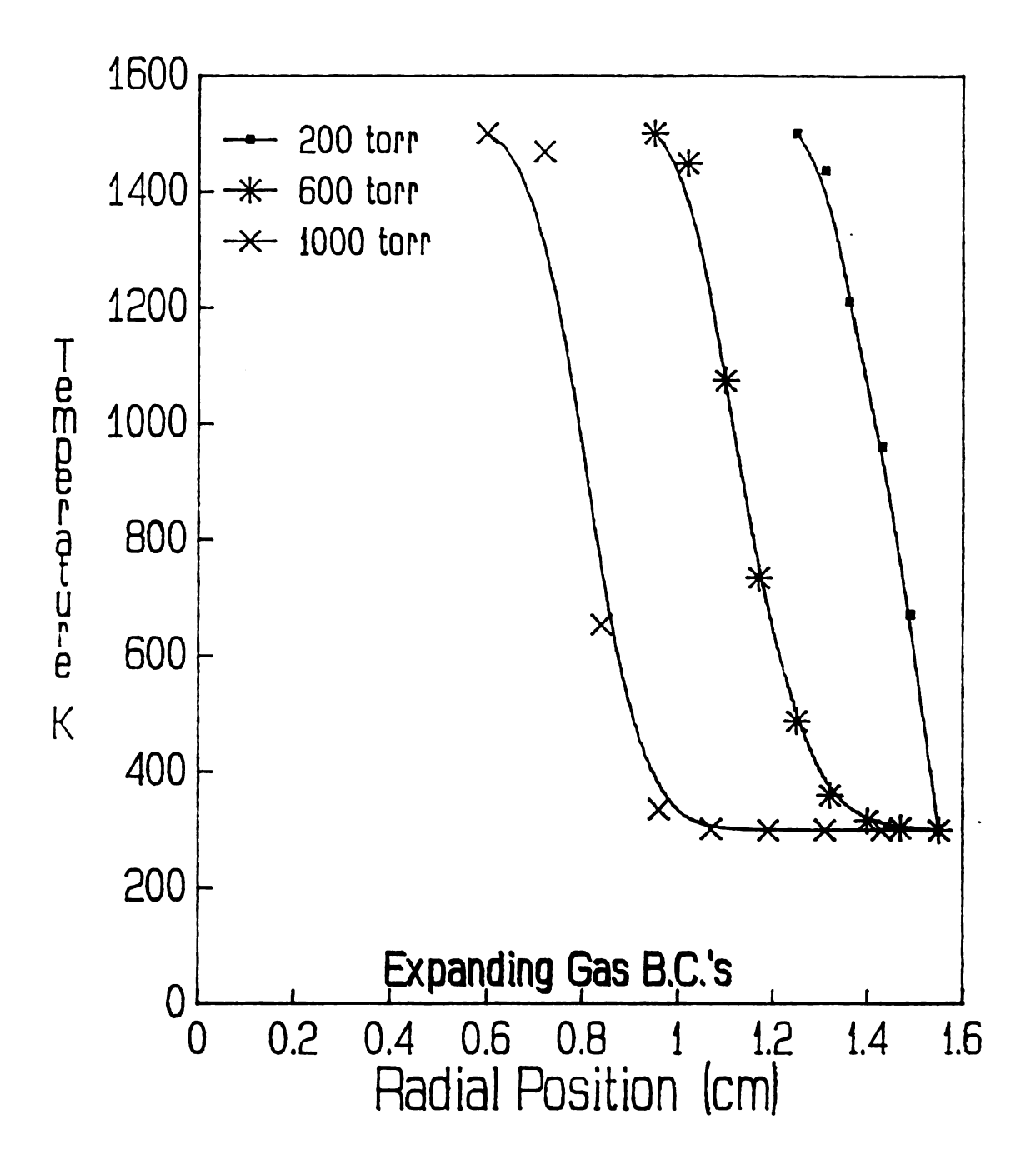


Figure 6.6 Expanding Gas Boundry Condition Radial Temperature Profiles (Exit Profiles)

N2 Non-Plasma Gas Exit-Temp. Radial Distributions, 200 Torr

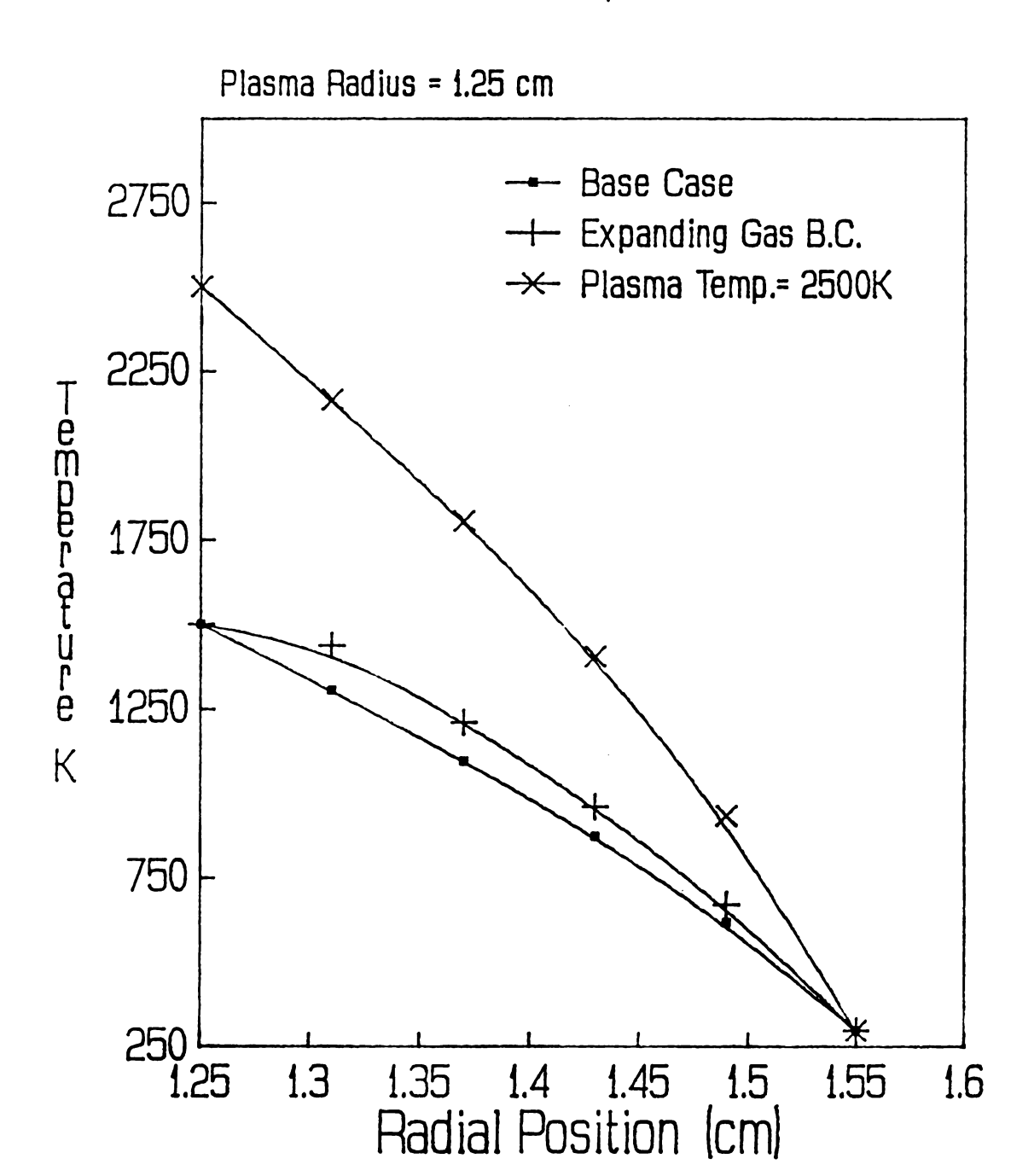


Figure 6.7 200 Torr Radial Temperature Distributions

N2 Non-Plasma Gas Exit Temp. Radial Distributions, 600 Torr

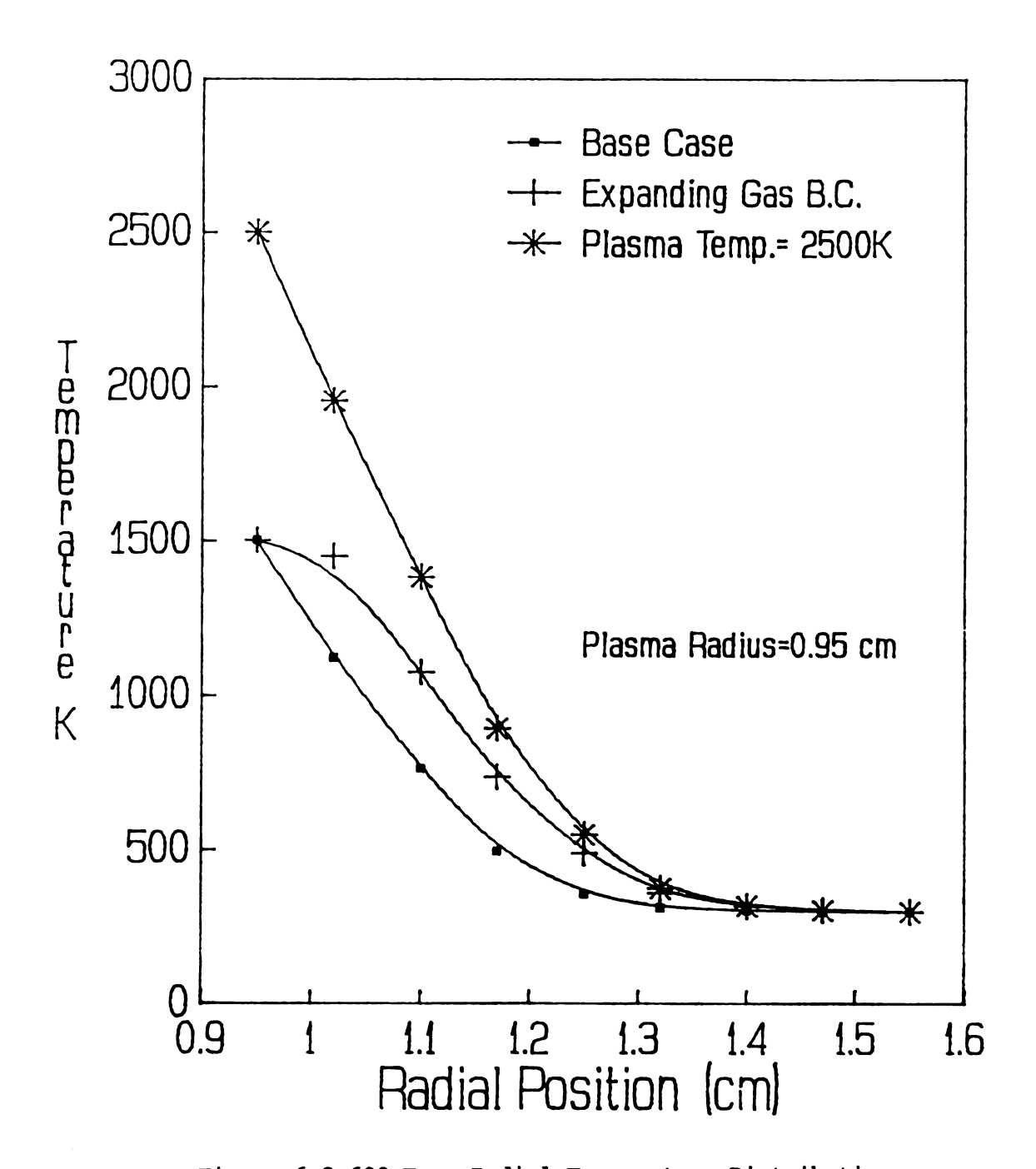


Figure 6.8 600 Torr Radial Temperature Distributions

N2 Non-Plasma Gas Exit Temp. Radial Distributions, 1000 Torr

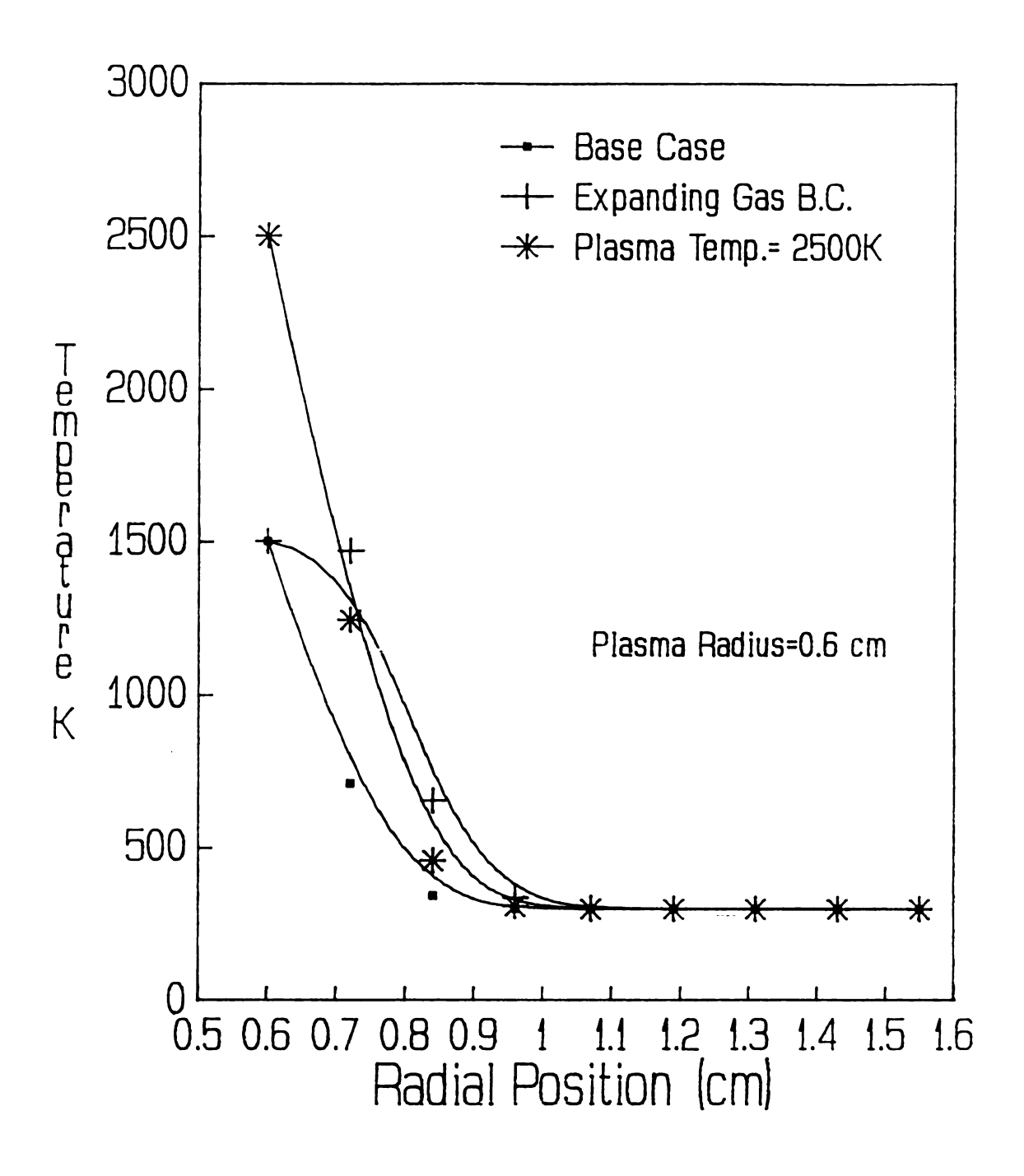


Figure 6.9 1000 Torr Radial Temperature Distributions

From the radial temperature distributions, mixing cup temperatures for the exit gas are calculated using the following equation.

$$T_{b} = \frac{\int 2\pi r T(r) U_{z}(r) dr}{\int 2\pi r U_{z}(r) dr}$$

Figure 6.10 illustrates the mixing cup temperatures for base case and expanding gas calculations. From this graph, it can be concluded that the expanding gas boundary condition causes higher mixing cup temperatures for all pressures, but still follows the same trend as the base case. Mixing cup temperatures range from 700 K at 1000 torr to 1450 K at 200 torr assuming a plasma temperature of 1500 K.

6.4 Summary

From a computer model, it is evident that conduction of the heat from the plasma to the quartz containment tube wall through non-reacting nitrogen gas cannot be ignored. To better understand the radial temperature profiles for high pressure plasmas, a more rigorous model, which incorporates turbulent mass and energy transfer, must be used. Nonetheless, a qualitative understanding of energy transfer mechanisms in microwave induced plasmas has been achieved in this simple modeling, and these results can be used to update other models which have neglected this effect.

Mixing cup temperatures calculated from the computer simulation runs range from 700 - 1450 K as the pressure changes from 1000 - 200 torr. As the pressure is increased, the mixing cup temperatures are decreased. A small difference is noted between the mixing cup temperatures calculated with the base case boundary conditions and the

N2 Gas Exit Temperatures Mixing Cup Averages

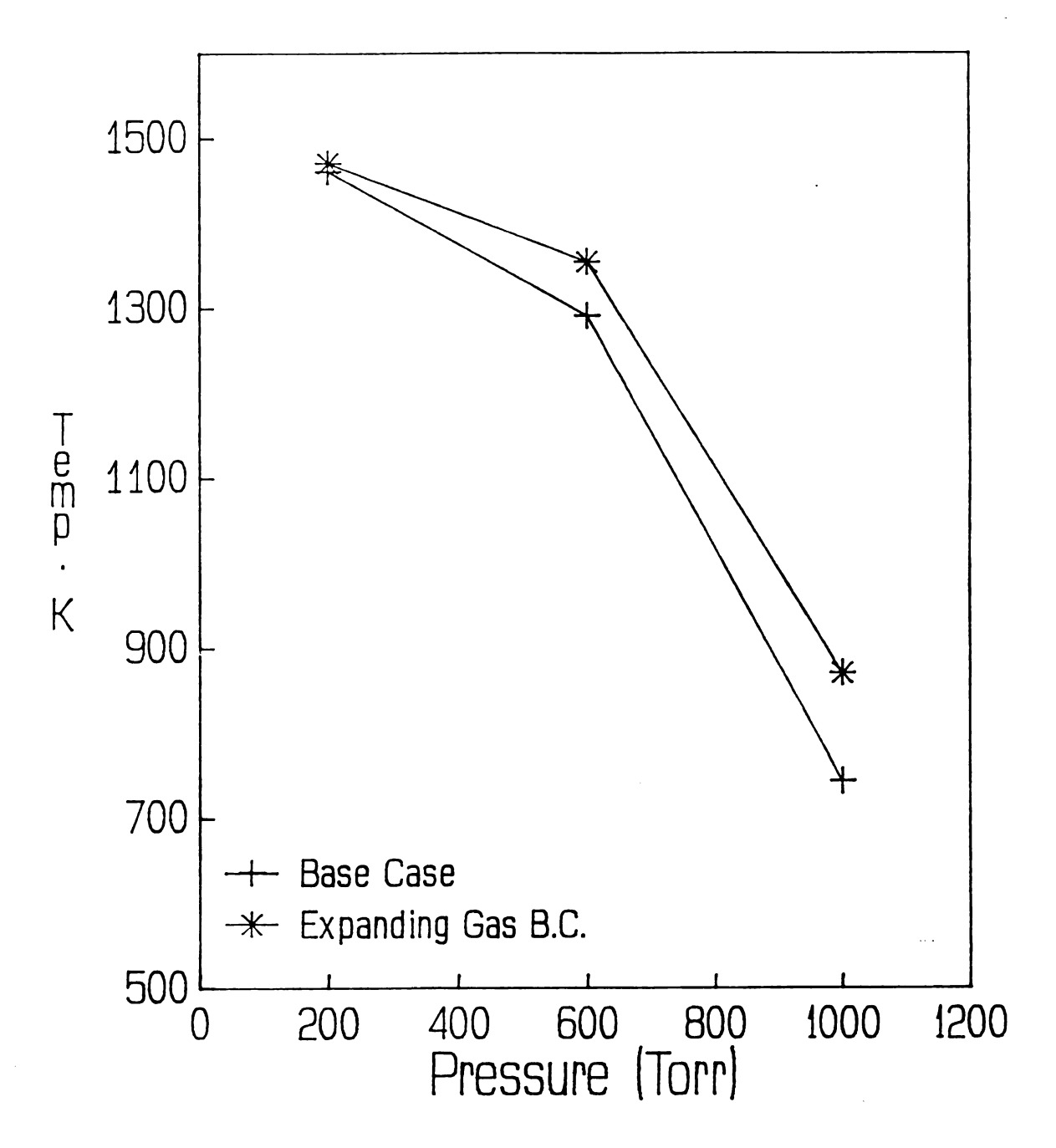


Figure 6.10 Mixing Cup Temperatures of Plasma Exit Gas

mixing cup temperatures calculated with the expanding gas boundary condition.

Chapter VII

Microwave Probe Development

7.1 Introduction

The need for development of a high temperature non-conducting (electrical) probe became apparent during research on a microwave plasma rocket engine. Although many methods exist for taking high temperature measurements, the measurement techniques are often not applicable in the microwave environment, and the techniques that can withstand the environment are either limited to low temperatures or give spatial averages of the temperature.

The conventional thermocouple and thermistor are limited in their use in an electromagnetic field because they are conductors and perturb the system if not located along node lines. Since a microwave plasma depends on the electromagnetic field properties, it is not easy to measure a perturbed system. All temperature measuring devices that use conductive materials are limited to certain places within the microwave field and therefore offer little, if any, worthwhile knowledge of the system under study.

Many spectroscopic techniques for measuring temperatures (gas and electronic - Chapman, Hoekstra, Brake, etc.) have been used but lack the accuracy desired to define the microwave system. The temperatures taken by emission spectroscopy are spatially averaged temperatures. Because plasmas do not give off enough light, lenses must be used to focus the emitted light on the monochromator slit opening.

The fluoroptic probe temperature sensing method is accurate in a microwave environment but lacks the high temperature capability needed for 1000 to 2000 °C measurements. Available fluoroptic probe systems have a 400 °C limit before the phosphor compound in the probes is deactivated.

A proposed solution to this problem is to use a ceramic sheath to protect the fluoroptic probe from being deactivated due to high temperatures. The protected probe takes the unsteady state temperature rise until the temperature nearly reaches its maximum limit (See Figure 7.1). The system is calibrated to obtain a set of temperature versus time curves that will then be used to accurately predict the temperature inside the plasma cavity (within the microwave field). The calibration technique assumes little or no absorption of microwave energy by the probe.

The first step in the development of a high temperature non-conducting probe is to narrow the field of possible ceramic materials by establishing the physical properties needed for an effective probe sheath. Melting point and the time needed for the temperature to rise from room temperature to the limit of the probe were the first two properties to be decided upon. To cover almost all foreseen experimental conditions, a melting point temperature limit of 2000 °C and a time limit of 10 minutes for the temperature rise were selected. A Gurney-Lurie chart for semi-infinite media was used to predict a thermal diffusivity necessary for the 10 minute temperature rise limit assuming a depth of one centimeter. According to these specifications, the ceramic chosen should have a thermal diffusivity of

High-Temperature, Microwave-Tolerant Probe Development

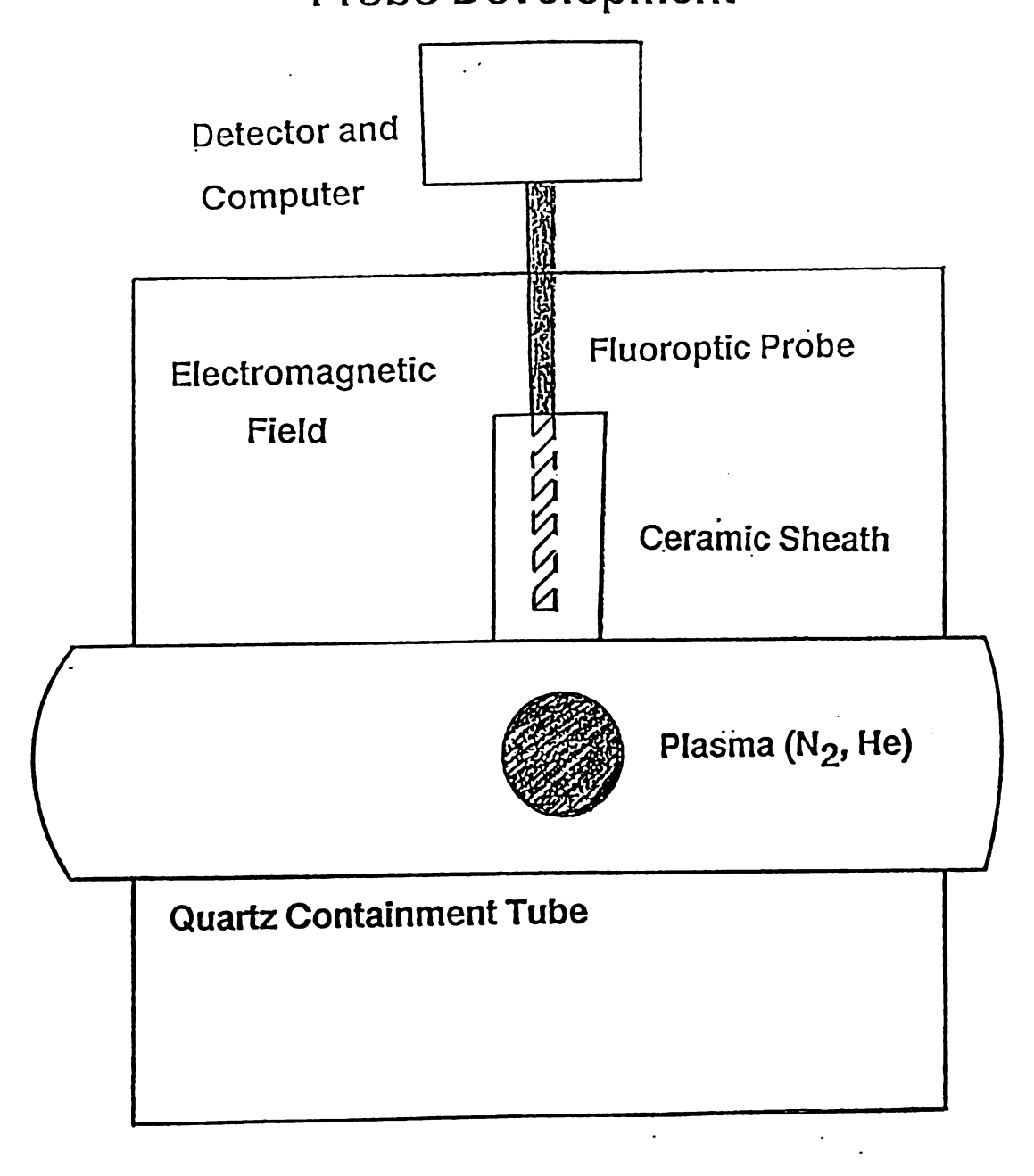


Figure 7.1 Concept Diagram of Microwave-Tolerant Probe

approximately 5 x 10^{-8} m²/s.

The two ceramic materials which have the above properties are yttria and magnesia. Magnesia has a melting point of over 3000 °C and yttria has a melting point near 2500 °C (Case [1987] and Industrial Publications [1984]). These materials are found to be satisfactory not only because of the above qualifications, but also because they are relatively well known and should not micro-crack under the anticipated high temperatures.

The final check of the material candidates before the fabrication of a probe sheath is the determination of the loss factor of each material in a microwave field. The loss factor is a measure of the microwave power absorbed by the material. The ceramic with the lowest loss factor is desired to keep the probe from being affected by the microwave field inside the cavity during experimental measurements. Since the loss factor is a function of temperature and electrical frequency, measurements are taken at a driving frequency of 2.45 GHz and several temperatures to characterize the lossiness of the ceramic materials.

7.2 Testing of Materials for Probe

The loss factors for yttria and magnesia are calculated using the method of Jow [1987]. In this method, the loss factor is calculated from the following parameters:

resonant cavity length and radius sample length and radius (assuming cylindrical samples) sample density and temperature resonant frequency change of empty to loaded cavity half-width of resonance peak at half-height in loaded cavity This experiment involved measuring the band resonant frequency (at 25 W input power) in an empty cavity, and then lowering the sample into the cavity and measuring the resulting change of the band resonant frequency and the band width at half-height. For sample temperatures above room temperature, the probes are heated with a heat gun and lowered into the cavity, and the measurements are taken while the probe cools. For a complete explanation of the theory involved, see Jow [1987].

To see the effects of a strong microwave environment (above 25 W) on the ceramic probe, a sample of yttria is placed in the maximum electromagnetic field position of the cavity and the resulting temperature rise measured for powers of 100 and 200 W. In this experiment, the quartz tube assembly is taken out of the cavity so that the only microwave absorbing entities are the yttria probe and the cavity walls. To ensure that as much of the radiation as possible is absorbed by the yttria sample, the holes bored into the microwave cavity body are covered with metal tape. This is also done to ensure the safety of the operator.

7.3 Discussion of Results

Using the TM_{012} mode, and the sweeping frequency perturbation method (Jow [1987]), the loss factors for yttria and magnesia are found to be 0.011 and 0.015, respectively. This loss factor data is good for temperatures up to 120 °C. The temperature limit is caused by the need for a teflon sample container because yttria and magnesia of necessary purity are most readily available in powder form. From

this information, it is evident that yttria is the preferred material for construction of a probe sheath.

Since the loss factor for yttria is lower than that for magnesia, the effects of an extreme electromagnetic field are measured on yttria only. Figure 7.2 shows the temperature versus time graph for yttria in microwave fields of 100 and 200 W. It can be seen that yttria heats up faster in the 200 W case than in the 100 W case, which is to be expected.

The results from this experiment are not conclusive enough to accept or reject yttria as a possible probe sheath material. Although it appears that yttria absorbs too much energy in a microwave environment to be useful as a probe sheath, the measurement technique was skewed and forced "all" of the microwave power to be coupled into the yttria. In a "best case" scenario, the cavity would have absorbed the energy instead of the yttria, and proved that yttria is an excellent sheath material. Unfortunately, this did not occur, but it is still possible that the yttria will not be the primary energy absorber in the microwave environment. Since the probe will be used in a plasma environment, the plasma, as a better coupling agent will absorb almost all of the microwave energy. Therefore, the yttria would not absorb as much energy and would be suitable as a probe sheath material. For this reason, more experiments must be conducted before the microwave resistant probe theory can be validated.

7.4 Summary

Selection of a ceramic material to construct a microwave

Microwave Heating of Yttria Probe Maximum Field Position

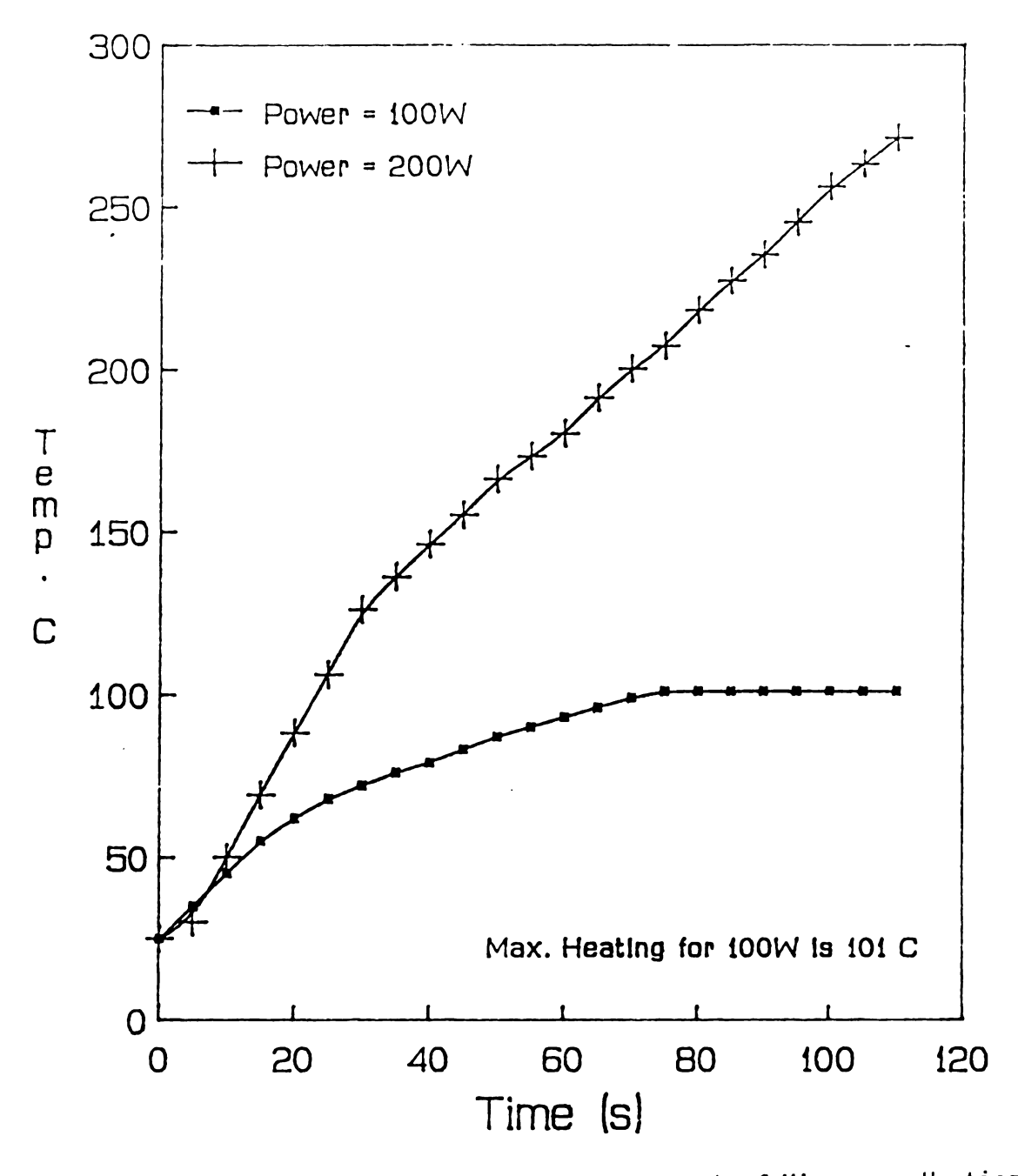


Figure 7.2 Temperature versus Time Graph of Microwave Heating of Yttria Probe

resistant probe sheath has been the focus of this study. Yttria and magnesia have the necessary high melting point (2500 and 3000 °C respectively) and thermal diffusivity for a temperature measurement of 1000 °C lasting no more than 10 minutes. Yttria was chosen for further research because it has a lower loss factor (0.011) than magnesia (0.015) in the temperature range of 25 to 120 °C (the measuring technique could not tolerate temperatures above 120 °C). Further research showed that although yttria has a lower loss factor than magnesia, it heats up 150 °C per minute in a 200 W electromagnetic field. However, these experiments were not run in a plasma environment where the plasma would absorb the majority of the energy. Therefore, more work must be completed in a plasma enviornment before determining whether or not yttria is suitable as a candidate material. If after further studies yttria is found to be an unsuitable sheath material, future development of a microwave resistant probe should use a material with a loss factor less than 0.011.

Chapter VIII

Conclusions

8.1 Introduction

The microwave electrothermal thruster is a potential propulsion system for deep space applications. In this concept, electrical power is used to heat the propellant through a microwave generated plasma. To help further the development of this system, the mechanisms of energy transfer to and within helium and nitrogen high pressure (200 - 1000 torr) microwave discharges were studied. Experimental techniques used in this investigation include emission spectroscopy, calorimetry, and photographic methods. The results of the calorimetry measurements were compared to results from a computer program modeling the heat transfer from the plasma to the quartz containment wall. The following paragraphs contain a summary of results of the experiments and computer modeling conducted during this investigation.

8.2 <u>Spectroscopy Measurements</u>

Bound electron temperatures, calculated from emission spectroscopy measurements on helium plasmas, are found to be affected by pressure and microwave power input. Under the operating conditions of this experiment, the electronic temperatures did not equal the electron temperatures because the system did not satisfy the local thermodynamic equilibrium condition. At 200 Torr, these temperatures are 3600 K for a 172 W input and 4400 K for a 246 W input. As the

pressure rises from 200 to 800 torr, these temperatures increase by approximately 1000 K. The electronic temperatures are not affected by cooling air and helium flow rates in the ranges of 0 to 4 scfm for air and 280 to 2520 sccm for helium at 800 torr. The helium flow rate affects the electronic temperatures in the 600 torr pressure case because the temperatures change from 5500 K to 5100 K with a change in flow rate of 280 to 1000 sccm.

8.3 Plasma Volume and Diameter Results

A 35 mm camera system was set up to photograph helium and nitrogen plasmas generated in a 33 mm I.D. quartz tube with a microwave input power of 246 W. Both helium and nitrogen discharges have a "threshold" pressure where the plasma volume and diameter change dramatically. Above this "threshold" pressure the plasma diameter became linearly dependent upon pressure. The "threshold" pressure for helium plasmas is approximately 200 torr. Nitrogen, since it is a diatomic gas, has a lower "threshold" pressure, around 100 torr for 246 W input power. Plasma diameters in the pressure range of 200 - 1000 torr for helium and nitrogen change from 31 to 7 mm and from 17 to 13 mm respectively. In the same pressure range, plasma volumes change from 46.71 to 4.59 cm³ for helium discharges and from 14.5 to 2.83 cm³ for nitrogen discharges.

8.4 Energy Balance Measurements

A calorimetry experiment was set up to calculate the partition of energy between the cavity, cooling air and working gas flows, for

nitrogen and helium plasmas in the 200 - 1000 torr pressure range. The results of the calorimetry experiment indicate that the amount of energy absorbed by the microwave cavity is dependent on the surface area of cavity exposed to the microwave environment. More easily put, the amount of power absorbed by the cavity depends on the cavity short length. The energy balance measurements indicate a 25% energy loss to the cooling water in the $\rm TM_{O11}$ mode and a 41% loss in the $\rm TM_{O12}$ mode. The power absorbed by the cavity is independent of both plasma pressure and input gas flow rate.

The amount of energy absorbed by the cooling air and plasma gas is pressure dependent. For most cases, the % $P_{\rm gas}$ varies from 10 - 16% as the pressure is increased from 200 - 800 torr. The % $P_{\rm air}$ is mode dependent and varies in this pressure range from 74 - 68 % in the TM_{011} mode and from 46 - 40% in the TM_{012} mode. The difference in the amount of energy absorbed by the cooling air in the two electromagnetic modes is equal to the difference in the amount of energy absorbed by the microwave cavity in the two modes. Over 75 % of the power input to the cavity has potential to be converted to thrust since the cavity wall losses are approximately 25 % over the experimental operating conditions of this study.

8.5 <u>Heat Conduction Model Results</u>

From a computer model of heat conduction from the plasma to the quartz tube wall through non-reacting nitrogen gas, it is evident that heat transfer between the plasma and the tube wall is important.

Using a simple energy transfer model, gas-wall interfacial temperature

differences of more than 500 K were calculated. This supports the conclusion that on the order of 75% of the power input into the cavity will be transferred to the plasma. The problem is to keep the power in the working fluid.

Mixing cup temperatures calculated from the computer model range from 700 - 1400 K as the pressure changes from 1000 - 200 torr. As the pressure increases, mixing cup temperatures decrease. Mixing cup temperatures calculated with the base case boundary conditions are similar to the mixing cup temperatures calculated with the expanding gas boundary conditions. The dramatic increase in mixing cup temperatures at low pressures can be attributed to the assumption that all the gas that flows through the plasma region exits at the plasma temperature. At low pressures, large plasma diameters cause the mixing cup temperatures to approach the plasma temperature of 1500 K.

8.6 Probe Development

In the selection of a ceramic material to construct a microwave resistant probe sheath, yttria and magnesia have the necessary high melting point (2500 and 3000 °C respectively) and thermal diffusivity for a temperature measurement of 1000 °C lasting no more than 10 minutes. Yttria was chosen for further research because it has a lower loss factor (0.011) than magnesia (0.015) in the temperature range of 25 to 120 °C (the measuring technique could not tolerate temperatures above 120 °C). Further research showed that although yttria has a lower loss factor than magnesia, it heats up 150 °C per minute in a 200 W electromagnetic field. However, these experiments

were not run in a plasma environment where the plasma would absorb the majority of the energy. Therefore, more work must be completed before determining whether or not yttria is suitable as a candidate material. If after further studies yttria is found to be an unsuitable sheath material, future development of a microwave resistant probe should use a material with a loss factor less than 0.011.

8.7 Summary

In this investigation, experiments and modeling efforts concentrated on helium and nitrogen microwave plasmas in the 200 to 1000 torr pressure range. Table 8.1 contains a brief summary of the experimental parameters used in this study. As research progresses, it becomes increasingly important to assemble complete data bases at various sets of operating conditions. An effort was made in this study to keep experimental parameters consistent so that a generalized body of data could be assembled on the microwave propulsion system under high pressure (200 - 1000 torr), low power (under 250 W) conditions.

Table 8.1. Summary Table of Experimental Parameters

| Parameter | Elect. Temp. | Plasma Meas. | Energy Balance | Computer Model |
|---------------------|-------------------|--------------------|---|-------------------|
| Gas | Не | He, N ₂ | He, N ₂ | N ₂ |
| Working Gas | | | | |
| Flow Range | | | | |
| (sccm) | 60 | 0 | 0 - 2000 | 5,000 |
| Air | | | | |
| Cooling Flow (scfm) | 0 - 3.5 | 3.5 | 0.5 | 4.5 |
| Electromagnet | ic | | | |
| Mode | TM 012 | TM 012 | TM ₀₁₂ , TM ₀₁₁ - | |
| Input Power (Watts) | 175 - 250 | 250 | 250 | - |
| Pressure | 200 - | 200 - | 200 - | 200 - |
| (torr) | 800 | 1000 | 800 | 1000 |

Chapter IX

Recommendations

9.1 Introduction

During the course of this investigation, many new directions for research have become evident. These new directions include modifications to existing experimental techniques as well as new experimental methods. The goals of these modifications are to simplify the procedures and increase the accuracy of the results. New experimental techniques are recommended to help gather data that was previously immeasurable. These modifications can be used as research continues in both low and high pressure and power regimes. Also, a future goal in plasma research is to unify the data taking so that all the plasma diagnostics presented in this study can be run simultaneously.

9.2 Spectroscopy

Emission spectroscopy measurements are very important in understanding the partition of energy within the plasma region.

Because of this, many aspects of this study can be modified to make better and more accurate measurements. A simple modification of the existing experimental system is the addition of a 10,000 Å diffraction grating to the monochromator. Using a 10,000 Å grating in combination with measurements in the U.V. range (below 3,000 Å) will enable a more complete understanding of the energy distribution within the microwave

plasma. To measure helium spectra in the U.V. range, a vacuum environment must be maintained between the monochromator and the emitting source. Measuring the spectra in the U.V. range will give us information on the relative population of the lower states. The most important state in the U.V. range is the "ls" state because all recombinations back to this state give off U.V. radiation.

Another modification to the present emission spectroscopy system is the addition of computer. The addition of a computer to take data will reduce error due to the integration of absorption peaks by hand. This will not only decrease experimental error, but will also increase the number of measurements taken during an experiment. One of the shortcomings this study is the lack of spatially resolved electronic temperature measurements. The use of a fiber-optic bundle is recommended for this purpose. Although a single strand of optical fiber is too insensitive for any plasma emission measurements to be taken, a bundle of these fibers should allow enough light to pass for the experiment to work. With these modifications, the distribution of energy within the electronic states of a plasma can be studied more accurately, and hopefully a better understanding will be gained in the process.

9.3 Plasma Volume and Diameter Measurements

Only two modifications to the plasma volume and diameter measurements are thought to be worthy of consideration. One of these modifications is the addition of a movie camera to the existing system. The movie camera should enable accurate measurements of the pressure range

at which the plasma constricts from the quartz containment wall. Not only would this critical pressure range be known, but also the shape, volume, and color change of the plasma could be measured in the 1- 1000 torr pressure range as well. A second modification of the current experimental technique is the use of $\rm H_2$ - $\rm N_2$ and $\rm H_2$ -He mixtures. Since hydrogen is too dangerous to work with at high pressures by itself in our present system, volume and diameter measurements could be made by using the mixtures. The existing system would need to have the entire flow system revamped in stainless steel before any thought of working with hydrogen is feasible. The expense and effort involved in these two modifications seem to be reasonable when compared with the amount of knowledge gained in the process. The ultimate goal of these modifications is to conduct high pressure hydrogen experiments.

9.4 Energy Balance

Although the energy balance technique used in this experiment is simple and successful, there are some modifications that would increase the amount of knowledge gained by this method. The addition of a 1500 W microwave source would enable calorimetry measurements in nitrogen plasmas over 400 torr. In this study, sustaining high pressure nitrogen plasmas was found to be difficult, if not impossible. By increasing the microwave input power, the stability of the plasma would increase and enable higher pressure measurements. Another modification would be to coat the inside of the brass cavity with silver or gold. This has been suggested by many previous investigators (Whitehair [1986], Hopwood [1986], Chapman [1986], etc.) as a

method for reducing the amount of energy absorbed by the cavity. By using new materials, the amount of energy absorbed by the cavity could be reduced and the overall efficiency increased.

9.5 Computer Modeling

The existing computer simulation represents a simple but useful model of the convective and conductive heat transfer from the plasma to the quartz tube wall. By inserting these results into a modified version of the program developed by Filpus [1986], a new understanding of the recombination processes downstream of the plasma can be achieved. To gain a better feel for the plasma processes, a computer simulation of a high pressure plasma is needed. Although Morin [1986] did a thorough job of modeling the plasma region, his work was done on low pressure discharges. To bring the capabilities of existing computer simulations up to high pressure microwave discharge modeling, a lot of work is needed to synthesize and update existing computer programs. It is hoped that the insights of this researcher, combined with the previous knowledge gained from my co-workers will enable the development of a new and better computer simulation of the microwave plasma processes.

9.6 Probe Development

Although one might think that the microwave resistant probe development was inconclusive, the concept is sound. To continue this work, it is recommended that more attention be paid to testing yttria and other ceramics in a plasma environment. In a plasma environment,

the sheath material should not absorb nearly as much energy as the plasma itself. Therefore, the sheath would be able to perform its duty of protecting the fluoroptic probe without changing the experimental results due to its own properties. Further work should be able to prove that the sheath concept is viable.



List of References

- 1. Bekefi, G., Principles of Laser Plasmas, Wiley & Sons, New York, 1976.
- 2. Bennet, C., and Myers, J., Momentum, Heat, and Mass Transfer, 2nd ed., McGraw-Hill, Inc., New York, 1974.
- 3. Brake, M., "A Theoretical and Experimental Investigation of the Chemical Kinetics of an Oxygen Microwave Discharge," Ph. D. Dissertation, Michigan State University, 1983.
- 4. Brodkey, R., The Phenomena of Fluid Motions, Ohio State University Press, Columbus, Ohio, 1967.
- 5. Bulirsch, R., and Stoer, J., "Numerical Treatment of Ordinary Differential Equations by Extrapolation Methods", Numerische Mathematik, 8(1), 1966.
- 6. Case, E., private communication, 1987.
- 7. Chapman, R., "Energy Distribution and Transfer in Flowing Hydrogen Microwave Plasmas," Ph. D. Dissertation, Michigan State University, 1986.
- 8. Cornelisse, J., Schoyer, H., and Wakker, K., Rocket Propulsion and Spaceflight Dynamics, Pitman Publishing Limited, London, 1979.
- 9. CRC Press, Inc., Handbook of Chemistry and Physics, 64th ed., 1984.
- 10. Fahien, R., Fundamentals of Transport Phenomena, McGraw-Hill, Inc., New York, 1983.
- 11. Filpus, W., "The Energetics of Hydrogen Atom Recombination, Ph. D. Dissertation, Michigan State University, 1986.
- 12. Gragg, W., "On Extrapolation Algorithms for Ordinary Initial Value Problems, J. SIAM Numerical Analysis, Series B, 2, 1965.
- 13. Griem, H., Plasma Spectroscopy, McGraw Hill, New York, 1964.
- 14. Hellund, E., *The Plasma State*, Reinhold Publishing, New York, 1961.

- 15. Hindmarsh, A., "Gear: Ordinary Differential Equation System Solver", Lawrence Livermore Laboratory Report, UCID-30001, Rev. 3, 1974.
- 16. Hopwood, J., Kubinec, M., Asmussen, J., and Brake, M., "Electronic Temperature Measurements of Helium Microwave Discharges," presented at 39th Annual Gaseous Electronics Conference, U. Wisconsin-Madison, 1986.
- 17. Howatson, A., An Introduction to Gas Discharges, Pergamon Press, Oxford, 1965.
- 18. Industrial Publications, Inc., Ceramic Data Book, 63rd ed., 1984.
- 19. Jow, J., Hawley, M., Finzel, M., Asmussen, J., Lin, H., and Manring, B., "Microwave Processing and Diagnosis of Chemically Reacting Materials in a Single-Mode Cavity Applicator," *IEEE Transactions on Microwave Theory and Techniques*, 35, 1435-42 [1987].
- 20. Krall, N., and Trivelpiece, A., Principles in Plasma Physics, McGraw Hill, New York, 1973.
- 21. Langmuir, I., "Plasma Oscillations", Phys. Rev., 33, 1939.
- 22. Mark, G., *Plasma Spectroscopy*, Elsevier Publishing, Amsterdam, 1968.
- 23. Morrin, T., "Collision Induced Heating of a Weakly Ionized Dilute Gas in Steady Flow", Ph. D. Dissertation, Michigan State University, 1985.
- 24. Rogers, J., "Properties of Steady State, High Pressure Argon Discharges," Ph. D. Dissertation, Michigan State University, 1982.
- 25. Stewart, P., "New Possibilities for Solar System Exploration", Aeronautics and Astronautics, 4, 12, 1966.
- 26. Sutton, G., and Ross, D., Rocket Propulsion Elements, 4th ed., John Wiley & Sons, Inc., New York, 1976.
- 27. Thompson, W., An Introduction to Plasma Physics, Pergamon Press, Oxford, 1962.
- 28. Tourin, R., Spectroscopic Gas Temperature Measurements, Elsvier Pub., Amsterdam, 1966.
- 29. Whitehair, S., "Experimental Development of a Microwave Electrothermal Thruster," Ph. D. Dissertation, Michigan State University, 1986.

APPENDIX

Program Sheath

C

```
č
      Variable Dictionary (IMSL Subroutine)
CCC
      Y - dependent variable - in this case it is the gas temperature
          at a specified grid point
C
C
      X - independent variable - in this case it is the length down
C
          the plasma tube
CCC
      N - the number of equations (input) to be solved (grid points)
С
     JM - maximum order of the rational approximation (usually set at
C
          6) must be less than 7
Č
     IDO- convergence type indicator; IND=2, specifies relative error
C
      H - on input H = the guess for the step size and on output H =
С
          the suggested value for the step size
C
Ċ
     HMIN - smallest permissible step size
C
CC
     TOL - tolerance for error control
C
      R - contains the absolute errors in each component for the
C
          current step
Č
C
     Variable Dictionary (Main Program Sheath)
С
C
      CASE - if case = 1 the plasma boundry temperature is constant
C
              and equal to the plasma temperature
C
              if case = 2 then the plasma boundry condition is that
C
             there is a energy flux across the boundry caused by the expansion of the "so called" plasma region due to the
C
             volume difference between the hot and cold gas
C
C
     MCOUNT - temporary variable which represents the line number so
Č
               that the radius can be calculated for a specific grid
CC
              point
C
      CVT - function routine to calculate heat capacity as a function
C
            of temperature (Cal / gmole K)
CCC
      D1 - diameter of the plasma (cm)
      D2 - diameter of the plasma containment tube (quartz tube)
C
C
      D3 - DIAMETER OF THE AIR COOLING TUBE (OUTER TUBE)
Č
      DISRAD - radial distance between grid points (D2-D1)/(LINE*2)
Č
С
      FRONT - TEMPORARY VARIABLE USED TO SEPARATE CASE 1 FROM CASE 2
C
C
      GBEG - TEMPORARY VARIABLE TO MAKE CALCULATING YPRIME EASIER
C
              (SAME WITH GBEG1 AND GBEGN)
Č
CC
      HC - heat transfer coefficient - calculated assuming that all
            resistance to heat transfer is between the air and the
C
           quartz tube wall (Weigand approximation) Cal / S Cm Cm K
00000
      HX - dummy variable used to hold H's place in data frie
       I - looping variable used in Do loop to evaluate Yprime(1)
```

```
С
        J - looping variable used in Do loop to initialize Y(J)
 Ċ
       KT - function routine to calculate thermal conductivity as a function of temperature ( Cal / S \mbox{Cm} K )
 С
 С
 C
 Č
       LINE - input variable - number of radial points in grid
 č
       ANI - gas velocity (gmoles/s)
C
C
С
       PATM - pressure of input gas in atm for easier input
С
Ċ
       PI - pi (3.14...)
Č
       PIN - pressure of input gas (correct units-cal/cm^3)
С
С
       PUTIN - temporary variable used to flag input file if an input
                file is to be used instead of input from the computer
С
č
                screen (same with putin2)
Č
       RAD - function routine to calculate the radius of the grid
С
              point from the line number (position from center of pipe)
С
С
CC
       RGAS - Ideal gas constant (1.98 Cal / gmole K)
        T - represents the temperature, used in KT, and CVT functions
С
C
C
       TI - input gas temperature
C
Č
       TP - plasma gas temperature
CC
       UBAIR - bulk air flow rate (cm/s)
       IMPLICIT REAL*8 (A-H,K,O-Z)
       EXTERNAL FCN, DIVPAG, FCNJ
       COMMON/DIMN/D1, D2, D3, DISRAD, ANI
       COMMON/GAS/RGAS, PI, UBAIR, PIN, Tp, ti, CASE
       DIMENSION Y(10), PARAM(50)
C THIS BLOCK INITIALIZES THE NEEDED VARIABLES FOR THE START OF THE
C PROGRAM AND THE SUBROUTINE FCN
       OPEN (10, FILE = 'KEEPIN.DAT', STATUS = 'OLD')
        RGAS = 1.98D0
       PI = 3.14159D0
            = 0.0D0
        GBEG = 0.000
        GBEGN= 0.0D0
        GBEG1= 0.0D0
        FRONT = 0.0D0
        IDO = 1
C THIS BLOCK IS THE INPUT READ, WRITE, AND PRINT STATEMENTS
       REWIND 10
      READ (10.*), H.PIN.TP.TI.D1.D2.D3.UBAIR.ANI.N.HMIN.TOL.CASE
PRINT *, 'DO YOU WANT TO USE OLD STEP SIZE AND PARAMETERS (Y=1)?'
READ *, PULIN
       IF (PUTIN. EQ. 1) THEN
        GO TO 50
       END IF
      PRINT *, 'ENTER THE STEP SIZE DESIRED (CM)' READ *, H
```

```
PRINT *, 'DO YOU WANT TO USE OLD PARAMETERS EXCEPT STEP SIZE?' READ *, PUTIN2
          IF (PUTINZ.EQ.1)THEN
GO TO 60
END IF
         OPEN (5, FILE = 'INDATA.DAT', STATUS = 'NEW')
         PRINT *, 'ENTER PLASMA TEMP., INPUT GAS TEMP. AND PRESS. (ATM)'
READ *, TP.TI, PATM
           PIN = 2.4218D-2*PATM
         PRINT ". 'ENTER PLASMA DIAMETER AND TUBE DIAMETERS (CM)' READ ". D1,D2,D3
         PRINT ". 'ENTER BULK AIR FLOW (CM/S), GAS (N2) FLOW (GMOLES/S)' READ ", UBAIR, ANI
         PRINT ", 'ENTER NO# OF RADIAL POINTS NEEDED ' READ ", N
         PRINT ", 'ENTER THE SMALLEST STEP SIZE, AND ERROR TOL' READ ", HMIN,TOL
         PRINT ", 'WHAT CASE IS BEING RUN? (1 OR 2)' READ ", CASE
        WRITE (5,"), 'STEP SIZE (H) = '.H,' GAS PRESSURE =',PIN WRITE (5,"), 'PLASMA TEMP. = '.TP,' INPUT GAS TEMP. =',TI WRITE (5,"), 'PLASMA DIAM. = ',D1,'INNER TUBE DIAM. = ',D2 WRITE (5,"), 'OUTER TUBE DIAMETER',D3 WRITE (5,"), 'BULK AIR FLOW = ',UBAIR,' MOLAR GAS FLOW = ',ANI WRITE (5,"), 'NUMBER OF RADIAL POINTS = ',N WRITE (5,"), 'SMALLEST STEP SIZE = ',HMIN,' ERROR TOL. = ',TOL WRITE (5,"), 'CASE NUMBER = ',CASE
         REWIND 10
         WRITE (10, "), H, PIN, TP, TI, D1, D2, D3, UBAIR, ANI, N, HMIN, TOL, CASE
         GO TO 80
         CONTINUE
         READ (10,"), H,PIN,TP,T1,D1,D2,D3,UBAIR,ANI,N,HMIN,TOL,CASE
GO TO 80
         CONTINUE
           REWIND 10
           READ (10, 1), HX, PIN, TP, TI, D1, D2, D3, UBAIR, ANI, N, HMIN, TOL, CASE
         CONTINUE
         PARAM(2)=HMIN
         PARAM(4)=10000
         LINE = N
            N1 = N + 1
         DISRAD = (D2-D1)/(2*LINE)
C SETTING THE INITIAL CONDITIONS FOR ALL RADIAL GRID POINTS
         DO 90 J=1,N
Y(J) = TI
         CONT INUE
         OPEN (15, FILE = 'OUTPUT.DAT', STATUS = 'NEW')
WRITE (15, *), ' START OF DATA OUTPUT'
```

50

60

80

90

```
WRITE (15,*), ' '
WRITE (15,3), (M,M=1,N)
WRITE (15,2), (RAD(M),M=2,N1)
WRITE (15,*), 'LENGTH', (' TEMP.
         FORMAT (8X,10(F8.2))
FORMAT (8X, RADIUS', 10(12, RADIUS'))
 3
 C THE NEXT BLOCK IS THE HEART OF THE PROGRAM - IT CALLS THE INTEGRATOR
         H = DMIN1(H,D1-X)
 100
         XEND = H + X
         CALL DIVPAG(IDO, N, FCN, fcnj, a, X, XEND, TOL, PARAM, Y)
         IF (IDO.GT.3)THEN
GO TO 500
END IF
        WRITE (15,1), X,(Y(M),M=1,N)
FORMAT (1X,F8.6,10(F8.2))
IF (X.LT.D1-HMIN)THEN
         GO TO 100
END IF
         GO TO 1000
C'THIS BLOCK IS TO HANDLE THE ERROR ROUTINE AND TO PRINT ANY NEEDED C INFORMATION WHICH MIGHT HELP DIAGNOSE PROBLEMS
         CONTINUE
500
        WRITE (15,*), 'TEMP.S = ',(Y(M),M=1,N)
WRITE (15,*), 'DISTANCE = ',X,'STEP SIZE = ',param(31)
       CONTINUE
1000
         STOP
         END
   THIS SUBROUTINE CONTAINS THE PARTIAL DIFFERENTIAL EQUATION IN
   AN ORDINARY DIFF. EQ. FORM AND CONTAINS THE BOUNDRY CONDITIONS AT THE TUBE WALL AND PLASMA GAS INTERFACE
        SUBROUTINE FCN (N, X, Y, YPRIME)
        IMPLICIT REAL*8 (A-H,K,O-Z)
        DIMENSION Y(N), YPRIME(N)
COMMON/GAS/RGAS, PI, UBAIR, PIN, Tp, ti, CASE
        COMMON/DIMN/D1, D2, D3, DISRAD, ANI
           TC=298
        HC = 0.368D0^{\circ}((UBAIR^{\circ}0.8D0)/(D3-D2)^{\circ}0.2D0)^{\circ}(D3/D2)^{\circ}0.45D0
        N1=N-1
        DO 2000 I=2,N1
        GBEG = 1.D0/(RAD(1+1)^*CVT(Y(1)))/(ANI/(PI^*D2^*D2/4)^*(1-
       +((RAD(1)+RAD(1+1))/D2)**2))
        YPRIME(I) = GBEG^{*}((RAD(I)^{*}KT(Y(I-1))^{*}((Y(I-1)-Y(I))/DISRAD))-
       +(RAD(1+1)*KT(Y(1))*(Y(1)-Y(1+1))/DISRAD))/DISRAD
2000 CONTINUE
      GBEGN = 1.D0/(RAD(N+1)*CVT(Y(N)))/(ANI/(PI*D2*D2/4)*(1-+((RAD(N)+RAD(N+1))/D2)**2))
       YPRIME(N) = GBEGN^{(RAD(N)^KT(Y(N-1))^((Y(N-1)-Y(N))/DISRAD))}
      +(RAD(N+1)*HC*(TC-Y(N))/DISRAD))/DISRAD
        IF (CASE .EQ. 1.D0) FRONT = RAD(1)*KT(TP)/DISRAD
IF (CASE .EQ. 2.D0) FRONT=(ANI*(1.D0-TI/TP)*(CVT(Y(1))+RGAS)
       +)/(3°D1°PI)
```

```
GBEG1 = 1.D0/(RAD(1)*CVT(Y(1)))/(ANI/(PI*D2*D2/4)*(1-+((RAD(2)+RAD(1))/D2)**2))
        YPRIME(1) = GBEG1*(FRONT*(TP-Y(1))-
       +(RAD(2)*KT(Y(1))*(Y(1)-Y(2))/DISRAD))/DISRAD
     RETURN
        END
C THIS FUNCTION CALCULATES THE HEAT CAPACITY BASED ON THE TEMPERATURE
        REAL FUNCTION CVT*8(T)
        IMPLICIT REAL*8 (A-H,K,O-Z)

COMMON/GAS/RGAS,PI,UBAIR,PIN,Tp,ti,CASE

CVT = 7.440D0 - 3.24D-3*T + 6.4D-6*T**2 - 2.79D-9*T**3
        RETURN
        END
C THIS FUNCTION CALCULATES THE THERMAL CONDUCTIVITY FROM THE TEMP.
       REAL FUNCTION KT*8(T)
IMPLICIT REAL*8 (A-H,K,O-Z)
KT = 5.258D-7*T**0.825D0
        RETURN
        END
C THIS FUNCTION CALCULATES THE RADIAL POSITION FROM THE LINE NO#
       REAL FUNCTION RAD*8(MCOUNT)
IMPLICIT REAL*8 (A-H,K,O-Z)
COMMON/DIMN/D1,D2,D3,DISRAD,ANI
        RAD = D1/2.D0 + DISRAD* (MCOUNT-1)
       RETURN
       END
C THIS IS A DUMMY FUNCTION BECAUSE THE SUBROUTINE WANTS IT
         real function fcnj
```

end

Experimental Procedure for Starting a Plasma

- 1) Turn on all the electronics for a warm-up period.
- 2) Start air and water cooling of plasma containment tube assembly (do not start water cooling of cavity yet because water can condense inside the cavity and change the cavity's electromagnetic characteristics)
- 3) Start the vacuum pump and open downstream valve to evacuate the plasma containment chamber to about 1 torr.
- 4) Begin working gas flow of 60 sccm.
- 5) Open water valve and start cooling the microwave cavity.
- 6) Turn on high voltage (microwave source) and increase the microwave input power to 80 W and check for microwave leaks in the system.
- 7) Tune cavity to the desired electromagnetic mode.

Short Length = 14.4 cm
$$TM_{012}$$
 mode Probe Depth = 0-2 cm TM_{011} mode TM_{012} mode

8) Once the plasma starts, increase the input power and pressure to the desired operating conditions. The cavity must be tuned constantly during the change to high pressure.

Safety Considerations

- Always make sure microwave power is turned off before turning on the microwave power source.
- 2) Don't put alot of power into the microwave cavity without a plasma already formed. Without a plasma in the cavity, there is nothing to absorb the energy, and it will either be reflected back towards the source or leak out and radiate the operator.
- 3) Always check microwave cables and the cavity for leaks before and during high power experiments. Also check the microwave cables for excess heat generated during the experiment. Another precaution is cooling the microwave cables with a fan.
- 4) Make sure that any openings in the cavity are covered with copper screen to keep the microwave radiation inside the cavity.
- 5) Check the pressure on the air-cooling tube. Make sure the pressure doesn't exceed 10 psi on this tube.
- 6) Always check the cavity during operation for heating during experiments. Increase the water if water cooling occurs.